DEMAND SIDE MANAGEMENT OF A RUN-OF-MINE ORE MILLING CIRCUIT

by

Björn Matthews

Submitted in partial fulfillment of the requirements for the degree

Master of Engineering (Electronic Engineering)

in the

Department of Electrical, Electronic and Computer Engineering
Faculty of Engineering, Built Environment and Information Technology
UNIVERSITY OF PRETORIA

September 2014

SUMMARY

DEMAND SIDE MANAGEMENT OF A RUN-OF-MINE ORE MILLING CIRCUIT

by

Björn Matthews

Supervisor(s):	Prof. Ian K. Craig
Department:	Electrical, Electronic and Computer Engineering
University:	University of Pretoria
Degree:	Master of Engineering (Electronic Engineering)
Keywords:	Demand side management, load shifting, milling circuit, model predictive control, real-time optimizer, run-of-mine ore, time-of-use tariff

In South Africa, where 75% of the worlds platinum is produced, electricity tariffs have increased significantly over recent years. This introduces challenges to the energy intensive mineral processing industry. Within the mineral processing chain, run-of-mine ore milling circuits are the most energy-intensive unit processes. Opportunities to reduce the operating costs associated with power consumption through process control are explored in this work.

In order to reduce operating costs, demand side management was implemented on a milling circuit using load shifting. Time-of-use tariffs were exploited by shifting power consumption of the milling circuit from more expensive to cheaper tariff periods in order to reduce overall costs associated with electricity consumption. Reduced throughput during high tariff periods was recovered during low tariff periods in order to maintain milling circuit throughput over a week long horizon.

In order to implement and evaluate demand side management through process control, a load shifting controller was developed for the non-linear Hulbert model. Implementation of the load shifting controller was achieved through a multi-layered control approach. A regulatory

linear MPC controller was developed to address technical control requirements such as milling circuit stability. A supervisory real-time optimizer was developed to meet economic control requirements such as reducing electricity costs while maintaining throughput.

Scenarios, designed to evaluate the sensitivities of the load shifting controller, showed interesting results. Mill power set-point optimization was found to be proportionally related to the mineral price. Set-points were not sensitive to absolute electricity costs but rather to the relationships between peak, standard, and off-peak electricity costs. The load shifting controller was most effective at controlling the milling circuit where weekly throughput was between approximately 90% and 100% of the maximum throughput capacity.

From an economic point of view, it is shown that for milling circuits that are not throughput constrained, load shifting can reduce operating costs associated with electricity consumption. Simulations performed indicate that realizable cost savings are between R16.51 and R20.78 per gram of unrefined platinum processed by the milling circuit. This amounts to a potential annual cost saving of up to R1.89 m for a milling circuit that processes 90 t/h at a head grade of 3 g/t.

OPSOMMING

AANVRAAGBESTUUR VIR 'N MAALKRING WAT ONBEHANDELDE ERTS MAAL

deur

Björn Matthews

Studieleier(s):	Prof. Ian K. Craig
Departement:	Elektriese, Elektroniese en Rekenaar-Ingenieurswese
Universiteit:	Universiteit van Pretoria
Graad:	Magister in Ingenieurswese (Elektroniese Ingenieurswese)
Sleutelwoorde:	Aanvraag-bestuur, in-tydse optimisering, maalkring, model-voorspellende beheer, onbehandelde erts, tyd-van-gebruiktarief, vragverskuiwing

In Suid-Afrika, waar 75% van die wêreld se platinum geproduseer word, het elektrisiteitspryse oor die afgelope jaar aansienlik toegeneem. Dit bied uitdagings aan die energie-intensiewe mineraalverwerkingsbedryf. In die mineraalprosesseringsbedryf is die maal van onbehandelde erts die mees energie-intensiewe proses. In die verhandeling word geleenthede ondersoek om die bedryfskoste wat verband hou met kragverbruik van die maalkringe te verminder.

Om bedryfskoste te verminder, is prosesbeheer gebruik om aanvraagbestuur op 'n maalkring te implementeer. Tyd-van-gebruiktariewe is benut deur die verskuiwing van die kragverbruik van die maalkring van duurder tariefperiodes na goedkoper periodes om die algehele elektrisiteitskoste te verminder. Daar is vir verminderde deurset tydens hoëtarief-periodes vergoed tydens laetarief-periodes sodat die gemiddelde deurset van die maalkring oor 'n periode van een week gehandhaaf kan word.

Aanvraagbestuur is geïmplementeer deur 'n vragverskuiwingbeheerder wat ontwikkel is vir die nie-lineêre Hulbert-model. Implementering van die vragverskuiwingbeheerder is bereik deur 'n multilaagbeheerbenadering. 'n Regulerende lineêre model-voorspellende beheerder is ontwikkel om tegniese beheervereistes soos maalkringstabiliteit te hanteer. 'n Toesighoudende

in-tydse optimiseerder is ontwikkel om ekonomiese beheervereistes, soos die vermindering van elektrisiteitskoste, te hanteer terwyl die deursettempo gehandhaaf word.

Scenario's is ontwikkel om die sensitiwiteit van die vragverskuiwingbeheerder te evalueer. Die resultate toon dat die maalkragkragverbruikstelpunt-optimisering proporsioneel verwant is aan die mineraalprys. Stelpunte is nie sensitief vir die absolute koste van elektrisiteit nie, maar eerder vir die verhouding tussen die piek-, standaard-, en af-piek-elektrisiteitskoste. Die lasverskuiwingbeheerder het die mees doeltreffende beheer oor die maalkring wanneer die deurset tussen ongeveer 90% en 100% is.

Vanuit 'n ekonomiese oogpunt word getoon dat vir maalkringe wat nie deursetbeperk is nie vragverskuiwing bedryfskoste, wat verband hou met elektrisiteitsverbruik, kan verminder. Simulasies wat uitgevoer is, dui daarop dat 'n kostebesparing van tussen R16.51 en R20.78 per gram van die ru-platinum verwerk deur die maalkring bereik kan word. Dit is 'n potensiële jaarlikse kostebesparing van tot R1.89 m vir 'n maalkring wat 90 t/h rou erts wat 3 g/t platinum bevat, prosesseer.

LIST OF ABBREVIATIONS

CV	Controlled variable
DMC	Dynamic matrix control
DOB	Disturbance observer
DSM	Demand side management
EE	Energy efficiency
INA	Inverse Nyquist array
MPC	Model predictive control
MPM	Model-plant mismatch
MV	Manipulated variable
PID	Proportional-integral-derivative
PSE	Product particle size
ROM	Run-of-mine
RTO	Real-time optimizer
SAG	Semi-autogenous
SID	System identification
TOU	Time-of-use

TABLE OF CONTENTS

CHAPTER 1

INTRODUCTION

Processing of run-of-mine (ROM) ore to pure metals is achieved through a number of processes as illustrated in Figure 1.1. ROM ore is first crushed, where after it is ground to liberate the minerals and then classified by size. These liberated minerals are then sent to a separation process where a concentrate is produced. If necessary, the liberated mineral stream may be returned to the mill to be reground. Reject material is discarded and the concentrate is sent to the downstream extraction process. The minerals are extracted from the concentrate to form a pure metal.

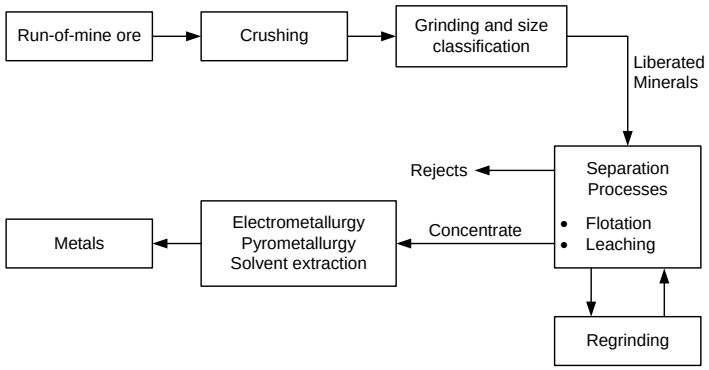

Figure 1.1: Simplified chain of processes in mineral processing and metallurgical plants, adapted from Hodouin (2011).

ROM ore milling circuits are commonly used to perform the crushing, grinding, and size classification processes in a single stage. ROM ore mills are often operated as semi-autogenous (SAG) mills with a high ball load (Powell, Morrell and Latchireddi, 2001). ROM ore milling circuits are the most energy-intensive unit process in a mineral processing plant (Wei and

Craig, 2009b).

The ROM ore milling circuit considered for this study consists of a SAG mill, a sump, and a hydrocyclone as shown in Figure 1.2. Two types of mills are commonly used for grinding, namely, ball mills and SAG mills (Wei and Craig, 2009b). Both types of mills use steel balls and ore as the grinding media, however, the ore fed to ball mills is first crushed while the ore fed to SAG mills is not. SAG mills are therefore used in milling circuits for single-stage crushing, grinding, and size classification (Craig, 2012).

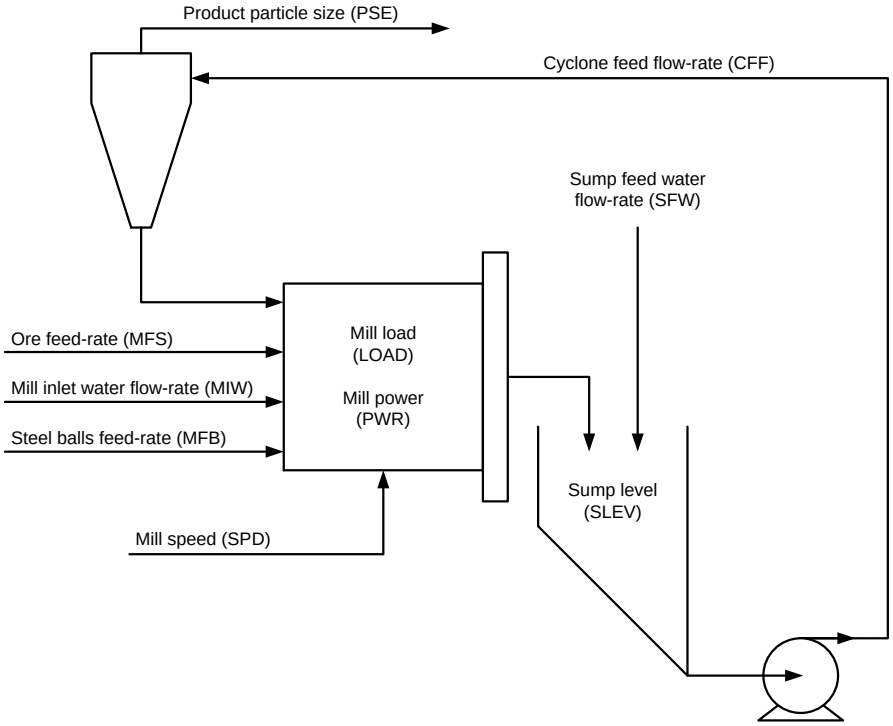

Figure 1.2: ROM ore milling circuit, adapted from Coetzee (2009).

The maximum ROM ore feed-rate to the SAG mill used in this study is approximately 100 t/h. Ore is mixed in the mill with steel balls, water, and the cyclone underflow. Within the mill, the water and ore mixture create a slurry which promotes grinding and flow through the mill. Slurry is discharged from the mill to the sump by either overflow or an end discharge grate. If an end discharge grate is used, the particles discharged from the mill are limited by the aperture of the grate.

The sump has two functions within the circuit, to maintain the density of the slurry, and act as a buffer within the circuit. Water is added to the slurry within the sump to achieve a

desired density and to facilitate transport through the circuit. Slurry is discharged from the sump to the hydrocyclone via a pump.

The hydrocyclone is used to split smaller in-specification (lighter) particles to the overflow and larger out-of-specification (heavier) particles to the underflow. In-specification particles are considered as particles smaller than 75 μm, while larger particles are considered out-of-specification. The product particle size distribution, referred to from here on as product particle size (PSE), is the percentage of particles in the overflow stream that are within specification. The underflow stream is returned to the mill for regrinding and makes up the circulating load. The overflow stream which consists predominantly of liberated minerals is sent to downstream separation processes.

Separation processes commonly used for mineral processing include flotation, leaching, and magnetic or gravimetric separation. In the case of platinum, the mineral considered in this study, flotation is generally used for separation (Craig and Koch, 2003; Wei, 2010). Recovery of platinum using flotation is a function of product particle size, illustrated in Figure 1.3.

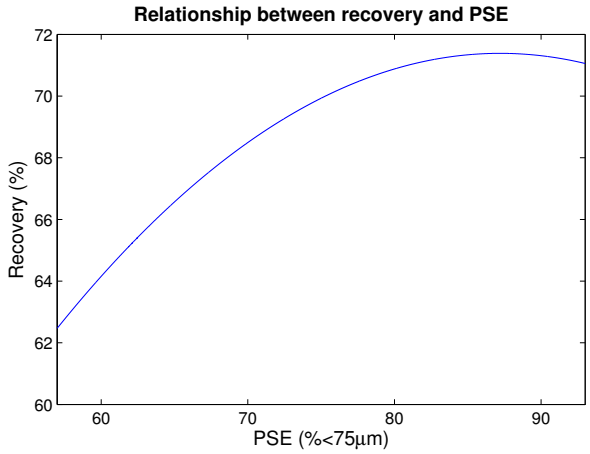

Figure 1.3: Recovery as a function of particle size, adapted from Wei (2010).

1.1 FEASIBILITY OF ROM ORE MILLING

ROM ore milling circuits were traditionally operated at maximum throughput, close to the peak power draw of the mill. This operating philosophy originates from the trade-off between low electricity costs and the high value of the milling circuit product (Craig and MacLeod,

1995; Coetzee, 2009). This is not necessarily the most feasible operating philosophy for South African ROM ore milling circuits in the future.

South Africa, where approximately 75% of the worlds platinum is produced (Jansen, 2012), has in recent years experienced rapidly increasing electricity tariffs. Electricity tariff increases result in increased operating expenses for ROM milling circuits, negatively impacting the profitability of mineral processing plants. This effect is further compounded by platinum price volatility and low platinum demand.

Reducing electricity-related operating costs through energy efficiency (EE) is one of the foremost challenges for mineral processing plants (Desbiens, Núñez, Del Villar, Hodouin and Poulin, 2008; Daniel, 2011). Two major opportunities exist for reducing the operating cost associated with the electrical power consumption of ROM ore milling circuits. Capital expenditure to retrofit high power consumption machinery with energy efficient machinery can reduce operating costs. Using process control to implement load shifting according to time-of-use (TOU) tariffs, a demand side management (DSM) instrument, presents an opportunity to reduce operating costs by reducing electricity demand during peak periods with little additional capital expenditure.

1.1.1 Electricity in South Africa

The South African electricity supply has come under stress in recent years as demand increased while capacity stagnated, resulting in decreasing reserve margins. In order to improve the reserve margin the South African electricity utility, Eskom, implemented a capacity expansion program (Eskom, 2007). Traditionally low electricity tariffs began increasing rapidly with an average annual tariff increase of 27% for the five year period 2008-2012, followed by annual increases of at least 8% for the foreseeable future (Eskom, 2012; NERSA, 2013).

In addition to the capacity expansion program a DSM program was implemented, where consumers are encouraged to reduce or manage their demand through cost-saving incentives or penalties. One of the key instruments used by Eskom for DSM is the TOU tariff structure. The tariff structure is designed to reduce peak demand through higher tariffs during peak periods and lower tariffs during standard and off-peak periods (Eskom, 2014b).

1.1.2 Demand side management

Demand side management was first introduced by Gellings and Limaye (1984) and formalized by Gellings (1985). DSM is a shift from the traditional supply-demand model to one where the consumer is given incentives to assist the electricity utility to manage their load shape. The load shape is indirectly controlled by consumers managing their demand.

DSM can be categorized into EE, TOU, demand response, and spinning reserve (Palensky and Dietrich, 2011). The categories range from long-term, permanent solutions, to short-term, temporary solutions. TOU solutions are considered as medium-term, optimized scheduling solutions. In order to take advantage of the cost-saving incentives offered through TOU tariffs, customers must shift their electrical load from peak periods to standard and off-peak periods. This process is known as load shifting (Gellings and Limaye, 1984).

The South African mining sector accounts for approximately 14% of the total electricity demand (Eskom, 2014a). Though the mining sector accounts for a large portion of the electricity demand, little has been published on the implementation of DSM, specifically load shifting, in the mineral processing sector. Load shifting in literature is typically focused on inert thermal processes, inert diffusion processes, mass transport processes, and logistics systems (Middelberg, Zhang and Xia, 2009; Zhang and Xia, 2010; Badenhorst, Zhang and Xia, 2011; van Staden, Zhang and Xia, 2011; Tang, Zheng and Zhang, 2014).

Applications of load shifting in the mining sector are limited to DSM of belt conveyor transport systems, a water pumping scheme, and a twin rock winder system for an underground mine. DSM was applied by formulating optimal switching control problems to exploit TOU tariffs (Middelberg et al., 2009; Zhang and Xia, 2010).

1.2 PROBLEM STATEMENT

In order to address the effect of increasing electricity tariffs, a decreasing platinum price, and reduced throughput on the economics of milling circuits, it was necessary to re-evaluate the control philosophy. It was hypothesized that the use of advanced control techniques to design a load shifting controller to control mill power draw according to TOU tariffs could realize operating cost savings. Process control was proposed rather than capital intensive solutions

which could include refurbishment of older more energy-intensive equipment to newer energy efficient equipment.

Operating cost savings could be realized by changing the profile over which electricity is used. Peak period electricity tariffs are up to seven times more expensive than off-peak tariffs. Therefore, taking advantage of cheaper electricity during off-peak periods by maximizing throughput while reducing throughput during peak and standard periods could offer electricity cost savings.

In order to implement the load shifting controller the revised control objectives had to meet both relevant traditional requirements as well as load shifting requirements. A load shifting controller, based on the revised control objectives, was developed to control the non-linear Hulbert milling circuit model. The load shifting controller comprises of a supervisory controller cascaded into a regulatory controller.

Linear model predictive control (MPC) was used to develop the regulatory controller, which is based on a linearization of the non-linear plant model. Regulatory control was used to satisfy control objectives which include maintaining milling circuit stability, set-point tracking, and maintaining the quality of the product by decreasing product size fluctuations.

A real-time optimizer (RTO), based on a non-linear objective function which maximizes profit associated with electricity cost and turnover of the milling circuit, was used as the supervisory controller. The supervisory controller was related to the plant model using equality constraints within the objective function. Supervisory control was used to maintain a specified average throughput over a seven day horizon while minimizing the cost of the associated power consumption.

1.2.1 Context of the problem

South Africa has in recent years experienced rapidly increasing electricity costs. As a result many energy-intensive industries have considered implementing both energy efficient technologies as well as demand side management strategies. Energy efficient technologies contribute to reducing the overall power consumption of a given plant. Demand side management strategies do not necessarily reduce the overall power consumption of a plant, but rather

change the demand characteristics of the plant.

Not only have electricity tariffs increased, but the reserve margin with which the electrical utility of South Africa operates, has decreased. The decreased reserve margin has resulted in reduced electricity security during peak periods. Demand side management has therefore been encouraged by the electricity utility in order to better control the demand curve of the utility.

Though South Africa is the worlds largest producer of platinum group metals, which is an energy-intensive process, little in the way of demand side management has been implemented in the sector. The traditional operating philosophy of the grinding process where throughput is maximized through power consumption maximization is generally still practiced (Coetzee, Craig and Kerrigan, 2010).

Decreased platinum prices compound the effect that electricity tariff increases have on the profitability of the grinding process. Lower platinum prices also tend to result in reduced output of the platinum mines which affects ore availability to milling circuits. These factors all contribute to reduced profitability of the processing of platinum.

1.2.2 Research gap

Though a few different implementations of DSM have been reported for the mining sector, DSM has not been reported as being implemented on milling circuits. RTOs have been implemented on milling circuits, however, none of the implementations reported in literature consider an economic performance function that takes the cost of electricity into account.

Control of the power consumption of a milling circuit according to electricity costs has not either been reported in literature. This work aims to show that the power consumption of a milling circuit can be manipulated according to electricity tariffs in order to increase the profitability of the milling circuit without compromising traditional control objectives that remain relevant.

1.3 RESEARCH CONTRIBUTION

This research presents a new type of controller for a milling circuit based on the Hulbert model. The load shifting controller is unique in both the regulatory as well as the supervisory controller aspects. Mill power draw is not traditionally directly controlled, which is unique to the 4×4 model predictive controller used at the regulatory control layer. Linear models of the relationship between mill speed and traditional controlled variables (CVs) as well as between mill power draw and traditional manipulated variables (MVs) are presented.

Control of mill power draw makes it possible to implement DSM on the milling circuit, which has not been reported in literature. DSM was implemented by shifting peak mill power draw to off-peak periods in the process known as load shifting. A supervisory controller, a RTO, which maximizes the profit of the milling circuit, was used to determine optimal mill power set-points for the regulatory controller.

Although economic optimization of milling circuits has been performed at the supervisory control layer, it has not been based on electricity tariffs. Economic optimization using process control to implement load shifting based on TOU tariffs has until now not been considered for a milling circuit.

Finally, some of the sensitivities applicable to the economic optimization of a milling circuit are presented. These sensitivities include sensitivity to platinum price, electricity tariffs, and milling circuit throughput. Consistent to literature it is shown that for a throughput constrained milling circuit it is not viable to implement DSM, however, for lower throughput cases it is shown to potentially reduce operating cost.

1.4 PUBLICATIONS

The following publications have resulted from this work:

- Matthews, B. and Craig, I. K. (2012). Demand side management by load shifting a run-of-mine ore milling circuit. *IFAC Automation in Mining, Mineral and Metal Processing* **2** (1): 84–89, http://dx.doi.org/10.3182/20120910-3-JP-4023.00061.

- Matthews, B. and Craig, I. K. (2013). Demand side management of a run-of-mine ore

milling circuit, *Control Engineering Practice* **21** (6): 759–768.

1.5 ORGANIZATION

Five chapters make up this dissertation. Chapter 2 presents a discussion on the literature around ROM ore milling circuit control, with a detailed description of the non-linear model used for this study. Chapter 2 also includes a discussion on the proposed control objectives for a milling circuit to operate economically with rising electricity costs.

Complete control of the ROM ore milling circuit is implemented based on both a regulatory and supervisory controller. Chapter 3 contains a discussion on the development of the regulatory MPC controller used to perform load shifting. Development of the RTO for supervisory control is discussed in Chapter 4. Integration considerations and results of the complete load shifting controller for the ROM ore milling circuit are presented and discussed in Chapter 5.

Chapter 6 contains concluding remarks as well as suggestions for further work in the field of DSM for ROM milling circuits.

CHAPTER 2

MILLING CIRCUITS

2.1 INTRODUCTION

Comminution is one of the key processes in the mineral processing chain as it is used to liberate the minerals from the ore body. ROM ore milling is usually the first and most expensive unit process in the mineral processing chain (Craig and MacLeod, 1995). Milling circuits are commonly used to perform the crushing, grinding, and classification required for mineral liberation.

Control of milling circuits has developed significantly since the 1960s, where early methods focused on classical control methods. Once milling circuits were identified as multivariable (Hulbert, Koudstaal, Braae and Gossman, 1981), investigation into multivariable control methods such as inverse Nyquist array (INA), μ-methods, and H_∞-control became more common in the literature. In the 1990s focus moved towards adaptive control with many architectures based on forms of MPC. The history of milling circuit control is further discussed in Section 2.2.

Optimization of the profitability of milling circuits was traditionally focused around maximizing throughput. This was primarily driven by high mineral price, demand, and low electricity tariffs. Traditional optimization techniques used for milling circuits are discussed in Section 2.3. According to changes in tariffs and mineral demand, traditional control objectives need to be re-examined. Updated milling control objectives based on relevant historical objectives and changing industry conditions are discussed in Section 2.4.

Adaptive control methods require a model to describe the process. Numerous phenomen-

ological models of varying complexity that describe the operation of milling circuits have been proposed in literature (e.g. Amestica, Gonzalez, Menacho and Barria, 1996; Morrison and Richardson, 2002; Morrell, 2004). The JKSimMet package, an industry-accepted tool, uses complex phenomenological models for milling circuit analysis, optimization, and design (Morrison and Richardson, 2002).

Complex models with many states are not necessarily desirable for process control owing to the increased complexity required for state estimation (Apelt, Asprey and Thornhill, 2002). Simplified process models that provide directional change information for the process variables have been shown to be effective when using feedback control (Le Roux and Craig, 2013). The Hulbert model is a reduced complexity non-linear model with five states and minimal parameters. The model was developed for the purposes of control and estimation and has been validated (Le Roux, Craig, Hulbert and Hinde, 2013). The Hulbert model was used to simulate the milling circuit process for this study and is described in Section 2.5.

2.2 HISTORY OF MILLING CIRCUIT CONTROL

Control of milling circuits has been a topic in literature since the late 1960s (Lynch and Dredge, 1969). Literature on milling circuit control has predominantly focused on three control objectives: maintain stability within the milling circuit, decrease product particle size fluctuations, and maximize milling circuit throughput (Atkins, Hinde, Lloyd and Mackay, 1974; Pauw, King, Garner and Van Aswegen, 1985; Craig and MacLeod, 1995).

A number of different milling circuit control implementations have been reported in both simulation and industrial environments. Early work on grinding circuit control focused on classical control methods. This early work was performed to determine whether classical control methods can be applied to grinding circuits for particle size distribution improvement (Atkins et al., 1974). Atkins and Hinde (1975) showed that disturbances are present in grinding circuits and that grinding circuits are not stable, which motivates the need for control.

Milling circuits were first identified as multivariable systems with significant interactions by Hulbert et al. (1981). Identification of milling circuits as multivariable promoted the development of multivariable controllers for the process. The first multivariable controllers

used for milling circuit control were designed using INA techniques (Hulbert and Woodburn, 1983; Hulbert, Craig, Coetzee and Tudor, 1990).

Hulbert et al. (1990) presented the first application where direct measurement of PSE was used to control a ROM ore milling circuit. Craig, Hulbert, Metzner and Moult (1992) expanded on this work by using steady-state optimization techniques to maximize throughput. Throughput was maximized while maintaining PSE by manipulating the mill load set-point for maximum power, i.e., power peak-seeking control. A multivariable power peak-seeking controller was also implemented on pebble milling circuits to achieve maximum throughput (Pauw et al., 1985).

Disturbances and model uncertainty are common in the control of milling circuits as ore acts as the main grinding medium (Craig and MacLeod, 1995). Model uncertainty promoted the development of a specification framework for robust multivariable control of milling circuits (Craig and MacLeod, 1995). Based on the specification framework, a robust multivariable controller was developed using μ-synthesis and -analysis methods (Craig and MacLeod, 1996). It was found that μ-methods are more powerful analysis than design tools owing to higher additional modeling costs compared to INA techniques.

H_∞ optimal control methods have been used to develop a robust milling circuit controller (Galán, Barton and Romagnoli, 2002). H_∞ control was shown to be more robust than decoupled PI control as PI controllers are susceptible to disturbances and model uncertainty. H_∞ controller synthesis was also found to be more systematic than PI controller synthesis with guarantees on stability and performance.

Constrained optimal control using Pontryagin's maximum principle for milling circuits has also been studied. Such optimal control implementations require comprehensive process models. In a two-part paper, a comprehensive model was developed, validated, and then used to develop optimal controllers (Rajamani and Herbst, 1991a; Rajamani and Herbst, 1991b). Optimal controllers were shown to achieve higher throughput than decoupled PI controllers over a wider range of operating conditions resulting from feed ore hardness disturbances. In further work by Herbst, Pate and Oblad (1992) a model was used for optimal control, estimation, and optimization.

Adaptive control has also been shown to be an applicable control strategy for milling cir-

cuit control (Najim, Hodouin and Desbiens, 1995). Adaptive control was shown to perform well for systems with strong interactions. Duarte, Sepúlveda, Castillo, Contreras, Lazcano, Giménez and Castelli (1999) performed a comparative experimental study using five different multivariable control strategies to control a copper ore milling plant. The five algorithms implemented were extended horizon, pole-placement, model reference, direct Nyquist array, and sequential loop closing algorithms. Adaptive extended horizon control was shown to perform best based on an economic analysis on recovery of copper.

Since the mid 1990s milling control literature predominantly focused on using MPC for control. An early form of MPC, dynamic matrix control (DMC), was compared to PID and learning automata control in a simulation study (Valenzuela, Bourassa, Najim and Del Villar, 1994). DMC exhibited the best performance while remaining simple to implement and tune.

Two model predictive controllers were developed using a phenomenological and black-box model of a milling circuit and tested in a simulation study (Niemi, Tian and Ylinen, 1997). The effect of dynamic interactions within the process was reduced using MPC while maintaining a simple structure as compared to multivariable control structures. Performance of MPC was shown to approach that of H_∞ control.

A number of studies have been performed where MPC was implemented on milling circuits and shown to exhibit better performance than decoupled PI(D) controllers. Ramasamy, Narayanan and Rao (2005) found MPC performed better than decoupled PI controllers with respect to interactions and robustness. Chen, Li and Fei (2008a) found that decoupled multi-loop PID controllers become sluggish owing to deteriorating process models, while MPC performs better owing to its inherent decoupling ability. Chen, Zhai, Li and Li (2007) showed that long-term stable operation of constrained MPC for an iron ore milling plant is possible.

Robust non-linear MPC of a ROM ore milling circuit was implemented by Coetzee et al. (2010) in a simulation study. Implementation issues regarding robust non-linear MPC included slow calculation times as compared to the process dynamics and the assumption of full state feedback which is not available on real plants. Practical implementation problems of MPC are also discussed in the work by Chen et al. (2008a). Problems that require considera-

tion are external disturbances, model-plant mismatch (MPM), and throughput optimization. Halldorsson, Fikar and Unbehauen (2005) have proposed methods to reduce calculation time for long prediction horizons using multi-rate MPC.

Large external disturbances and MPM in milling circuit control are common problems for most control methodologies (Chen et al., 2008a). Disturbance observers (DOBs) have been developed for milling circuit control in order to attenuate these large external disturbances. Yang, Li, Chen and Li (2010) implemented feedforward control using a DOB in combination with feedback MPC for a milling circuit. Results of the simulation study showed that the DOB improved the disturbance rejection of the control scheme. Olivier, Craig and Chen (2012) implemented two different forms of DOBs using Bode's ideal cut-off and fractional order filters for the Q-filter. The DOBs were found to attenuate disturbances as well as MPM for a milling circuit under PI control.

Improved state and parameter estimation for model-based controllers can improve milling circuit control performance (Apelt et al., 2002). State and parameter estimation has been shown to effectively identify MPM for a ROM ore milling circuit (Olivier, Huang and Craig, 2012; Olivier and Craig, 2013; Naidoo, Olivier and Craig, 2013). Once MPM is identified the process control model can be updated according to changes in the parameters identified. Methods shown to effectively identify MPM include dual particle filter estimation (Olivier, Huang and Craig, 2012), partial correlation analysis (Olivier and Craig, 2013), and a combined neural network and particle filter estimation approach (Naidoo et al., 2013).

2.3 MILL THROUGHPUT MAXIMIZATION

At steady-state conditions in a milling circuit, throughput is equivalent to the feed-rate of ore to the circuit. In a survey by Wei and Craig (2009b), approximately 80% of respondents reported that ore feed-rate to the mill is used as an MV. Throughput can therefore not be directly controlled as a CV owing to the use of ore feed-rate as an MV (Chen et al., 2008a). Control structures that use an objective function can, however, be formulated to achieve certain targets for MVs through the use of weighting functions. Choice of MV target weights present a trade-off between control objectives as increased circuit throughput generally results in a decline of PSE (Coetzee et al., 2010).

Increased throughput of a milling circuit at constant PSE will result in increased turnover owing to increased volumes produced over the same period. Throughput maximization is therefore often considered for economic optimization of milling circuits. Decreased PSE fluctuations through stabilizing control which results in reduction of ore feed-rate fluctuations has been shown to result in increased throughput (Atkins and Hinde, 1975; Valenzuela et al., 1994; Duarte et al., 1999; Chen et al., 2007). Set-point optimization is, however, the most common tool used to implement throughput maximization.

The importance of on-line set-point optimization with respect to interacting constraints applicable to milling circuits was identified in early milling circuit control literature (Cutler and Perry, 1983). Work by Pauw et al. (1985) and Craig et al. (1992) on power peak-seeking control are examples of set-point optimization to achieve maximum throughput. Power peak-seeking controllers for milling circuits were implemented to adjust the mill load set-point to achieve maximum mill power. An assumption for power peak-seeking control is that maximum throughput occurs at maximum mill power. More recently, it has been shown that maximum throughput does not occur at maximum mill power but rather at a slightly lower mill power (Powell, van der Westhuizen and Mainza, 2009).

Set-point optimization approaches which have been implemented on milling circuits include fuzzy-logic rule based optimization (Borell, Bäckström and Söderberg, 1996; Chen, Li and Fei, 2008b; Steyn, Brooks, de Villiers, Muller and Humphries, 2010) and RTO (Radhakrishnan, 1999; Lestage, Pomerleau and Hodouin, 2002). Steyn et al. (2010) implemented an additional supervisory model predictive controller within the linear operating region determined by the fuzzy-logic controller. Radhakrishnan (1999) implemented a RTO to maximize milling circuit profit using an objective function to generate a response surface. A RTO implemented by Lestage et al. (2002) was designed to achieve maximum throughput as a function of process constraints based on a steady-state model.

2.4 CONTROL OBJECTIVES

Milling circuits are inherently difficult processes to control owing to strong external disturbances, non-linearities, strong interactions, and large time delays (Craig, 2012). The primary control objective for milling circuits is stabilization (Atkins and Hinde, 1975). Secondary control objectives have also been identified for milling circuits at the supervisory or optim-

ization control layers. Secondary control objectives are generally aimed at improving the profitability of the milling circuit (Craig and MacLeod, 1995).

A common control objective addressed at the supervisory control layer is maximization of throughput while maintaining product particle size within a specified range (Craig et al., 1992; Herbst et al., 1992; Borell et al., 1996; Radhakrishnan, 1999; Lestage et al., 2002; Chen et al., 2008a; Steyn et al., 2010). Maximization of throughput directly increases the production rate of milling circuits. Simple throughput maximization will, however, not necessarily increase the turnover of a milling circuit operation. The goal of a milling circuit operation is to liberate the precious metal particles from the ore body so that downstream concentration and extraction is possible. In addition to throughput maximization it is therefore important to maintain product particle size within an acceptable range. The supervisory controller developed by Steyn et al. (2010) for example was developed with the aim of minimizing the power per fines produced ratio to improve energy efficiency of the milling circuit.

Craig and MacLeod (1995) expanded on the secondary control objectives by considering the broader economics of milling circuits. Secondary control objectives were given as

1. improve the quality of the product by
   (a) increasing the fineness of grind, and
   (b) decreasing product size fluctuations,
2. maximize throughput,
3. minimize the steel consumed per ton of fines produced,
4. minimize the power consumed per ton of fines produced.

These control objectives are not all complementary and certain trade-offs are necessary. A trade-off between fineness of grind and milling circuit throughput relates to the objective to maximize throughput while maintaining a certain product particle size. It is important that PSE is as fine as economically possible as recovery in the downstream separation process is dependent on PSE (see Figure 1.3). To minimize losses Craig et al. (1992) show that it is also important to minimize deviations in PSE.

Minimization of power consumed per ton of fines produced is often not considered as a control objective. Traditionally throughput is maximized rather than minimizing power consumption owing to the high value of the milling circuit product as compared to the low cost of electricity, specifically in South Africa (Craig and MacLeod, 1995; Coetzee, 2009). Optimization of mill power draw is therefore not considered as maximum throughput generally occurs when mill power is close to its maximum (Powell et al., 2009).

High electricity tariff increases and lower platinum prices suggest that the trade-off between power consumption and throughput may no longer be a valid trade-off. In addition the trade-off assumes that there is more ore available than the throughput capacity of the milling circuit, i.e. the milling circuit is throughput constrained. When this is not the case the trade-off between power consumption and throughput also needs to be reconsidered.

Revised secondary control objectives to implement a load shifting controller on a milling circuit were formulated as follows

1. maintain the quality of the product by decreasing product size fluctuations,

2. maintain a specified average throughput over a seven day horizon, and

3. minimize the costs associated with power consumption.

Specified average throughput is considered to be the average ore output of the mining operation, relating to the availability of ore to be ground. Average throughput is considered over a seven day horizon to account for the weekly TOU electricity tariff structure in South Africa. Minimization of ball consumption is not considered a secondary control objective as it was a constant input and not used as an MV.

2.5 HULBERT MILLING CIRCUIT MODEL

The Hulbert model consists of four modules, the feeder, mill, sump, and hydrocyclone modules. The structure is such that arbitrary circuit configurations may be designed using different combinations of the modules (Coetzee, 2009). Five states, fines, rocks, solids, steel balls, and water are used to describe the constituents of the milling circuit. Rocks are defined as ore that is too large to pass through the end discharge grate of the mill. Solids are defined

as coarse and fine ore. Coarse ore is defined as ore that can discharge from the mill but is out-of-specification, thus larger than 75 μm. Fines, or fine ore, is defined as ore that is in-specification and thus smaller than 75 μm.

The milling circuit configuration used for this study with the volumetric flow-rates around the circuit is given in Figure 2.1. Subscripts used to distinguish between the different states and flow-rates are defined in Table 2.1. Model parameters are given in Table 2.2 with states, inputs, and outputs in Table 2.3.

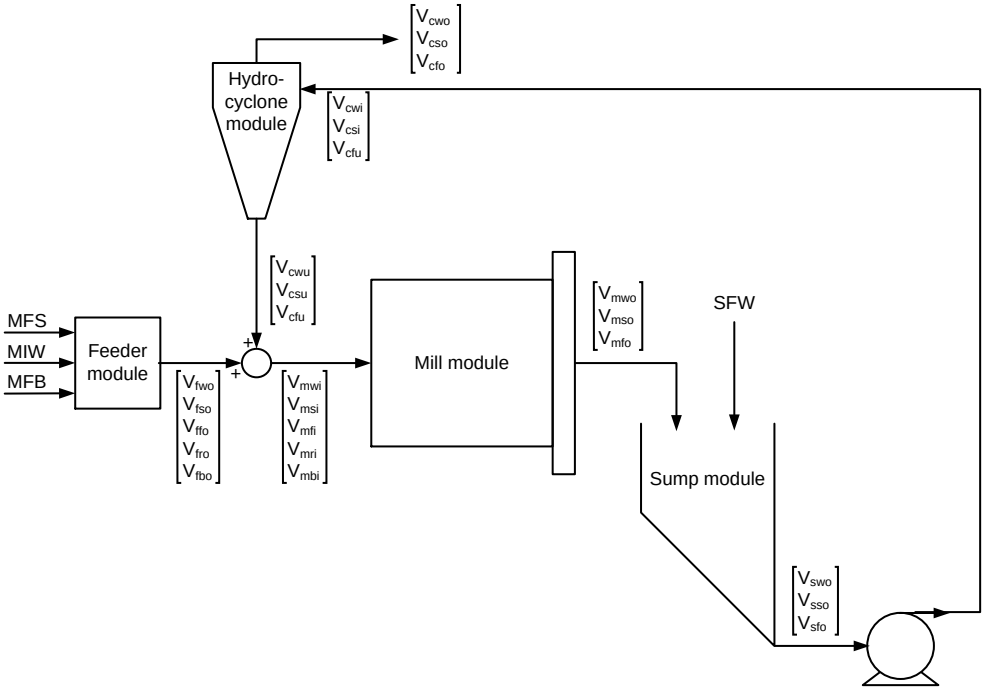

Figure 2.1: Volumetric flow-rates around the ROM ore milling circuit model.

Table 2.1: Subscripts used for states and volumetric flow-rates.

Subscript	Description
$V_{\Delta--}$ or $X_{\Delta-}$	c-cyclone, f-feeder, m-mill, s-sump
$V_{-\Delta-}$ or $X_{-\Delta}$	b-balls, c-coarse, f-fines, r-rocks, s-solids, w-water
$V_{-\Delta}$	i-inflow, o-outflow, u-underflow

Table 2.2: Mill model parameters.

Parameter	Nom	Description
α_f	0.1	Fraction of fines in the ore. [dimensionless]
α_r	0.1	Fraction of rock in the ore. [dimensionless]
D_s	3.2	Density of feed ore. [kg/m^3]
D_b	7.85	Density of steel balls. [kg/m^3]
ϕ_f	28	Power per fines produced. [kWh/t]
ϕ_r	69	Rock abrasion factor. [kWh/t]
ϕ_b	94	Steel abrasion factor. [kWh/t]
P_{max}	2000	Maximum mill motor power. [kW]
v_{mill}	100	Mill volume [m^3]
$v_{P_{max}}$	0.45	Fraction of mill volume filled for maximum power. [dimensionless]
$\varphi_{P_{\max}}$	0.51	Rheology factor for maximum mill power. [dimensionless]
ε_{ws}	0.6	Maximum water-to-solids volumetric ratio at zero slurry flow. [dimensionless]
V_V	40	Volumetric flow per "flowing volume" driving force. [1/h]
δ_{P_v}	1	Power-change parameter for volume. [dimensionless]
δ_{P_s}	1	Power-change parameter for fraction solids. [dimensionless]
α_P	0.82	Fraction power reduction per fractional reduction from maximum mill speed. [dimensionless]
α_{ϕ_f}	0.01	Fractional change in kW/fines produced per change in fractional filling of mill. [dimensionless]
χ_P	0	Cross-term for maximum power. [dimensionless]
ε_C	184	Cyclone coarse split fraction. [dimensionless]
α_{su}	0.16	Fraction of solids in the underflow of the cyclone. [dimensionless]
C_1	0.6	Cyclone constant. [dimensionless]
C_2	0.7	Cyclone constant. [dimensionless]
C_3	3	Cyclone constant. [dimensionless]
C_4	3	Cyclone constant. [dimensionless]

Table 2.3: Model states, inputs, and outputs.

Variable	Description
	States
X_{mb}	Holdup of balls in the mill. [m^3]
X_{mf}	Holdup of fine ore in the mill. [m^3]
X_{mr}	Holdup of rock in the mill. [m^3]
X_{ms}	Holdup of solids in the mill (coarse and fine ore). [m^3]
X_{mw}	Holdup of water in the mill. [m^3]
X_{sf}	Holdup of fine ore in the sump. [m^3]
X_{ss}	Holdup of solids in the sump (coarse and fine ore). [m^3]
X_{sw}	Holdup of water in the sump. [m^3]
	Inputs
CFF	Flow-rate of slurry from the sump to the cyclone. [m^3/h]
MFB	Feed-rate of balls to the mill. [t/h]
MFS	Feed-rate of solids to the mill (rocks, coarse, and fine ore). [t/h]
MIW	Flow-rate of water to the mill. [m^3/h]
SFW	Flow-rate of water to the sump. [m^3/h]
SPD	Fraction of mill speed for maximum power. [dimensionless]
	Outputs
PSE	Product particle size. [$\% < 75\mu m$]
LOAD	Fraction of mill filled. [dimensionless]
SLEV	Level of the sump. [m^3]
PWR	Power draw of the mill motor. [kW]
TPT	Throughput (course and fine ore). [t/h]
φ	Rheology factor. [dimensionless]

2.5.1 Feeder module

The feeder module is a simple model that takes the feed-rate of ore to the mill and divides it into the ore streams used within the milling circuit (rocks, solids, and fines). The module also converts the feed-rates to volumetric flow-rates which are used throughout the milling circuit. More complex models for real feeders such as vibratory feeders can be used in place of the simple feeder module.

Volumetric outflow-rates of the feeder module are given by

$$V_{fwo} \triangleq MIW, \tag{2.1}$$

$$V_{fso} \triangleq (1-\alpha_r)\cdot\frac{MFS}{D_s}, \tag{2.2}$$

$$V_{ffo} \triangleq \alpha_f\cdot\frac{MFS}{D_s}, \tag{2.3}$$

$$V_{fro} \triangleq \alpha_r\cdot\frac{MFS}{D_s}, \tag{2.4}$$

$$V_{fbo} \triangleq \frac{MFB}{D_b}. \tag{2.5}$$

2.5.2 Mill module

The mill module was developed with the capability of modeling rod, ball, autogenous, or SAG mills. The mill model is similar to other models found in literature but adds the effect of power and slurry rheology to the breakage functions. Volumetric flow-rates entering the mill are related to flow-rates from the feeder module and underflow-rates from the hydrocyclone module by

$$\begin{bmatrix} V_{mwi} \\ V_{msi} \\ V_{mfi} \\ V_{mri} \\ V_{mbi} \end{bmatrix} = \begin{bmatrix} V_{fwo}+V_{cwu} \\ V_{fso}+V_{ccu}+V_{cfu} \\ V_{ffo}+V_{cfu} \\ V_{fro} \\ V_{fbo} \end{bmatrix}. \tag{2.6}$$

Five states related to the holdup within the mill are considered. These states are holdup of water (X_{mw}), holdup of solids (X_{ms}), holdup of fines (X_{mf}), holdup of rock (X_{mr}), and holdup of steel balls (X_{mb}). Mill load is considered as the total holdup within the mill as a

ratio of mill volume, given by

$$LOAD \triangleq \frac{X_{mw} + X_{ms} + X_{mr} + X_{mb}}{v_{\text{mill}}}. \tag{2.7}$$

A rheology factor relates the effect slurry fluidity and density have on the performance of the mill (Shi and Napier-Munn, 2002). The rheology factor is lowest when the ratio X_{ms}/X_{mw} approaches 1.5, and highest when X_{ms}/X_{mw} approaches 0. Rheology factor is defined as

$$\varphi \triangleq \left(\frac{\max\left[0, \left(X_{mw} - \left(\frac{1}{\varepsilon_{ws}} - 1\right) \cdot X_{ms}\right)\right]}{X_{mw}} \right)^{0.5}. \tag{2.8}$$

The effect of slurry rheology on power consumption is given by

$$Z_r = \frac{\varphi}{\varphi_{P_{\max}}} - 1, \tag{2.9}$$

and the effect of mill load on power consumption is given by

$$Z_x = \frac{LOAD}{v_{P_{\max}}} - 1. \tag{2.10}$$

The effect of slurry rheology on mill power is lowest when φ approaches the optimal rheology factor ($\varphi_{P_{\max}}$). The effect of mill load is lowest when the fraction of the mill filled ($LOAD$) approaches the optimal mill filling ($v_{P_{\max}}$). Mill power consumption is given by

$$PWR = P_{\max} \cdot \left[1 - \delta_{P_v} \cdot Z_x^2 - 2 \cdot \chi_P \cdot \delta_{P_v} \cdot \delta_{P_s} \cdot Z_x \cdot Z_r - \delta_{P_s} \cdot Z_r^2\right] \cdot SPD^{\alpha_P}. \tag{2.11}$$

Production of fines from rock and coarse ore are not independently considered. Production of fines within the mill is characterized by

$$FP \triangleq \frac{PWR}{D_s \cdot \phi_f \left[1 + \alpha_{\phi_f} \left(LOAD - v_{P_{\max}}\right)\right]}. \tag{2.12}$$

Coarse and fine ore are broken into indeterminable ratios from rock. Rock consumption is considered rather than yield of coarse and fine ore from rock. Rock consumption is given by

$$RC \triangleq \frac{1}{D_s \cdot \phi_r} \cdot PWR \cdot \varphi \cdot \left(\frac{X_{mr}}{X_{mr} + X_{ms}}\right). \tag{2.13}$$

Steel balls are used to facilitate grinding within the mill. Over time the steel balls are ground away and therefore steel ball consumption is considered. Ball consumption is given by

$$BC \triangleq \frac{1}{D_b \cdot \phi_b} \cdot PWR \cdot \varphi \cdot \left(\frac{X_{mr}}{X_{mr} + X_{ms}} \right). \tag{2.14}$$

Fines production, rock consumption, and ball consumption are highest when mill power is maximized.

Changes to the holdups within the mill are given by

$$\frac{dX_{mw}}{dt} \triangleq V_{mwi} - V_{mwo}, \tag{2.15}$$
$$\frac{dX_{ms}}{dt} \triangleq V_{msi} - V_{mso} + RC, \tag{2.16}$$
$$\frac{dX_{mf}}{dt} \triangleq V_{mfi} - V_{mfo} + FP, \tag{2.17}$$
$$\frac{dX_{mr}}{dt} \triangleq V_{mri} - RC, \tag{2.18}$$
$$\frac{dX_{mb}}{dt} \triangleq V_{mbi} - BC. \tag{2.19}$$

Volumetric outflow-rates from the mill are given by

$$V_{mwo} \triangleq V_V \cdot \varphi \cdot X_{mw} \cdot \left(\frac{X_{mw}}{X_{mw} + X_{ms}} \right), \tag{2.20}$$
$$V_{mso} \triangleq V_V \cdot \varphi \cdot X_{ms} \cdot \left(\frac{X_{mw}}{X_{mw} + X_{ms}} \right), \tag{2.21}$$
$$V_{mfo} \triangleq V_V \cdot \varphi \cdot X_{mf} \cdot \left(\frac{X_{mw}}{X_{mw} + X_{ms}} \right). \tag{2.22}$$

Rocks and steel balls are considered larger than the end discharge grate aperture and therefore cannot leave the mill. Rock and ball flow-rates from the mill are therefore zero ($V_{mro} = V_{mbo} \triangleq 0$).

2.5.3 Mixed-sump module

The mixed-sump, or sump, module is modeled based on the assumption that all constituents are fully mixed. Only three of the five states are considered in the model as rocks and steel balls cannot enter the sump owing to the end discharge grate on the mill. Volumetric flow-rates entering the sump are related to mill outflow-rates by

$$\begin{bmatrix} V_{swi} & V_{ssi} & V_{sfi} \end{bmatrix}^{\mathrm{T}} = \begin{bmatrix} V_{mwo} & V_{mso} & V_{mfo} \end{bmatrix}^{\mathrm{T}}. \tag{2.23}$$

Changes to the holdups within the sump module are given by

$$\frac{dX_{sw}}{dt} \triangleq V_{swi} + SFW - V_{swo}, \tag{2.24}$$

$$\frac{dX_{ss}}{dt} \triangleq V_{ssi} - V_{sso}, \tag{2.25}$$

$$\frac{dX_{sf}}{dt} \triangleq V_{sfi} - V_{sfi}. \tag{2.26}$$

Sump level is defined as

$$SLEV \triangleq X_{sw} + X_{ss}. \tag{2.27}$$

Cyclone feed density is defined as

$$CFD \triangleq X_{sw} + D_s \cdot \left(\frac{X_{ss}}{X_{ss} + X_{sw}} \right). \tag{2.28}$$

Volumetric outflow-rates from the mixed-sump module are given by

$$V_{swo} \triangleq CFF \cdot \left(\frac{X_{sw}}{X_{ss} + X_{sw}} \right), \tag{2.29}$$

$$V_{sso} \triangleq CFF \cdot \left(\frac{X_{ss}}{X_{ss} + X_{sw}} \right), \tag{2.30}$$

$$V_{sfo} \triangleq CFF \cdot \left(\frac{X_{sf}}{X_{ss} + X_{sw}} \right). \tag{2.31}$$

2.5.4 Hydrocyclone module

The hydrocyclone is a classification device that splits a slurry feed based on weight. Lighter particles are sent via the cyclone overflow to downstream processes, while heavier particles are sent via the cyclone underflow back to the mill for regrinding. The hydrocyclone, or cyclone, module models particle size and density by accounting for the effect of angular velocity of the particle within the cyclone, the slurry density and viscosity. The model is based on the empirical cyclone models of Nageswararao, Wiseman and Napier-Munn (2004). Volumetric flow-rates into the cyclone are related to outflow-rates of the sump by

$$\begin{bmatrix} V_{cwi} & V_{cci} & V_{cfi} \end{bmatrix}^{\mathrm{T}} = \begin{bmatrix} V_{swo} & V_{sso} - V_{sfo} & V_{sfo} \end{bmatrix}^{\mathrm{T}}. \tag{2.32}$$

Cyclone volumetric underflow-rates are calculated by

$$V_{ccu} \triangleq V_{cci} \cdot \left(1 - C_1 \cdot e^{-CFF/\varepsilon_C}\right) \cdot \left(1 - \left[\frac{F_i}{C_3}\right]^{C_4}\right) \cdot \left(1 - P_i^{C_5}\right), \tag{2.33}$$

$$V_{cwu} \triangleq V_{cwi} \cdot \left(\frac{V_{ccu} - F_u \cdot V_{ccu}}{F_u \cdot V_{cwi} + F_u \cdot V_{cfi} - V_{cfi}}\right), \tag{2.34}$$

$$V_{cfu} \triangleq V_{cfi} \cdot \left(\frac{V_{ccu} - F_u \cdot V_{ccu}}{F_u \cdot V_{cwi} + F_u \cdot V_{cfi} - V_{cfi}}\right), \tag{2.35}$$

where

$$F_u \triangleq 0.6 - (0.6 - F_i) \cdot e^{-V_{ccu}/\alpha_{su}\varepsilon_C}, \tag{2.36}$$

$$F_i \triangleq \frac{V_{csi}}{V_{cwi} + V_{csi}}, \tag{2.37}$$

$$P_i \triangleq \frac{V_{cfi}}{V_{csi}}. \tag{2.38}$$

Volumetric overflow-rates are given by

$$V_{cwo} \triangleq V_{cwi} - V_{cwu}, \tag{2.39}$$

$$V_{cfo} \triangleq V_{cfi} - V_{cfu}, \tag{2.40}$$

$$V_{cco} \triangleq V_{cci} - V_{ccu}. \tag{2.41}$$

Product particle size is defined as

$$PSE \triangleq \frac{V_{cfo}}{V_{cco} + V_{cfo}}. \tag{2.42}$$

Product throughput of the milling circuit is given by

$$TPT \triangleq V_{cco} + V_{cfo}. \tag{2.43}$$

2.6 CONCLUSION

Economic optimization based on electricity cost minimization of milling circuits has not appeared in open literature as far as can be ascertained. High electricity tariffs have become significant to the point where alternative control philosophies should be investigated. In order to perform such an investigation, control objectives for a load shifting controller were formulated as follows

1. maintain stability of the milling circuit

2. maintain the quality of the product by decreasing product size fluctuations,

3. maintain a specified average throughput over a seven day horizon, and

4. minimize the costs associated with power consumption.

These control objectives form the basis of the load shifting controller developed to investigate the potential for cost savings through milling circuit load shifting. In order to evaluate the potential efficacy of the load shifting controller the non-linear Hulbert milling circuit model was used as the process model for this simulation study.

CHAPTER 3

REGULATORY CONTROLLER

3.1 INTRODUCTION

In order to perform power load shifting on a milling circuit it is necessary to control mill power draw. Traditionally mill power draw was not controlled for ROM ore milling circuits. Therefore, a controller had to be developed to control traditional CVs of the milling circuit as well as mill power draw according to set-points derived by a supervisory controller. The regulatory controller is independently considered in this chapter.

The first design choice in developing a controller for the non-linear milling circuit model was to choose a control structure. The control structure had to be multivariable as the plant exhibits strong interactions (Hulbert et al., 1981). Additional characteristics of ROM ore milling circuits that have an impact on the choice of controller include large time delays, time varying characteristics, non-linearities, and constraints on MVs and CVs (Coetzee, 2009). Ore acts as one of the main grinding mediums in a ROM ore milling circuit and it is therefore also important that the controller accounts for uncertainty (Craig and MacLeod, 1995).

It has been shown that model-based optimal controllers exhibit better control performance compared to decoupled PI(D) controllers (Herbst et al., 1992). Based on the requirements for the multivariable controller, a model predictive controller was chosen to control the milling circuit. MPC exhibits a number of desirable characteristics with respect to milling circuit control (Muller and De Vaal, 2000; Chen et al., 2007). A number of characteristics of MPC that motivate its use for milling circuit control are given below.

- Constrained MPC effectively handles interacting multivariable systems through its co-

ordinated approach (Ramasamy et al., 2005).

- MPC can effectively predict the future states of a system with large time delays (Chen et al., 2008a).
- Compared to other multivariable control structures MPC offers similar performance with simpler design (Niemi et al., 1997).
- The structure of MPC is such that constraints can easily be implemented (Chen et al., 2007).
- MPC has been shown to outperform decoupled PI controllers with respect to decoupling and robustness (Ramasamy et al., 2005).

Based on the above-mentioned characteristics, MPC was used to control the ROM ore milling circuit. Although recent research has focused on using different forms of MPC to control milling circuits, it is not the dominant control structure used in the mineral processing industry. In a recent survey by Wei and Craig (2009b), 63% of respondents reported that decoupled PI control is used, while only 7% reported the use of MPC.

Coetzee (2009) used non-linear MPC to implement robust control of a milling circuit. Non-linear MPC was shown to be effective for the control of a milling circuit in the presence of large disturbances. Though non-linear MPC was shown to be effective, implementation issues were identified. The main implementation issue was the long calculation time for a short prediction and control horizon.

Linear MPC was used to provide stabilizing control and implement mill power draw control for the non-linear milling circuit in order to perform load shifting. Decoupled PI control could be used to implement stabilizing control, however, the different operating points at which the milling circuit must operate to implement load shifting present MPM limitations. The state estimator used in the MPC structure provides a degree of inherent MPM correction.

Though linear MPC inherently provides disturbance rejection through the state estimator, it may be susceptible to large disturbances (Yang et al., 2010). If such large disturbances are experienced for a particular plant DOBs may be implemented. Additional disturbance rejection has the potential to improve the performance of the linear controller (Olivier, Craig

and Chen, 2012; Olivier, Huang and Craig, 2012; Olivier and Craig, 2013; Naidoo et al., 2013).

In order for a control strategy to fall into the MPC class three criteria must be met (Camacho and Bordons, 2004)

- a *mathematical model* is used to predict the outputs at future time instances,
- an *objective function* is minimized by calculating the optimal control sequence, and
- a *receding horizon* strategy is used by moving the horizon a step forward at each time step.

This chapter will address the above three points, concluding with simulation results of the regulatory controller and a synthesis thereof.

3.2 CONTROLLED AND MANIPULATED VARIABLES

In the survey by Wei and Craig (2009b), respondents were asked to indicate the controlled and manipulated variables used for the control of their milling circuits. Most commonly used CVs, in order, are sump level, product particle size, sump discharge slurry density, feed ratio, and mill load. Most commonly used MVs, in order, are flow-rate of water to the sump, flow-rate of water to the mill, feed-rate of solids to the mill, and flow-rate of slurry to the cyclone.

CVs used in this study are product particle size (PSE), sump level (SLEV), mill load (LOAD), and mill power draw (PWR). PSE is controlled as it is a measure of the quality of the product produced by the milling circuit. Economic turnover of the milling circuit can be related to the product particle size by

$$Turnover \propto Product\ particle\ size \times Throughput. \tag{3.1}$$

Throughput is not directly controlled in milling circuits as under steady-state conditions the milling circuit throughput rate is equivalent to the feed-rate of solids to the mill. Feed-rate of solids to the mill is used as an MV and throughput therefore cannot be controlled. Control of throughput will be further discussed in conjunction with MV weight tuning in

Section 3.4.2.

SLEV is controlled to maintain milling circuit stability as it exhibits open loop unstable characteristics (Atkins et al., 1974). If SLEV is not controlled the sump tends to either run dry or overflow. The sump is used within the milling circuit as a buffer and tight control of the sump level is therefore not necessary. If the sump runs dry the sump discharge pump will cavitate. If the sump overflows valuable minerals within the slurry may be lost.

LOAD is controlled as it has an effect on the mill power draw as indicated in equations (2.10) and (2.11). This is illustrated by the mill power versus mill load grind curves developed by Powell et al. (2009). Mill power has a parabolic relationship to mill load as illustrated in Figure 3.1.

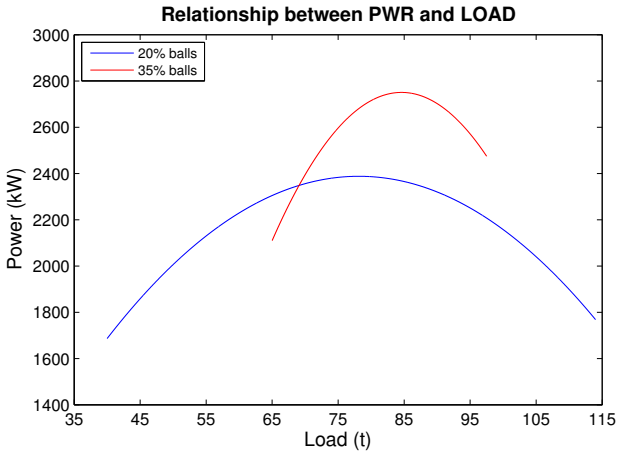

Figure 3.1: Power-load curve, adapted from Powell et al. (2009).

Finally, PWR is controlled so that power load shifting can be achieved. It is important to note that PWR is not an independent output of the milling circuit and other outputs, such as LOAD, have an effect on mill power draw. These interdependencies are accounted for in the weight selection for the controller. Depending on the relative importance of the CVs the controller can be tuned to control one more tightly than another through weight selection.

In order to attain functional controllability it is necessary to use at least four MVs to control the four chosen CVs (Skogestad and Postlethwaite, 2006). Based on the Hulbert model there are six variables available to be used as MVs. The four MVs used for this study are flow-rate of slurry from the sump to the cyclone (CFF), feed-rate of solids to the mill (MFS), flow-rate

of water to the sump (SFW), and fraction of mill speed for maximum power (SPD). Flow-rate of water to the mill (MIW) and feed-rate of balls to the mill (MFB) are not used as MVs.

MIW is not used as an MV as in order to maintain a relatively constant solids-to-water ratio within the mill it is ratio controlled based on the feed-rate of solids to the mill. MFB is generally not used as a manipulated variable as reported in the survey by Wei and Craig (2009b). MFB is therefore simulated as a constant input at the nominal feed-rate.

CFF, MFS, and SFW were chosen as manipulated variables as they are traditionally used for the output-input pairings to control PSE, LOAD, and SLEV. These output-input pairings were made between PSE and SFW, LOAD and MFS, and SLEV and CFF (Napier-Munn and Wills, 2006; Chen et al., 2007). Traditionally PWR is not directly controlled, however in order to develop a load shifting controller it is necessary to have direct control over PWR.

The fraction of mill speed for maximum power draw was chosen as an MV primarily to control PWR. Based on the mill power model (see Section 2.5.2), PWR is dependent on the effect of the mill load, slurry rheology, and mill speed. Mill power draw can be approximated to

$$PWR = P_{\max} \cdot \left[1 - \left(\frac{LOAD}{v_{P_{\max}}} - 1\right)^2 - \left(\frac{\varphi}{\varphi_{P_{\max}}} - 1\right)^2\right] \cdot SPD^{\alpha_P}. \tag{3.2}$$

In order to change PWR it is therefore necessary to manipulate LOAD, φ, or SPD as $v_{P_{\max}}$, $\varphi_{P_{\max}}$, and α_P are constant parameters. LOAD cannot be effectively used as an MV as it is used as one of the CVs. Additionally the percentage of the mill filled is constrained between 30% and 50%. Z_x is therefore effectively constrained between 0 and 0.1111, which means that the mill holdup can at most reduce mill power draw by 11.11%.

The slurry rheology factor, φ, also cannot be used to control the mill power draw as it cannot be manipulated owing to ratio control of MIW. Ratio control of MIW results in a relatively constant solids-to-water ratio which means that the slurry rheology will not significantly change within the mill with minimal influence on PWR.

The only variable that can therefore be used to effectively manipulate the mill power draw is the fraction of mill speed for maximum power draw. SPD is constrained between 70% and 100%. Based on the fraction of power reduction per fractional reduction from maximum mill

speed, PWR can therefore be reduced by up to 37.26% by manipulating SPD. In order to use SPD as an MV, it is necessary to have some form of variable speed control. Respondents in a recent survey reported that 90% of them used an electric motor as an actuator for mill speed.

The operating point of the milling circuit for the CVs, MVs, and states is presented in Table 3.1. In addition to the operating point, constraints and weights are presented in the table. Constraints will be further discussed in Section 3.4.1 and weights in Section 3.4.2.

3.3 LINEAR PLANT MODELING

The plant to be controlled for this simulation study was the non-linear model of a milling circuit as described in Section 2.5. In order to use linear MPC, it was necessary to develop a linear model based on the non-linear model. The linear plant model is given by

$$\Delta\mathbf{Y}(s) = \mathbf{G}(s)\Delta\mathbf{U}(s), \tag{3.3}$$

where

$$\Delta\mathbf{Y}(s) = \begin{bmatrix} \Delta PSE(s) \\ \Delta LOAD(s) \\ \Delta SLEV(s) \\ \Delta PWR(s) \end{bmatrix}, \tag{3.4}$$

$$\Delta\mathbf{U}(s) = \begin{bmatrix} \Delta CFF(s) \\ \Delta MFS(s) \\ \Delta SFW(s) \\ \Delta SPD(s) \end{bmatrix}, \tag{3.5}$$

and

$$\mathbf{G}(s) = \begin{bmatrix} G_{11}(s) & G_{12}(s) & G_{13}(s) & G_{14}(s) \\ G_{21}(s) & G_{22}(s) & G_{23}(s) & G_{24}(s) \\ G_{31}(s) & G_{32}(s) & G_{33}(s) & G_{34}(s) \\ G_{41}(s) & G_{42}(s) & G_{43}(s) & G_{44}(s) \end{bmatrix}. \tag{3.6}$$

The model was developed based on the non-linear Hulbert model with the parameters given in Table 2.2. System identification (SID) based on random step perturbations to the MVs was used to identify the model. MV perturbations were applied to the non-linear model around the

Table 3.1: Milling circuit operating point, constraints, and weights.

Variable	Min	Max	OP	W	Description
			States		
X_{mb}	0	20	6.22	–	Holdup of balls in the mill. [m^3]
X_{mf}	0	50	3.24	–	Holdup of fine ore in the mill. [m^3]
X_{mr}	0	50	16.98	–	Holdup of rock in the mill. [m^3]
X_{ms}	0	50	8.78	–	Holdup of ore in the mill (coarse and fine ore). [m^3]
X_{mw}	0	50	8.01	–	Holdup of water in the mill. [m^3]
X_{sf}	0	30	1.26	–	Holdup of fine ore in the sump. [m^3]
X_{ss}	0	30	3.43	–	Holdup of ore in the sump (coarse and fine ore). [m^3]
X_{sw}	0	30	15.14	–	Holdup of water in the sump. [m^3]
			Controlled variables		
LOAD	30	50	40.0	10	Percentage of the mill filled. [%]
PSE	60	90	82.0	200	Product particle size. [% $< 75\mu$m]
PWR	1550	2000	1855	200	Power draw of the mill motor. [kW]
SLEV	2	38	18.6	10	Level of the sump. [m^3]
TPT	0	200	92.0	–	Throughput (course and fine ore). [t/h]
			Manipulated variables		
CFF	400	500	470.4	0.001	Flow-rate of slurry from the sump to the cyclone. [m^3/h]
MFB	0	4	2	–	Feed-rate of balls to the mill. [t/h]
MFS	0	200	92.0	0.004	Feed-rate of ore to the circuit. [t/h]
MIW	0	100	30.7	–	Flow-rate of water to the mill. [m^3/h]
SFW	0	400	304.3	0.001	Flow-rate of water to the sump. [m^3/h]
SPD	70	100	92.7	1	Percentage of mill speed for maximum power. [%]

operating point given in Table 3.1. The linear model was identified and validated using black-box modeling with the System Identification Toolbox in MATLAB (Ljung, 1988; Ljung, 1999). Changes were applied to only one MV at a time in order to isolate the effect of that MV on the relevant CVs. Time constants of the linear model are given in hours.

3.3.1 Product particle size

3.3.1.1 PSE-CFF

PSE exhibited a time delayed first-order response to a change in CFF. In order to improve the model fit, a zero was added to the model form. The linear model was fitted to the step response data (see Figure 3.2) to give the following transfer function

$$G_{11}(s) = \frac{-8.386 \times 10^{-3}(1 - 2.259s)}{(1 + 0.513s)} e^{-0.011s}. \tag{3.7}$$

3.3.1.2 PSE-MFS

PSE exhibited a time delayed first-order response to a change in MFS. The linear model was fitted to the step response data (see Figure 3.2) to give the following transfer function

$$G_{12}(s) = \frac{-9.440 \times 10^{-2}}{(1 + 0.472s)} e^{-0.014s}. \tag{3.8}$$

3.3.1.3 PSE-SFW

PSE exhibited a first-order response to a change in SFW. The linear model was fitted to the step response data (see Figure 3.2) to give the following transfer function

$$G_{13}(s) = \frac{4.699 \times 10^{-2}}{(1 + 0.363s)}. \tag{3.9}$$

3.3.1.4 PSE-SPD

PSE exhibited a time delayed second-order response to a change in SPD. In order to improve the linear model fit, a zero was included to the model form. The linear model was fitted to the step response data (see Figure 3.2) to give the following transfer function

$$G_{14}(s) = \frac{9.127 \times 10^{-2}(1 + 9.723s)}{(1 + 7.078s)(1 + 0.596s)} e^{-0.014s}. \tag{3.10}$$

3.3.2 Mill load

3.3.2.1 LOAD-CFF

LOAD exhibited a time delayed second-order response to a change in CFF. In order to improve the linear model fit, a zero was included in the model form. The linear model was fitted to the step response data (see Figure 3.3) to give the following transfer function

$$G_{21}(s) = \frac{0.353(1 + 4.000s)}{(1 + 10.114s)(1 + 0.599s)} e^{-0.014s}. \tag{3.11}$$

3.3.2.2 LOAD-MFS

LOAD exhibited a second-order response to a change in MFS. In order to improve the linear model fit, a zero was included in the model form. The linear model was fitted to the step response data (see Figure 3.3) to give the following transfer function

$$G_{22}(s) = \frac{1.286(1 + 2.379s)}{(1 + 8.707s)(1 + 0.498s)}. \tag{3.12}$$

3.3.2.3 LOAD-SFW

LOAD exhibited a time delayed second-order response to a change in SFW. In order to improve the linear model fit, a zero was included in the model form. The linear model was fitted to the step response data (see Figure 3.3) to give the following transfer function

$$G_{23}(s) = \frac{-0.385(1 + 4.583s)}{(1 + 14.179s)(1 + 0.621s)} e^{-0.014s}. \tag{3.13}$$

3.3.2.4 LOAD-SPD

LOAD exhibited a time delayed second-order response to a change in SPD. In order to improve the linear model fit, a zero was included in the model form. The linear model was fitted to the step response data (see Figure 3.3) to give the following transfer function

$$G_{24}(s) = \frac{-1.054(1 + 3.600s)}{(1 + 11.155s)(1 + 0.967s)} e^{-0.064s}. \tag{3.14}$$

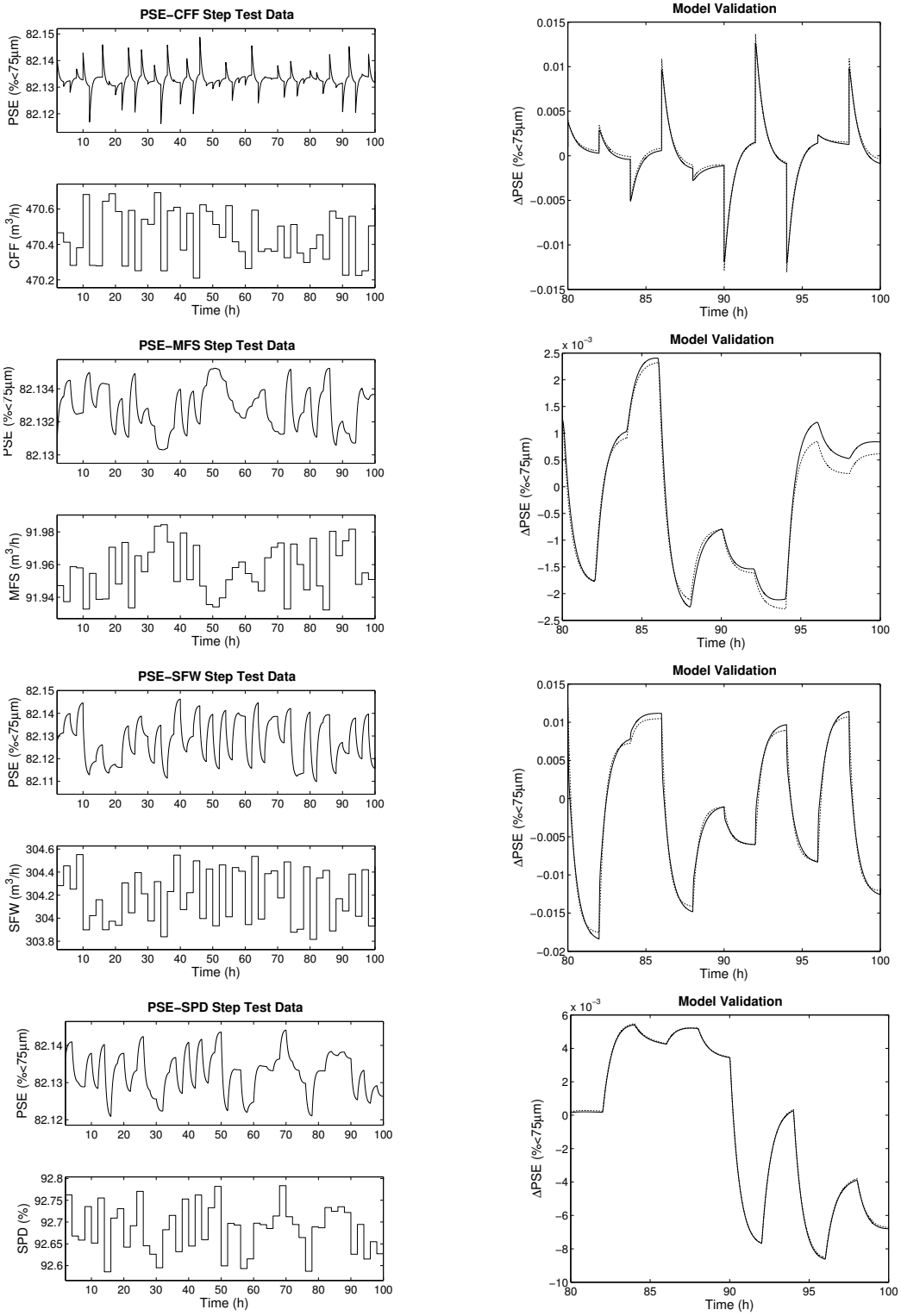

(a) PSE vs MVs. **(b)** Non-linear vs linear model.

Figure 3.2: Change in PSE in response to random perturbations to the MVs. The linear model (dotted line) is compared to the non-linear model (solid line).

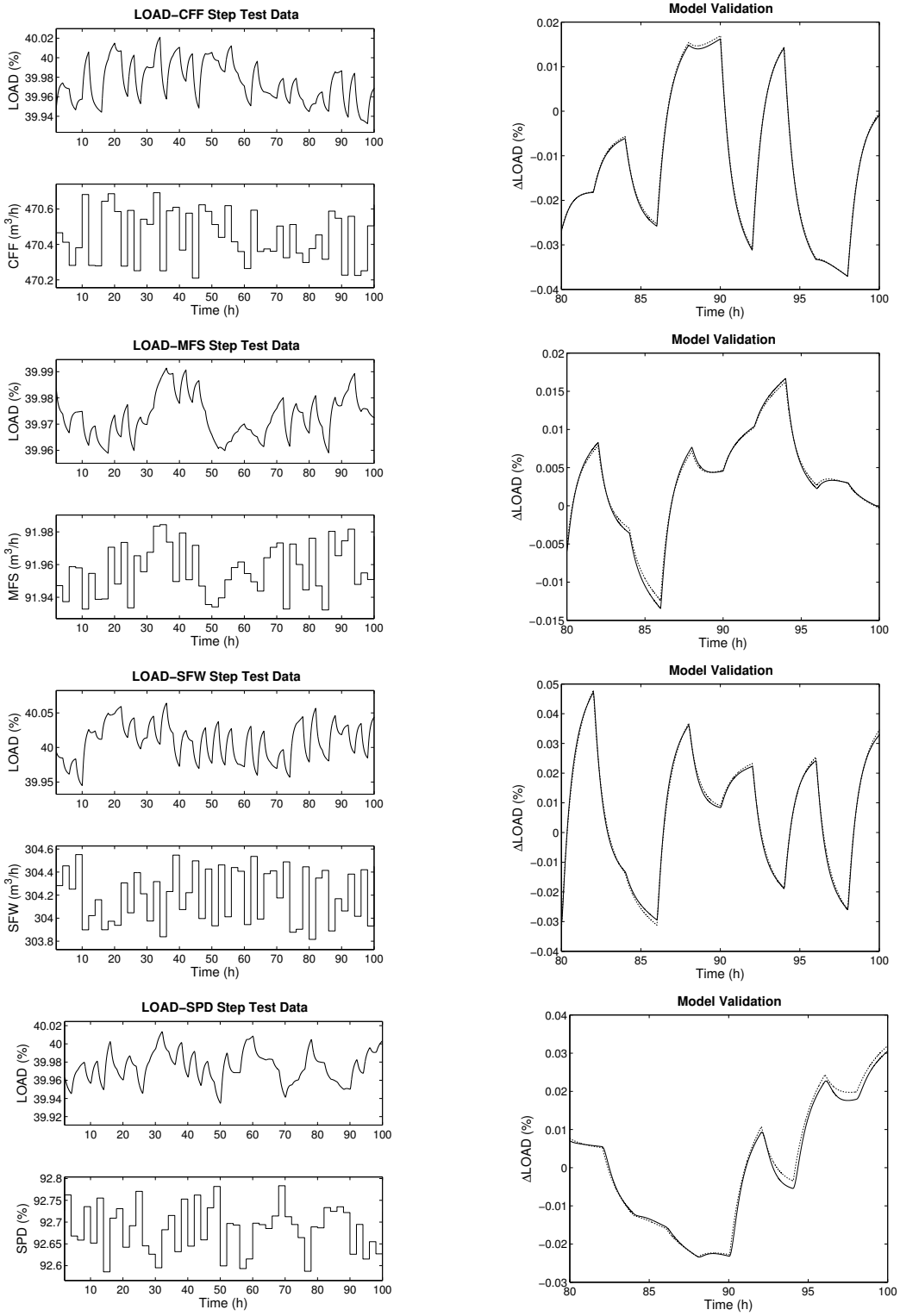

(a) LOAD vs MVs. **(b)** Non-linear vs linear model.

Figure 3.3: Change in LOAD in response to random perturbations to the MVs. The linear model (dotted line) is compared to the non-linear model (solid line).

3.3.3 Sump level

3.3.3.1 SLEV-CFF

SLEV exhibited a time delayed integrating response to a change in CFF. The linear model was fitted to the step response data (see Figure 3.4) to give the following transfer function

$$G_{31}(s) = \frac{-0.533}{s} e^{-0.014s}. \tag{3.15}$$

3.3.3.2 SLEV-MFS

SLEV exhibited a time delayed integrating response to a change in MFS. The linear model was fitted to the step response data (see Figure 3.4) to give the following transfer function

$$G_{32}(s) = \frac{0.934}{s} e^{-0.6s}. \tag{3.16}$$

3.3.3.3 SLEV-SFW

SLEV exhibited an integrating response to a change in SFW. The linear model was fitted to the step response data (see Figure 3.4) to give the following transfer function

$$G_{33}(s) = \frac{0.572}{s}. \tag{3.17}$$

3.3.3.4 SLEV-SPD

SLEV exhibited a time delayed integrating response to a change in SPD. The linear model was fitted to the step response data (see Figure 3.4) to give the following transfer function

$$G_{34}(s) = \frac{-0.925}{s} e^{-0.71s}. \tag{3.18}$$

3.3.4 Mill power

3.3.4.1 PWR-CFF

PWR exhibited a time delayed second-order response to a change in CFF. In order to improve the linear model fit, a zero was included in the model form. The linear model was fitted to

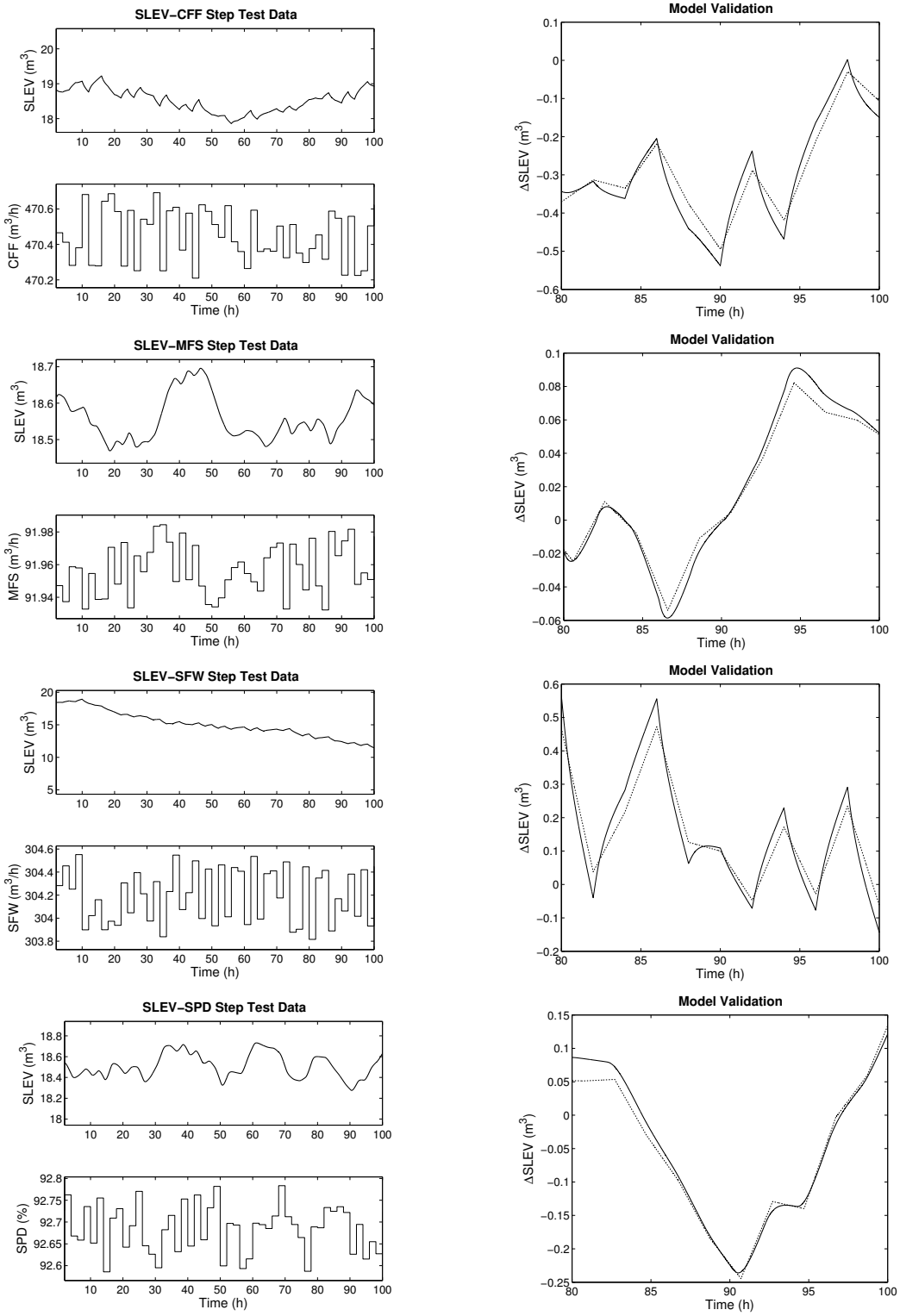

(a) SLEV vs MVs. **(b)** Non-linear vs linear model.

Figure 3.4: Change in SLEV in response to random perturbations to the MVs. The linear model (dotted line) is compared to the non-linear model (solid line).

the step response data (see Figure 3.5) to give the following transfer function

$$G_{41}(s) = \frac{3.484 \times 10^{-3}(1 + 4.416s)}{(1 + 10.048s)(1 + 0.585s)} e^{-0.014s}. \tag{3.19}$$

3.3.4.2 PWR-MFS

PWR exhibited a time delayed second-order response to a change in MFS. In order to improve the linear model fit, a zero was included in the model form. The linear model was fitted to the step response data (see Figure 3.5) to give the following transfer function

$$G_{42}(s) = \frac{12.509(1 + 2.698s)}{(1 + 8.522s)(1 + 0.481s)} e^{-0.014s}. \tag{3.20}$$

3.3.4.3 PWR-SFW

PWR exhibited a time delayed second-order response to a change in SFW. In order to improve the linear model fit, a zero was included in the model form. The linear model was fitted to the step response data (see Figure 3.5) to give the following transfer function

$$G_{43}(s) = \frac{-3.714(1 + 5.065s)}{(1 + 13.984s)(1 + 0.596s)} e^{-0.014s}. \tag{3.21}$$

3.3.4.4 PWR-SPD

PWR exhibited a time delayed second-order response to a change in SPD. In order to improve the linear model fit, a zero was included in the model form. The linear model was fitted to the step response data (see Figure 3.5) to give the following transfer function

$$G_{44}(s) = \frac{10.983(1 + 2.812s)}{(1 + 1.887s)(1 + 0.001s)} e^{-0.014s}. \tag{3.22}$$

Although the linear model for PWR-SPD compares well to the non-linear model response, it could be argued that the over-damped second-order transfer function could be simplified to a first-order transfer function. The analytical argument follows that given $(\tau_{p1} = 1.887) \gg (\tau_{p2} = 0.001)$, if $\tau_{p2} \to 0$, a similar response could be achieved. Figure 3.6 illustrates the different responses for the proposed PWR-SPD linear model given by

$$G_1(s) = \frac{10.983(1 + 2.812s)}{(1 + 1.887s)(1 + 0.001s)} e^{-0.014s}, \tag{3.23}$$

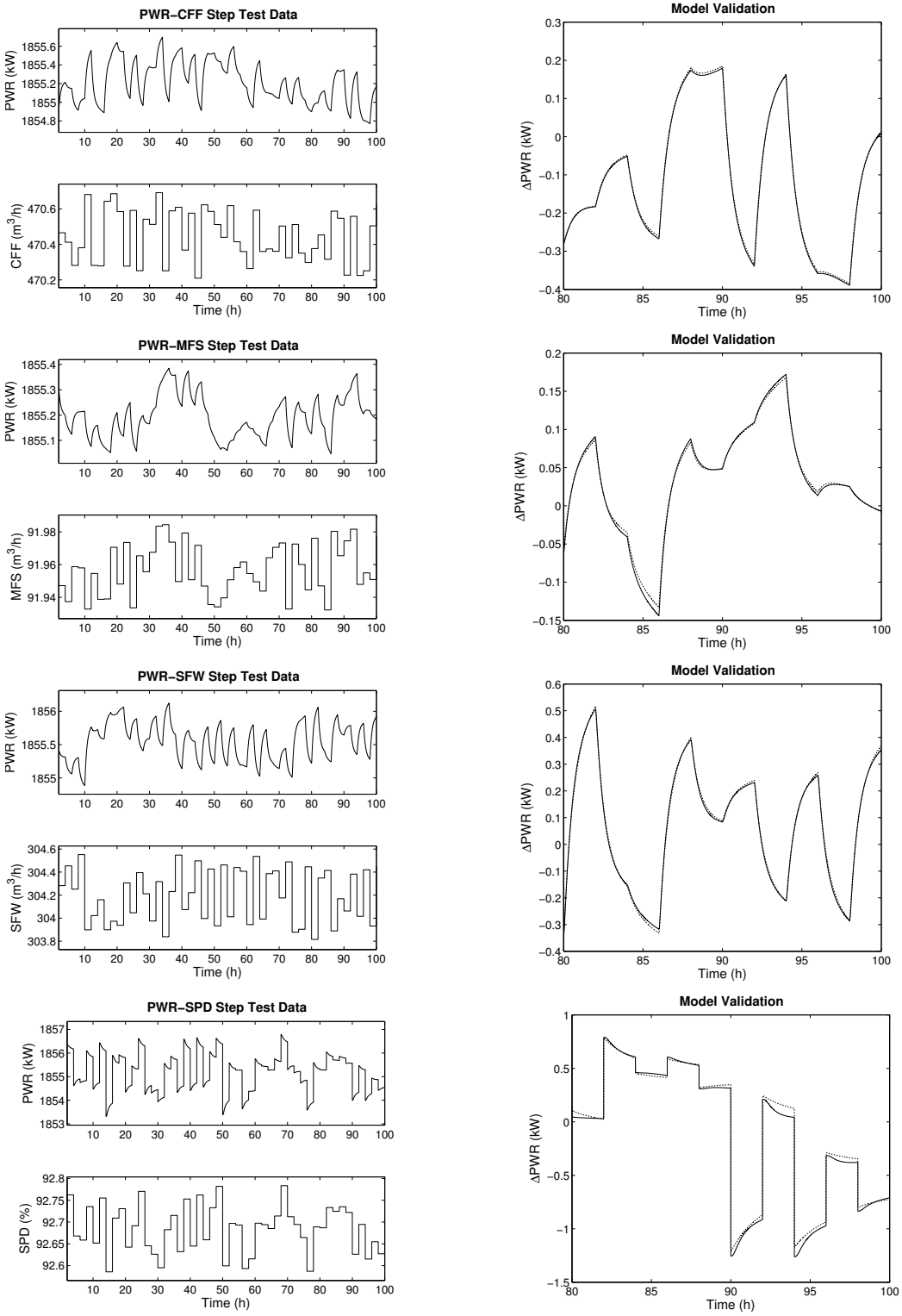

(a) PWR vs MVs. **(b)** Non-linear vs linear model.

Figure 3.5: Change in PWR in response to random perturbations to the MVs. The linear model (dotted line) is compared to the non-linear model (solid line).

and

$$G_2(s) = \frac{10.983(1 + 2.812s)}{(1 + 1.887s)} e^{-0.014s}. \tag{3.24}$$

As can be observed from the step response data, specifically in Figure 3.6b, the response of the models $G_1(s)$ and $G_2(s)$ differ significantly between 0.014 h and 0.020 h. Without the pole τ_{p2} the transfer function effectively has a discontinuity which the MPC controller cannot handle. This effect could be eliminated by removing the zero, however, the decay over time requires the zero.

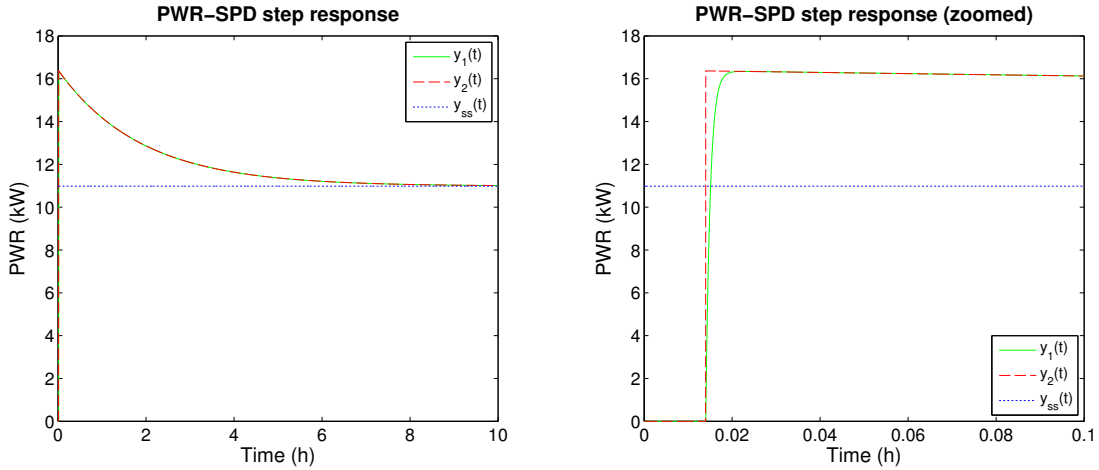

(a) PWR-SPD step response. **(b)** PWR-SPD step response (zoomed).

Figure 3.6: PWR-SPD step response for the second-order transfer function (blue line) compared to the simplified first-order transfer function (red line).

These effects can be identified in the non-linear model through the simplified power equation,

$$PWR = P_{\max} \cdot \left[1 - \left(\frac{LOAD}{v_{P_{\max}}} - 1\right)^2 - \left(\frac{\varphi}{\varphi_{P_{\max}}} - 1\right)^2\right] \cdot SPD^{\alpha_P}. \tag{3.25}$$

PWR responds very rapidly to a change in SPD. As PWR changes, so does the load within the mill as less slurry is discharged. This changes the rheology factor (φ) as the properties of the slurry begin to change. As the mill load and rheology factor move away from the optimal load ($v_{P_{max}}$) and rheology factor ($\varphi_{P_{max}}$), so the mill power draw begins to decay.

Step responses of the linear models for PSE, LOAD, and PWR compared very well to the non-linear model responses. Linear models for SLEV exhibited satisfactory responses given the

desired modeling effort which was limited to first- and second-order linear responses.

3.4 OBJECTIVE FUNCTION

MPC is used to control a plant by predicting the plant output based on control moves that may be made. Predicted plant output, calculated inputs, and constraints are formulated into an objective function to achieve certain performance objectives for the system. The objective function for the regulatory controller was given by

$$\begin{aligned} V(\mathbf{u},\mathbf{x}_0) &= \sum^{N_p}\Big((\mathbf{y}_{sp}-\mathbf{y}_{nom})-\mathbf{g}\left(\mathbf{x}_0,(\mathbf{u}-\mathbf{u}_{nom})\right)\Big)^{\mathrm{T}}\cdot\mathbf{Q}\cdot \\ &\quad \Big((\mathbf{y}_{sp}-\mathbf{y}_{nom})-\mathbf{g}\left(\mathbf{x}_0,(\mathbf{u}-\mathbf{u}_{nom})\right)\Big)+\sum^{N_c}\Delta\mathbf{u}^{\mathrm{T}}\mathbf{R}\Delta\mathbf{u}, \end{aligned} \tag{3.26}$$

where $\mathbf{u}$ represents the MVs, $\mathbf{x}$ the states with initial states $\mathbf{x}_0$, $\mathbf{y}_{sp}$ the set-points, $\mathbf{y}$ the CVs, $\mathbf{Q}$ the weights on the CVs, and $\mathbf{R}$ the rate of change weights on the MVs.

The function $\mathbf{g}(\mathbf{x}_0,\mathbf{u})$ represents the time domain response of the linear plant model described in the previous section. The function can be expressed as

$$\mathbf{g}(\mathbf{x}_0,\mathbf{u})=\mathcal{L}^{-1}\left(\mathbf{G}(s)\cdot\mathbf{U}(s)\right), \tag{3.27}$$

where

$$\mathbf{y}(t)=\mathbf{g}\left(\mathbf{0},\mathbf{u}(t)-\mathbf{u}_{nom}(t)\right)+\mathbf{y}_{nom}(t). \tag{3.28}$$

The objective function was minimized by calculating optimal values for $\mathbf{u}$. This was performed subject to constraints on the CVs, MVs, as well as the rate of change of the MVs,

$$\begin{aligned} &\min_{\mathbf{u}} V(\mathbf{u},\mathbf{x}_0), \\ &s.t.\ \ \mathbf{y}\in\mathbb{Y},\mathbf{u}\in\mathbb{U}, \\ \mathbb{Y} &= \{\mathbf{y}\in\mathbb{R}^{n_y}|\mathbf{y}_l\le\mathbf{y}\le\mathbf{y}_u\}, \\ \mathbb{U} &= \{\mathbf{u}\in\mathbb{R}^{n_u}|\mathbf{u}_l\le\mathbf{u}\le\mathbf{u}_u\}, \\ \mathbf{y}(t) &= \mathbf{g}\left(\mathbf{0},\mathbf{u}(t)-\mathbf{u}_{nom}(t)\right)+\mathbf{y}_{nom}(t) \\ &|\Delta\mathbf{u}|\le\Delta\mathbf{u}_{max}. \end{aligned} \tag{3.29}$$

The regulatory controller was implemented using the Model Predictive Control Toolbox in MATLAB (Bemporad, Morari and Ricker, 2004). The mathematical model used was the linear plant model described in the previous section. Constraints and weights of the objective function are discussed in the subsections that follow.

3.4.1 Constraints

CV and MV constraints were implemented as hard constraints. The controller could therefore not violate any of the constraints. Upper and lower constraints on the CVs were given by $\mathbf{y}_u$ and $\mathbf{y}_l$ respectively, where

$$\mathbf{y}_u = \begin{bmatrix} PSE_{max} \\ LOAD_{max} \\ SLEV_{max} \\ PWR_{max} \end{bmatrix} = \begin{bmatrix} 90.0 \\ 50.0 \\ 38.0 \\ 2000 \end{bmatrix}, \quad \text{and} \quad \mathbf{y}_l = \begin{bmatrix} PSE_{min} \\ LOAD_{min} \\ SLEV_{min} \\ PWR_{min} \end{bmatrix} = \begin{bmatrix} 60.0 \\ 30.0 \\ 2.0 \\ 1550 \end{bmatrix}. \tag{3.30}$$

Upper and lower constraints on the MVs were given by $\mathbf{u}_u$ and $\mathbf{u}_l$ respectively, where

$$\mathbf{u}_u = \begin{bmatrix} CFF_{max} \\ MFS_{max} \\ SFW_{max} \\ SPD_{max} \end{bmatrix} = \begin{bmatrix} 500.0 \\ 200.0 \\ 400.0 \\ 100.0 \end{bmatrix}, \quad \text{and} \quad \mathbf{u}_l = \begin{bmatrix} CFF_{min} \\ MFS_{min} \\ SFW_{min} \\ SPD_{min} \end{bmatrix} = \begin{bmatrix} 400.0 \\ 0.0 \\ 0.0 \\ 70.0 \end{bmatrix}. \tag{3.31}$$

Upper and lower CV and MV constraints used were commonly used constraints for the control of the Hulbert model (Coetzee et al., 2010; Olivier, Craig and Chen, 2012). These constraints were defined to ensure that the operating point at which the circuit operates was physically relevant.

MV maximum rate of change constraints were given by

$$|\Delta \mathbf{u}_{max}| = \begin{bmatrix} 1.00 \\ 0.20 \\ 1.00 \\ 0.50 \end{bmatrix}. \tag{3.32}$$

MV rate constraints were used to prevent sudden or unrealistic changes to the MVs. Constraints on CFF and SFW allow a maximum flow-rate change of 1 m^3/h every sampling interval (10 s). The constraint on MFS allowed the solids feed-rate to change by 0.2 t/h every 10 s. The constraint on SPD allowed the mill speed to change by a maximum of 0.5% every 10 s.

3.4.2 Weights

The relative importance of the CVs and MVs was taken into account by the controller through the weights used in the objective function. Two weighting matrices, **Q** and **R**, were used to implement the relative weights on the CVs and MVs respectively. The term *relative weights* is important as the weights were used to rate the importance of maintaining each CV at its set-point as well as rating the importance of minimizing changes to each MV.

The weighting matrices were formulated as diagonal matrices and contribute to the objective function as follows,

$$Contrib_Q = (\mathbf{y_{sp}} - \mathbf{y})^{\mathrm{T}} \begin{bmatrix} Q_{PSE} & 0 & 0 & 0 \\ 0 & Q_{LOAD} & 0 & 0 \\ 0 & 0 & Q_{SLEV} & 0 \\ 0 & 0 & 0 & Q_{PWR} \end{bmatrix} (\mathbf{y_{sp}} - \mathbf{y}), \tag{3.33}$$

where

$$\mathbf{y_{sp}} - \mathbf{y} = \begin{bmatrix} PSE_{sp} - PSE \\ LOAD_{sp} - LOAD \\ SLEV_{sp} - SLEV \\ PWR_{sp} - PWR \end{bmatrix}, \tag{3.34}$$

and

$$Contrib_R = \begin{bmatrix} \Delta CFF \\ \Delta MFS \\ \Delta SFW \\ \Delta SPD \end{bmatrix}^{\mathrm{T}} \begin{bmatrix} R_{CFF} & 0 & 0 & 0 \\ 0 & R_{MFS} & 0 & 0 \\ 0 & 0 & R_{SFW} & 0 \\ 0 & 0 & 0 & R_{SPD} \end{bmatrix} \begin{bmatrix} \Delta CFF \\ \Delta MFS \\ \Delta SFW \\ \Delta SPD \end{bmatrix}. \tag{3.35}$$

The contributions could be simplified to

$$\begin{aligned} Contrib_Q \quad = \quad & Q_{PSE} (PSE_{sp} - PSE)^2 + Q_{LOAD} (LOAD_{sp} - LOAD)^2 + \\ & Q_{SLEV} (SLEV_{sp} - SLEV)^2 + Q_{PWR} (PWR_{sp} - PWR)^2, \end{aligned} \tag{3.36}$$

and

$$Contrib_R = R_{CFF} (\Delta CFF)^2 + R_{MFS} (\Delta MFS)^2 + R_{SFW} (\Delta SFW)^2 + R_{SPD} (\Delta SPD)^2. \tag{3.37}$$

In order to tune the weights through relationships between the CVs and MVs, the squared relationships in (3.36) and (3.37) had to be taken into account. Individual CV and MV weights were therefore considered as

$$\begin{aligned} Q_y &= W_y^2, \\ R_u &= W_u^2. \end{aligned} \tag{3.38}$$

In order to compare the relative importance of the weights the following relationship was used,

$$W_{PSE} \times |PSE_{sp} - PSE| = W_{SLEV} \times |SLEV_{sp} - SLEV| \,. \tag{3.39}$$

If then, for example, a 1 unit deviation in PSE from its set-point would be equivalent to a 10 unit deviation in SLEV from its set-point, $W_{PSE} = 10 \times W_{SLEV}$.

Weights were used in order to implement the control objectives given in Section 2.4. The control objectives were formulated as certain trade-offs, with the most important being the stability of the milling circuit. Stability of the milling circuit required only that LOAD and SLEV, which are open loop unstable, remain within their respective operating ranges. This meant that their relative weights can be chosen lower than that of PSE.

Set-point deviation equivalents as well as the weights for the CVs are given in Table 3.2. At first inspection the relative weight between PSE and PWR appears to be high considering the control objectives where that PSE is considered a more important CV than PWR. During tuning it was, however, found that when PWR remained relatively stable, variations in PSE could be reduced. Relaxed weights on SLEV and LOAD allowed the control effort to be focused on PSE and PWR in accordance with the control objectives.

Table 3.2: Relative CV weight choices.

CV	$\lvert CV_{sp} - CV \rvert$	W_{CV}
PSE	1%	200
LOAD	20%	10
SLEV	20 m^3	10
PWR	1 kW	200

MV weights were chosen to be smaller than CV weights so that correction of set-point devi-

ation was prioritized over control action in order to improve set-point tracking. MV weights were, however, also used to reduce unnecessary control action by penalizing changes to MVs. If a change in an MV could, however, improve the set-point tracking, relative weights between the MVs and CVs allowed for adequate control action to be taken.

The relationship between the MV weights and CV weights was set so that the effect of a 200 kW set-point deviation in PWR on the objective function was equivalent to a 1% change in SPD. This relationship ensured that the penalties on control moves had a lower priority than set-point tracking. Relative weights according to control action movement are given in Table 3.3.

Table 3.3: Relative MV weight choices.

MV	$\|\Delta MV\|$	W_{MV}
CFF	0.001 m^3/h	0.001
MFS	0.004 t/h	0.004
SFW	0.001 m^3/h	0.001
SPD	1%	1

As can be seen from the MV weight choices, CFF and SFW had the lowest weights. This was implemented to reduce MV movement of both MFS and SPD. SPD should primarily be changed to adjust PWR and choosing a higher weight in relation to the other MV weights resulted in reduced use of SPD to control the milling circuit. This was similar for MFS as it related to the milling circuit throughput and was therefore kept as high as possible with movement penalized more than that of CFF and SFW.

3.5 RECEDING HORIZON CONTROLLER TUNING

Receding horizon control is achieved by iteratively solving an optimal control problem for a finite prediction horizon at some sampling interval (Mayne, Rawlings, Rao and Scokaert, 2000). The objective function was minimized at each iteration using the system state at that instant as the initial state for the optimal control problem. Iteration of the finite horizon control problem effectively achieved an infinite horizon, or receding horizon control.

Prediction horizon should be chosen to cover the longest dynamics (or settling time, T_s) of the linear model. The number of prediction steps, N_p, was calculated based on the sampling interval of the controller, ΔT_{MPC}. Control horizon was chosen so that control action occurred across the prediction horizon (Seborg, Edgar and Mellichamp, 2004). The regulatory controller was tuned by first determining the sampling interval, then the number of prediction steps, and finally the number of control moves. Resulting MPC settings are summarized in Table 3.4.

Table 3.4: MPC settings.

Sampling interval	Prediction steps	Control moves	Blocking vector
10 s	30	6	[3 3 4 5 7 8]

3.5.1 Sampling interval

The sampling interval of the controller was chosen based on the fastest dynamics within the milling circuit. By inspection it is evident that the fastest dynamics occur within the SLEV loops owing to the integral action,

$$\Delta SLEV = \begin{bmatrix} \frac{-0.533}{s}e^{-0.014s} & \frac{0.934}{s}e^{-0.6s} & \frac{0.572}{s} & \frac{-0.925}{s}e^{-0.71s} \end{bmatrix} \begin{bmatrix} \Delta CFF \\ \Delta MFS \\ \Delta SFW \\ \Delta SPD \end{bmatrix}, \tag{3.40}$$

the fastest of which are the SLEV/CFF and SLEV/SFW loops owing to the small time delays with gains of -0.533 and 0.572 respectively.

The sampling interval was therefore chosen to give the controller time to change the MVs so that the sump will neither run dry nor overflow within a sampling interval. In order to determine the amount of time it would take for the sump to run dry or overflow from the nominal sump level the worst case conditions for CFF and SFW were chosen. The worst case scenario was where CFF was at its maximum (500 m^3/h) and SFW was at its minimum (0 m^3/h). At these flow-rates it would take 134 s for the sump to run dry from its nominal level of 18.6 m^3.

In addition to maintaining control of SLEV, increases in the sampling interval deteriorated

controller performance. The sampling interval of the non-linear model is 10 s (as also chosen by Craig and MacLeod (1995)) and therefore the sampling interval of the controller had to be implemented as a multiple of 10 s for implementation in MATLAB. Increasing the sampling interval to 20 s significantly deteriorated the performance of specifically PSE and PWR as illustrated in Figure 3.7 and 3.8.

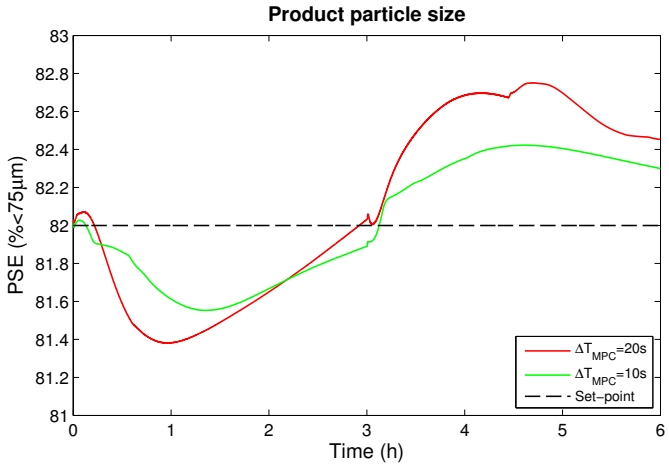

Figure 3.7: PSE response for different sampling intervals.

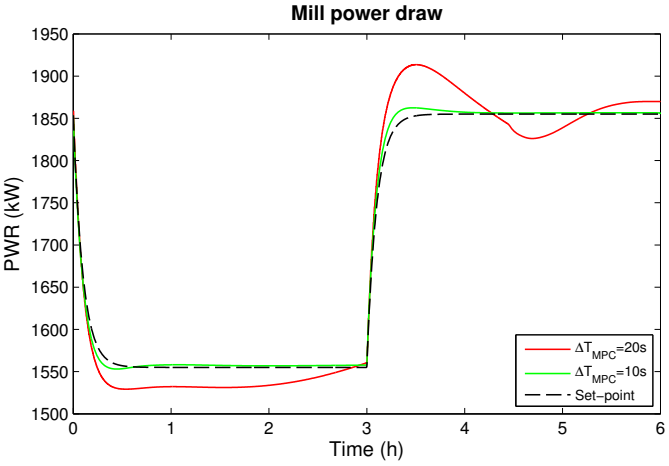

Figure 3.8: PWR response for different sampling intervals.

PSE and PWR were the two most important CVs and as a result of the poor performance the sampling interval was chosen to be 10 s. This allowed for approximately 13 samples for the controller to respond to decreasing SLEV. Although this is a large margin, the primary choice of the low sampling interval is the tighter control of PSE and PWR.

3.5.2 Prediction horizon

It is recommended that the prediction horizon be chosen to cover the longest dynamics of the plant (Seborg et al., 2004). Considering the linear model of the milling circuit, the longest dynamics were found in the LOAD/SFW loop. The settling time, considered as the time it takes to reach and remain within $\pm 5\%$ of the steady-state gain of the step response, was 35 h. This prediction horizon resulted in 12600 prediction steps (N_p).

Such a large prediction horizon was undesirable as for a 4×4 plant with six control actions the optimization problem became infeasible. By considering the control objectives, (see Section 2.4) a trade-off was made in considering which loop the prediction horizon was based on. With this in mind the control loops for PSE were considered. The longest dynamics of these loops are found in the PSE/SPD loop, for which the settling time is 13 h, resulting in 4680 prediction steps.

Coetzee et al. (2010) successfully implemented a robust non-linear MPC controller for the Hulbert milling circuit model with a small prediction horizon, 60 s or 6 steps. The reduced computational time as a result of such a small prediction horizon was desirable. Based on these results the prediction horizon for the controller was initially chosen as 100 s and tested.

Increasing the prediction horizon resulted in improved stability and performance of the controller. The prediction horizon was increased in 100 s increments to 500 s. In order to test the performance the PWR set-point was changed from the nominal operating point, $1,855$ kW, to $1,555$ kW, and then returned to the nominal operating point after 3 h. Performance was measured by the integral square error (ISE) and maximum set-point deviation ($\Delta_{\max}$). These results are presented in Figures 3.9 to 3.12 and Table 3.5.

Results of the performance tests of the controller indicate that the best performance, based on the maximum set-point deviation and ISE metrics, was for a prediction horizon of 200 s. Performance of PSE for this prediction horizon was, however, in conflict with the secondary control objectives, specifically the objective *"maintain the quality of the product by decreasing product size fluctuations"*. Inspection of Figure 3.9 reveals that for a prediction horizon of 200 s an oscillation occurred in PSE over the intervals $t = (0, 0.5)$ and $t = (3, 3.5)$.

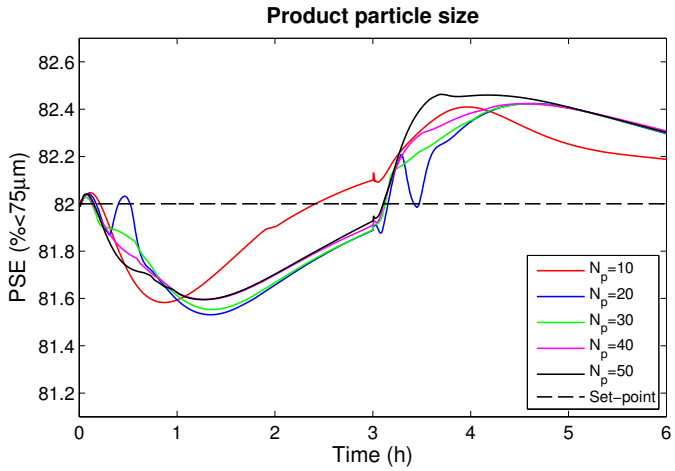

Figure 3.9: PSE response for different prediction horizons.

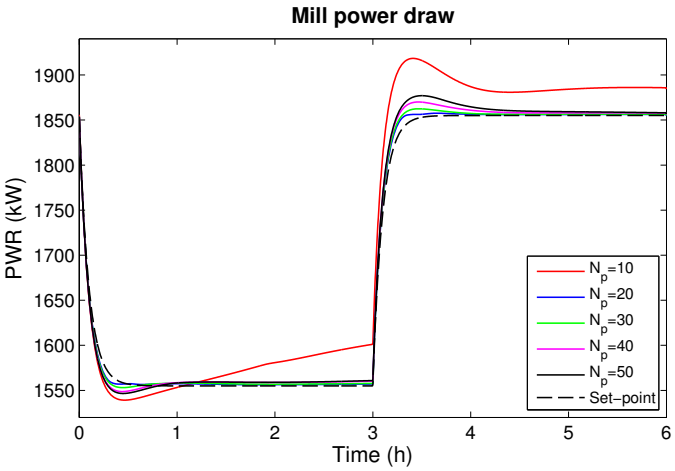

Figure 3.10: PWR response for different prediction horizons.

The prediction horizon was therefore chosen as 300 s as the combination of PSE and PWR performance were best. Performance of PSE was best for a horizon of 100 s, however, the performance of PWR was very poor for this horizon. Performance of LOAD improved as the horizon increased, while the performance of SLEV deteriorated. Owing to the control objectives, these were not key metrics considered for the controller tuning, as long as they remained within the relevant operating ranges.

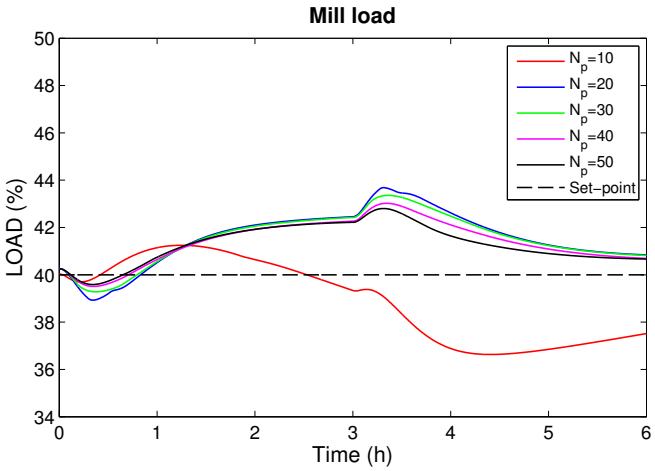

Figure 3.11: LOAD response for different prediction horizons.

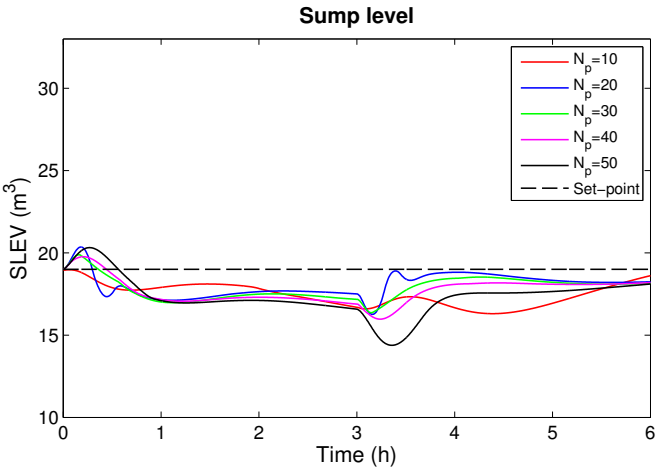

Figure 3.12: SLEV response for different prediction horizons.

3.5.3 Control horizon

The control horizon was initially chosen as three control moves. Increasing the control horizon with a fixed prediction horizon was shown to improve the performance of the controller up to a certain point. Through this method the control horizon was increased to six control moves. Further increasing the number of control moves resulted in increased computational intensity while performance remained the same.

In order to prevent the control action from being too aggressive, the control action was distributed across the prediction horizon. This distribution was implemented using a blocking

Table 3.5: Effect of prediction horizon on performance.

		Prediction Horizon				
		100 s	200 s	300 s	400 s	500 s
PSE	Δ_{max}	0.417	0.469	0.447	0.423	0.463
	ISE	0.416	0.613	0.610	0.607	0.695
PWR	Δ_{max}	71.99	13.66	16.62	21.92	25.47
	ISE	6799	96.00	168.6	386.8	591.8
LOAD	Δ_{max}	3.368	3.683	3.356	3.022	2.801
	ISE	24.21	23.00	21.00	17.03	14.48
SLEV	Δ_{max}	2.695	2.734	2.636	3.029	4.618
	ISE	17.15	8.686	10.77	13.84	24.39

vector which denoted how many prediction steps each control move persisted. The blocking vector was chosen to allow successive control moves to persist longer to prevent sluggish control action. Blocking vectors for three to six control moves are given in Table 3.6.

Table 3.6: Blocking vectors for different control horizons.

Control moves	Blocking vector
3	[3 9 18]
4	[3 5 9 13]
5	[3 4 5 7 11]
6	[3 3 4 5 7 8]

In order to compare the performance of the controller depending on the number of control moves implemented, the integral square error (ISE) and maximum set-point deviation were calculated as for the prediction horizon performance tests. Results are presented in Figures 3.13 to 3.16 and Table 3.7.

Again, as discussed in the previous section, PSE and PWR were the two most important CVs as long as LOAD and SLEV remain within the respective operating regions. The performance metrics used indicated that performance of the controller for PSE, PWR, and SLEV was best for six control moves. Performance of LOAD was best for four control moves, however it did

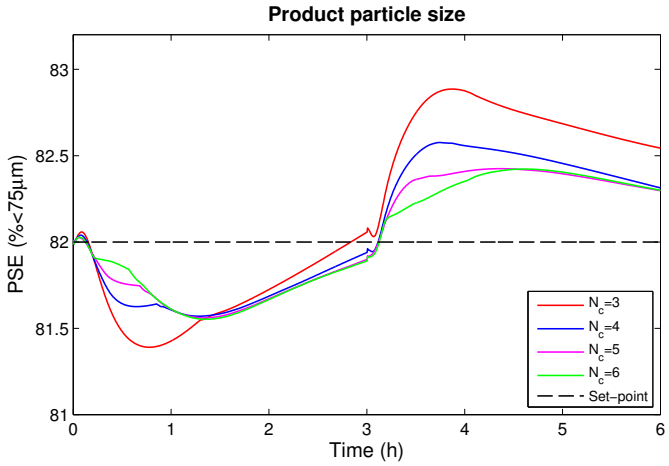

Figure 3.13: PSE response for different numbers of control moves.

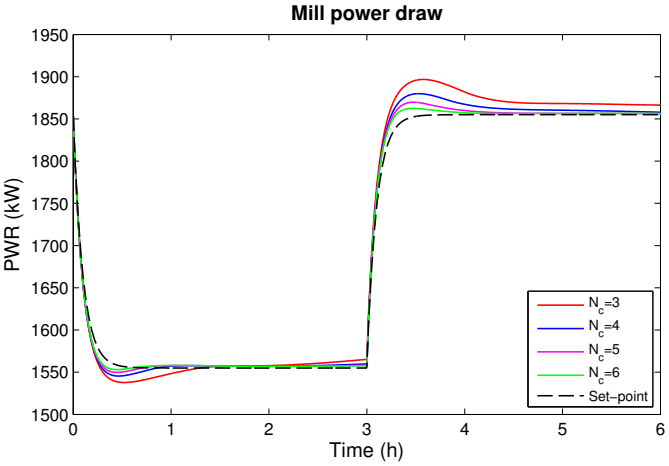

Figure 3.14: PWR response for different numbers of control moves.

not significantly deteriorate for six control moves and remained stable.

3.6 RESULTS

In order to test the regulatory controller, simulations were performed to evaluate the response of the controller with regards to PWR set-point tracking. The purpose of the regulatory controller was to reduce the power draw of the milling circuit when electricity costs were high and increase the power draw when costs were low. These changes in PWR had to minimally disturb the operation of the rest of the milling circuit, i.e. maintain the remaining CVs at their nominal operating points.

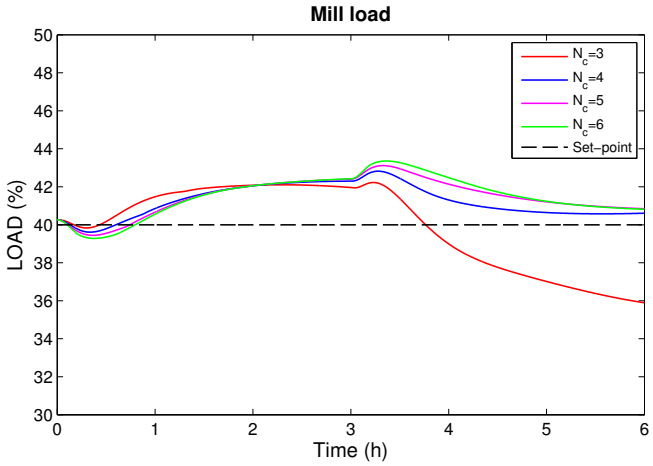

Figure 3.15: LOAD response for different numbers of control moves.

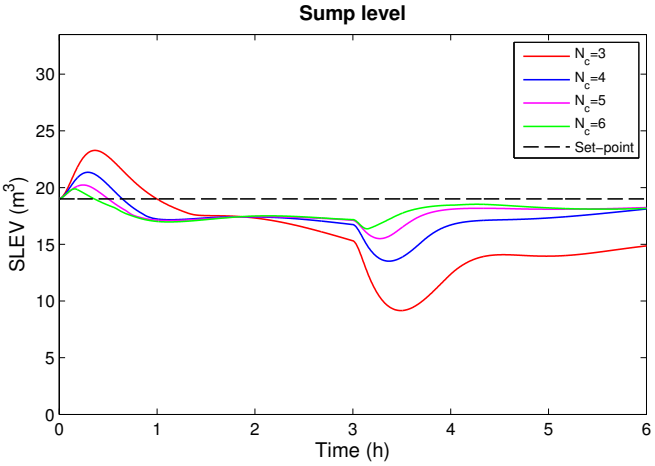

Figure 3.16: SLEV response for different numbers of control moves.

3.6.1 Simulation setup

The PWR set-point was changed while maintaining the set-points of PSE, LOAD, and SLEV. Set-points for PSE, LOAD, and SLEV were kept at the nominal operating points of 82.0%, 40%, and 18.6 m^3 respectively. PWR was changed according to the TOU electricity tariff table for a weekday as given in Table 3.8. Applicability of the TOU tariff structure to load shifting is further discussed in the following chapter.

Measurement noise was not considered for the simulations. The Kalman estimator used to estimate the states of the system, based on the linear model, was primarily used to reject

Table 3.7: Effect of control horizon on performance.

		Control moves			
		N_c=3	N_c=4	N_c=5	N_c=6
PSE	Δ_{max}	0.886	0.576	0.439	0.447
	ISE	1.852	0.904	0.665	0.610
PWR	Δ_{max}	42.88	27.07	19.60	16.61
	ISE	1962	657.9	288.2	168.6
LOAD	Δ_{max}	4.106	2.821	3.115	3.356
	ISE	28.53	13.97	18.83	21.00
SLEV	Δ_{max}	9.844	5.486	3.497	2.636
	ISE	133.8	31.36	14.29	10.77

Table 3.8: PWR set-points according to TOU tariff periods.

Period	Tariff	PWR_{sp} (kW)
00:00 - 06:00	Off-peak	1950
06:00 - 07:00	Standard	1800
07:00 - 10:00	Peak	1600
10:00 - 18:00	Standard	1800
18:00 - 20:00	Peak	1600
20:00 - 22:00	Standard	1800
22:00 - 24:00	Off-peak	1950

noise on the measured outputs. State estimation was not the focus of this work and therefore noise rejection performance was not considered.

3.6.2 Simulation results

Simulation results for the CVs and MVs are presented in Figure 3.17. The results are presented with the relevant constraints and set-points.

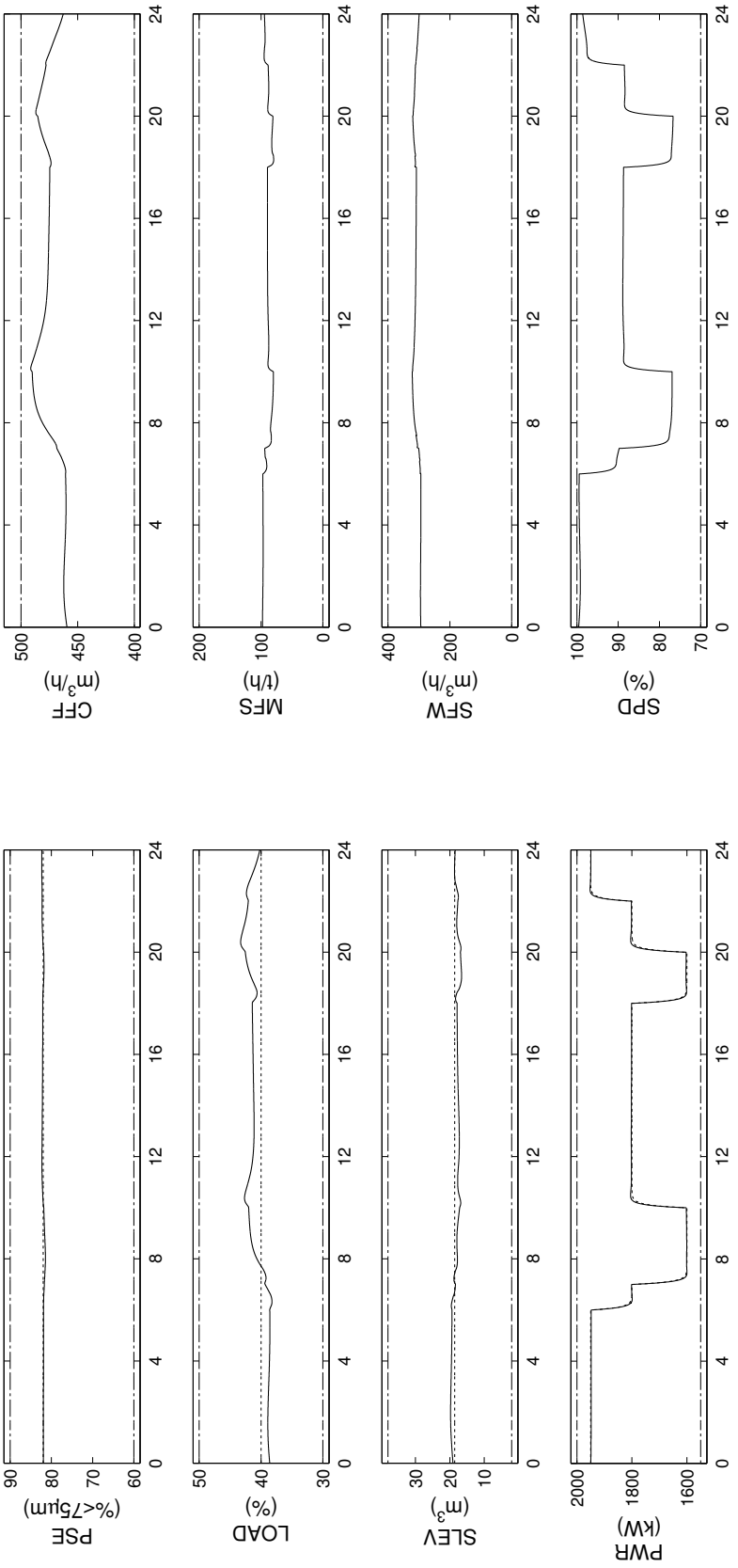

(a) CV responses for the simulation.

(b) MV responses for the simulation.

Figure 3.17: Solid lines indicate CVs and MVs, dotted lines the set-points, and dash-dotted lines the constraints.

Performance in terms of set-point tracking was satisfactory for PSE and PWR. Variations in PSE were very small with long time dynamics which would minimally affect the downstream extraction processes (McKee, 1991). Set-point tracking of LOAD and SLEV was not very accurate which was to be expected. In order to perform load shifting it is necessary to change the operating point of the non-linear model which may also result in the linear model not being valid any more. As per the discussion on weight choice in Section 3.4.2, LOAD and SLEV were designed to allow a degree of fluctuation in order to achieve tighter control of PSE and PWR.

None of the CVs or MVs violated the constraints. CFF, MFS, and SFW remained significantly far from the constraints. This indicates that the controller did not run at its limit and would have room to maneuver in the presence of disturbances (Olivier, Craig and Chen, 2012). SPD approached the constraint during periods where PWR was maximized as expected.

3.7 CONCLUSION

The regulatory controller was based on linear MPC and designed to control the non-linear plant given by the Hulbert model. The linear model was developed using SID to give a sufficiently accurate representation of the non-linear model using first- and second-order transfer functions for the controller. SID, chosen over Jacobian linearization owing to simplicity of implementation, was shown to be effective for milling circuit control.

The controller was developed to meet the control objectives of maintaining milling circuit stability, controlling mill power draw, and minimizing PSE variations. Concerns around milling circuit stability were predominantly addressed by the use of the MPC structure. In order to control PWR the controller had to be modified from the traditional 3×3 controller to a 4×4 controller. The additional CV was PWR and the additional MV introduced was SPD. Minimization of PSE variations was addressed by tuning the weights of the controller to prioritize control between the CVs.

The regulatory controller achieved the desired control objectives. Minor variations in PSE were observed, however, long time dynamics of these variations were considered acceptable as they would minimally affect downstream processes. The milling circuit exhibited stable behavior with room for the MVs to maneuver in the presence of disturbances.

CHAPTER 4

SUPERVISORY CONTROLLER

4.1 INTRODUCTION

Optimization of milling circuit control was traditionally performed by considering only throughput maximization (see Section 2.3). Throughput maximization is generally implemented by maximizing the power draw of the mill (Pauw et al., 1985; Craig et al., 1992). Changing industry conditions, which include higher peak electricity tariffs, lower platinum demand and price, and a drive towards energy efficiency bring to question whether maximization of throughput can still be considered an optimal economic operating model (Desbiens et al., 2008; Daniel, 2011).

TOU tariffs, developed by electricity utilities to decrease peak demand and increase off-peak demand, present a cost saving opportunity for milling circuit operators. Real-time optimization of profit, based on the trade-off between mill power draw (operating expense) and throughput (turnover), has the potential to improve the economics of a milling circuit. In this chapter the development of such a RTO to be implemented at the supervisory control layer is described.

4.2 REAL-TIME OPTIMIZER

In order to calculate set-points for the mill power load shifting controller, a non-linear objective function was developed to be minimized. The objective function was developed as a loss function based on turnover and the costs associated with electricity consumption. In order to take dynamic changes of mineral price, electricity tariffs, and throughput availabil-

ity into account, the loss minimization function was implemented as a RTO, formulated as follows,

$$\begin{aligned} & \min_{\mathbf{u}_{SS}} L(\mathbf{u}_{SS}, \mathbf{y}_{SS}), \\ & s.t.\ \ \mathbf{y}_{SS} \in \mathbb{Y}, \mathbf{u}_{SS} \in \mathbb{U}, \\ \mathbb{Y} &= \{\mathbf{y}_{SS} \in \mathbb{R}^{n_y} | \mathbf{y}_l \leq \mathbf{y}_{SS} \leq \mathbf{y}_u\}, \\ \mathbb{U} &= \{\mathbf{u}_{SS} \in \mathbb{R}^{n_u} | \mathbf{u}_l \leq \mathbf{u}_{SS} \leq \mathbf{u}_u\}, \\ |\Delta \mathbf{u}_{SS}| &\leq \Delta T_{RTO}/\Delta T_{MPC} \times \Delta \mathbf{u}_{max}, \\ TPT_{ave} &= \frac{1}{168} \times \sum_{t=1}^{168/\Delta T_{RTO}} \Delta T_{RTO} \times u_{SS_2}(t). \end{aligned} \tag{4.1}$$

The RTO was implemented with a sampling interval, ΔT_{RTO}, of 30 min. This interval was chosen based on the frequency at which the TOU tariffs change (f_{TOU}). The TOU tariffs used as input to the RTO were hourly based which is a sampling frequency of $f_{RTO} = 2 \times f_{TOU}$. It was also necessary that the sampling interval of the supervisory controller be a multiple of the sampling interval of the regulatory controller, $\Delta T_{RTO} = 1800 \times \Delta T_{MPC}$ in this case.

Minimization of the objective function was formulated with a window of $N = 168$ h (7 days). The window was made this length in order to take advantage of cheaper electricity over weekends where throughput can be increased to compensate for lower throughput during the week when electricity is on average more expensive.

4.2.1 Objective function

The objective function was given by

$$L(\mathbf{u}_{SS}, \mathbf{y}_{SS}) = \sum_{t=1}^{N/\Delta T_{RTO}} \left[C_t(\mathbf{y}_{SS}) - I_t(\mathbf{u}_{SS}, \mathbf{y}_{SS}) \right], \tag{4.2}$$

where $C_t(\mathbf{y})$ is the cost associated with electricity consumption, $I_t(\mathbf{u}, \mathbf{y})$ is the turnover attributed to the ROM ore milling circuit, and N is the window over which the objective function was evaluated. Turnover and electricity cost functions are discussed below. The variables used for the turnover and electricity cost functions are summarized in Table 4.1.

4.2.1.1 Turnover

The effect that load shifting has on the basic profitability of the milling circuit had to be evaluated to assess the benefits of load shifting. Turnover associated with the milling circuit

Table 4.1: Variables used for the supervisory control objective function.

Variable	Units	Description
$L(\mathbf{u}_{SS}, \mathbf{y}_{SS})$	ZAR	Loss as a function of steady-state MVs and CVs.
$I_t(\mathbf{u}_{SS}, \mathbf{y}_{SS})$	ZAR	Turnover as a function of steady-state MVs and CVs.
$C_t(\mathbf{y}_{SS})$	ZAR	Electricity cost as a function of steady-state CVs.
N	h	Window over which $L(\mathbf{u}_{SS}, \mathbf{y}_{SS})$ is evaluated.
ΔT_{RTO}	h	Sampling interval of the RTO.
HG	g/t	Approximate head grade of ore.
P_{ADJ}	ZAR/g	Price of the product at the output of the flotation process.
P_{market}	ZAR/ozt	Market price for platinum.
u_{SS_2}	t/h	Steady-state feed-rate of ore to the mill (MFS_{SS}).
y_{SS_1}	%	Steady-state product particle size (PSE_{SS}).
y_{SS_4}	kW	Steady-state mill power draw (PWR_{SS}).
$\vartheta(y_{SS_1})$	fraction	Recovery within flotation process as a function of PSE_{SS}.
$c(t)$	ZAR/kWh	Electricity tariff at time t.

product was given by

$$I_t(\mathbf{u}_{SS}, \mathbf{y}_{SS}) = \Delta T_{RTO} \times HG \times P_{ADJ} \times u_{SS_2}(t) \times \vartheta(y_{SS_1}(t)), \tag{4.3}$$

where ΔT_{RTO} is the sampling interval in hours, HG is the approximate head grade of the mined ore given as 3 g/t, u_{SS_2} is the steady-state feed-rate of ore to the mill (MFS) which relates to the throughput over an hour, and $\vartheta(y_{SS_1}(t))$ is the recovery in percent within the flotation circuit as a function of steady-state PSE (y_{SS_1}). The relationship between recovery and particle size, as given in Figure 1.3, is

$$\vartheta(y_{SS_1}(t)) = -0.009776 y_{SS_1}^2(t) + 1.705 y_{SS_1}(t) - 2.955. \tag{4.4}$$

Mineral price, P_{ADJ}, is the price of the product at the output of the flotation circuit. The price is adjusted from the market price of refined platinum to the separated product, or concentrate, produced by the flotation circuit. This adjustment was made so that a comparison of the electricity costs of only the milling circuit can be made to the income associated with the process itself. Adjusted price was given by

$$P_{ADJ} = (0.032) \times (0.75) \times P_{market}, \tag{4.5}$$

where 0.032 is the conversion factor between gram and troy ounce, 0.75 represents the percentage of the costs associated with the mining, liberation, and separation processes upstream of the refining process (Cramer, 2008), and P_{market} is the market price for platinum, given as R16000 /ozt.

4.2.1.2 Electricity costs

Electricity consumption was calculated based on the average mill power draw every half hour. Electricity cost was then calculated based on the half-hourly electricity consumption billed at the applicable TOU tariff for that half hour. This function was given by

$$C_t(\mathbf{y}_{SS}) = \Delta T_{RTO} \times y_{SS_4}(t) \times c(t), \tag{4.6}$$

where y_{SS_4} is the steady-state mill power draw given by PWR in (2.11) and $c(t)$ is the applicable TOU tariff for the given period in ZAR/kWh as given in Tables 4.2 and 4.3.

Table 4.2: Eskom time-of-use periods (Eskom, 2014b).

Period	Weekdays	Saturdays	Sundays
00:00 - 06:00	Off-peak	Off-peak	Off-peak
06:00 - 07:00	Standard	Off-peak	Off-peak
07:00 - 10:00	Peak	Standard	Off-peak
10:00 - 12:00	Standard	Standard	Off-peak
12:00 - 18:00	Standard	Off-peak	Off-peak
18:00 - 20:00	Peak	Standard	Off-peak
20:00 - 22:00	Standard	Off-peak	Off-peak
22:00 - 24:00	Off-peak	Off-peak	Off-peak

4.2.2 RTO plant model

The objective function (4.2) was related to the milling circuit model through the steady-state linear plant model used for the regulatory controller (see Section 3.3). Steady-state models for the transfer functions $G_{31}(s)$, $G_{32}(s)$, $G_{33}(s)$, and $G_{34}(s)$ were calculated as the gain at the end of the sampling interval ($t = 30$ min) as these transfer functions contain integrators

Table 4.3: Eskom time-of-use tariffs (ZAR/kWh) (Eskom, 2011; Eskom, 2014b).

Tariff period	High demand season (Jun.-Aug.)		Low demand season (Sep.-May)	
	2011/12	2014/15	2011/12	2014/15
Peak	1.958	2.285	0.548	0.745
Standard	0.510	0.692	0.336	0.513
Off-peak	0.273	0.376	0.235	0.325

and cannot reach steady-state. The steady-state model was given by

$$\mathbf{y}_{SS} = \mathbf{G}_{SS} \cdot \mathbf{u}_{SS}, \tag{4.7}$$

where $\mathbf{G}_{SS}$ was given by

$$\begin{bmatrix} -7.0 \times 10^{-3} & -9.5 \times 10^{-2} & 4.5 \times 10^{-2} & 0.108 \\ 8.1 \times 10^{-2} & 4.8 \times 10^{-2} & -7.0 \times 10^{-2} & -1.050 \\ -0.385 & 0.438 & 0.339 & -0.442 \\ 3.577 & 8.990 & 1.605 & 73.570 \end{bmatrix}. \tag{4.8}$$

In order to ensure that the minimization of the objective function remained true to the linear plant model, the steady-state linear plant model was used as an equality constraint for the objective function.

4.2.2.1 Constraints

In addition to using the steady-state model as equality constraints, input and output constraints to the non-linear model were included. CV constraints used in the objective function were made 10% tighter than those used by the regulatory controller as in Table 3.1 while the MV constraints remained the same. Resulting CV constraints were given by

$$\begin{aligned} \mathbf{y}_l &= \begin{bmatrix} 63.0 & 32.0 & 5.6 & 1550 \end{bmatrix}^{\mathrm{T}}, \\ \mathbf{y}_u &= \begin{bmatrix} 87.0 & 48.0 & 34.4 & 1950 \end{bmatrix}^{\mathrm{T}}. \end{aligned} \tag{4.9}$$

In addition to constraints on the CVs and MVs, average throughput of the milling circuit was implemented using an equality constraint. Average throughput refers to the throughput

over the seven day period for which the optimization was done. The throughput constraint was implemented as

$$TPT_{ave} \times 24 \times 7 = \sum_{t=1}^{N/\Delta T_{RTO}} \Delta T_{RTO} \times u_{SS_2}(t), \tag{4.10}$$

where TPT_{ave} is the average throughput over the seven day period (24 h $\times$ 7) and $u_{SS_2}(t)$ is the steady-state of MFS at time t.

The throughput constraint originated from the assumption that ore could be supplied to the milling circuit at a certain rate, i.e. a buffer in the form of a silo or storage facility lay between the source of ore and milling circuit. The average throughput rate of the milling circuit had to therefore be the same as the average feed-rate of ore supplied to the milling circuit over a seven day period.

4.2.2.2 RTO outputs

Optimal set-points, $\mathbf{y}_{sp}$, were calculated based on the optimal steady-state inputs, $\mathbf{u}_{SSopt}$, using the steady-state linear plant model given by

$$\mathbf{y}_{sp} = \mathbf{G}_{SS} \cdot \mathbf{u}_{SSopt}. \tag{4.11}$$

4.3 RESULTS

Economic performance of the milling circuit was sensitive to three key levers, throughput, mineral price, and electricity tariffs. The focus of this section is on the sensitivities to mineral and electricity tariffs. Sensitivity to throughput variations will be illustrated in the following chapter. For all simulations run the target hourly average throughput was kept constant at 90 t/h.

4.3.1 Mineral price sensitivity

In order to determine the sensitivity to mineral price the electricity tariff was kept constant for the simulation. Prices used were based on the 2014/15 tariff structure for MegaFlex during the high demand period (see Table 4.3). The mineral price was varied between R10, 000 /ozt and R16, 000 /ozt. Figure 4.1 illustrates the sensitivity of the PWR set-point to mineral price.

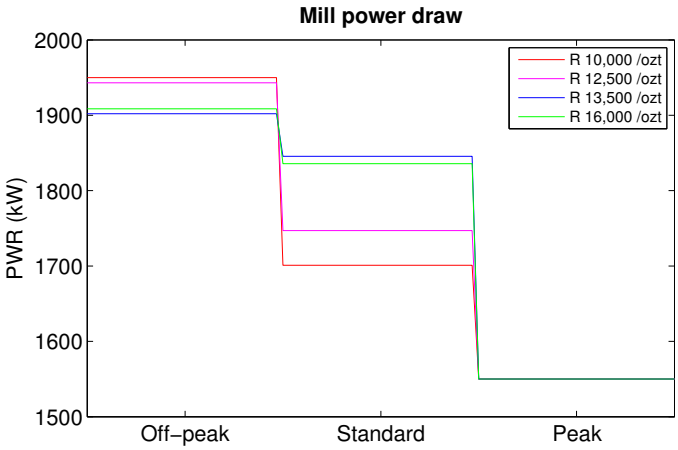

Figure 4.1: Sensitivity of the PWR set-point to changes in the mineral price.

The relationship between the optimized PWR set-point and mineral price was of a proportional nature. What can be seen is that as the mineral price increased, it became more economically viable to operate the milling circuit with a higher power draw during standard tariff periods while maintaining throughput. As the mineral price decreased, the power draw during standard tariff periods was reduced while it was increased during off-peak tariff periods in order to maintain throughput at the lowest electricity cost.

Peak PWR for all three cases remained at the lower limit. This is owing to the large difference between peak and off-peak or standard tariffs and the relatively short period over which peak tariffs last.

4.3.2 Electricity tariff sensitivity

In order to determine the sensitivity to the electricity tariff the mineral price was kept constant at R16, 000 /ozt. The electricity tariffs used were based on the 2011/12 and 2014/15 tariff structures for MegaFlex during both the high and low demand periods (see Table 4.3). The sensitivities to electricity tariff are illustrated in Figure 4.2.

The optimized PWR set-points were driven by the relationship between electricity tariffs during the different periods, i.e. peak, standard, and off-peak. Set-point optimization was not sensitive to the absolute electricity tariff. This is clearly evident when comparing the set-points calculated based on 2011/12 tariffs (blue line) and 2014/15 tariffs (green line) for

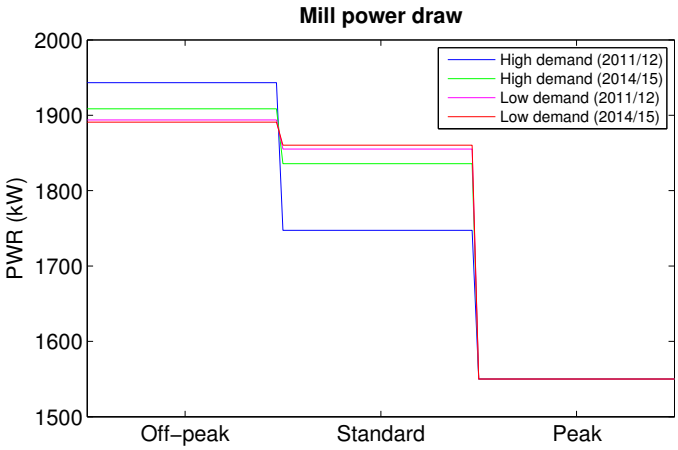

Figure 4.2: Sensitivity of the PWR set-point to changes in the electricity tariff.

the high demand period in Figure 4.2.

If the baseline tariff is considered as the off-peak tariff, then for the 2011/12 tariffs the standard tariff was 87% higher with the peak tariff 617% higher. For the 2014/15 tariffs in comparison, the standard tariff was 84% higher while the peak tariff was only 508% higher than the off-peak tariff for that year. This relational difference is what drove the off-peak PWR set-point to be lower for 2014/15 tariffs than 2011/12 tariffs even though the absolute cost of electricity between the periods increased by approximately 11% p.a. This was the same case, though to a lesser extent, for the low demand periods.

4.4 CONCLUSION

The supervisory controller was developed to minimize the electricity cost associated with running the mill while maintaining a specified weekly average throughput. A non-linear objective function based on the steady-state linear plant model was used to mathematically represent negative profit.

It was found that the relationship between PWR set-point choice and mineral price was a proportional relationship as would be expected. What was interesting is the fact that the relationship between the absolute electricity tariff and PWR set-points is not proportional. PWR set-points are relative to the variation between peak, standard, and off-peak tariffs as the difference between the tariffs presents larger cost saving opportunities for load shifting.

CHAPTER 5

LOAD SHIFTING CONTROLLER

5.1 INTRODUCTION

The complete control structure used for this study is given in Figure 5.1. The process model used was the non-linear Hulbert model as discussed in Chapter 2. Regulatory control was provided by the linear MPC controller as discussed in Chapter 3. Supervisory control was provided via optimal PWR set-points as calculated by the RTO discussed in Chapter 4. Though not considered in this study, the control loop could be extended to include peripheral tools such as DOBs as well as state and parameter estimators (Olivier, Craig and Chen, 2012; Olivier and Craig, 2013; Naidoo et al., 2013).

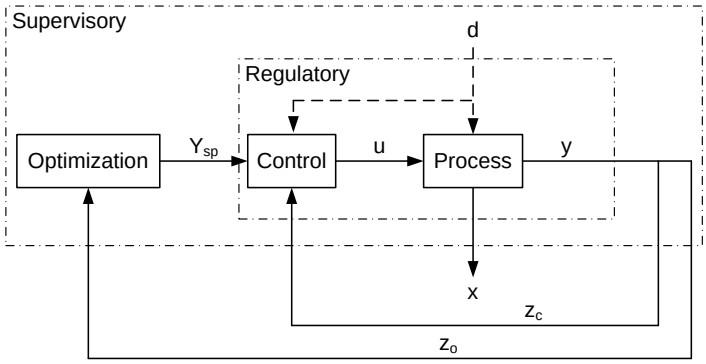

Figure 5.1: Complete control structure.

The complete load shifting controller is presented in this chapter along with some of the design considerations required to integrate the regulatory and supervisory control layers. Scenarios for different throughput requirements are presented along with the simulation res-

ults. These results are analyzed according to technical control objectives as well as economic objectives.

5.2 REGULATORY AND SUPERVISORY LAYER INTEGRATION

Set-points were calculated by the supervisory controller (RTO) and sent to the regulatory controller (MPC). In order to integrate the two layers it was necessary to consider three aspects, the sampling interval of the two controllers, which of the set-points calculated by the RTO were implemented, and whether filtering was applied to the set-points.

5.2.1 Sampling interval

The sampling interval of the RTO (ΔT_{RTO}) was significantly larger than that of the MPC controller (ΔT_{MPC}). The sampling interval of the RTO was chosen to be half of the interval between TOU tariff changes as per the tariff structure (Table 4.2). The sampling interval of the MPC controller was chosen to be as long as possible while still meeting requirements of the fast SLEV dynamics to maintain circuit stability. Regulatory control was used for set-point tracking with a faster time-scale and supervisory control for economic optimization at a medium time-scale (Engell, 2007).

In order to simulate the two controllers for the complete closed loop control in the simulation environment it was necessary that the sampling intervals be a multiple of each other. The simulation interval used was that of the MPC controller as the RTO sampling interval multiplied into the interval. The MPC sampling interval was 10 s and the RTO sampling interval was 30 min. The relationship between the sampling intervals was $\Delta T_{RTO} = 180 \times \Delta T_{MPC}$.

5.2.2 Set-point implementation

Within the RTO optimal set-points for PSE, LOAD, SLEV, and PWR were calculated. Simultaneous implementation of all four optimal set-points decreased the stability of the ROM ore milling circuit. As discussed in Section 2.4, it was important to minimize variations in PSE as well as maintain milling circuit stability. The PSE set-point was chosen in order to maximize recovery downstream from the milling circuit, i.e. the set-point had to be 87% to achieve maximum flotation recovery as indicated in Figure 1.3.

Theoretically, the PSE set-point should be kept at the maximum recovery value, however, there is a trade-off between PSE and throughput (Bauer and Craig, 2008), i.e. the higher the PSE the lower the throughput, resulting in milling circuits usually being operated below the maximum recovery PSE value (Duarte et al., 1999). RTO results indicated that PSE should be 81.2%, 81.8%, and 82.9% during peak, standard, and off-peak periods respectively. To reduce variations in PSE though, the PSE set-point was maintained at 82% which lies in the middle of the range of the RTO results, while still allowing for higher throughput.

Additional design choices were made to improve milling circuit stability. Set-points for LOAD and SLEV were maintained at the nominal values, which were in the middle of the respective operating regions. By maintaining the SLEV set-point and marginally relaxing SLEV control, control of PSE was improved. Similarly, maintaining the LOAD set-point while allowing increased variations in LOAD, improved control of PSE and PWR. Therefore, only the PWR set-point was changed according to the supervisory controller.

5.2.3 Set-point filtering

The set-point change mechanism used to implement the PWR set-point changes had an influence on the performance of the controller. Figure 5.2 illustrates the difference in controller performance when the PWR set-point was changed using a step change, ramp change, or first-order filtered change.

The step change mechanism occurred at the time of the set-point change. For the ramp change mechanism the set-point was changed using a ramp persisting for 0.2 h with the gradient,

$$m = \left(PWR_{sp}(old) - PWR_{sp}(new)\right)/0.2. \tag{5.1}$$

The filtered set-point change was implemented by filtering the set-point step change with a first-order filter with time constant of 0.1 h, given by

$$G(s) = \frac{1}{0.1s + 1}. \tag{5.2}$$

Step changes to the PWR set-point resulted in poor controller performance, specifically with respect to PSE and SLEV. Sudden change of PWR caused erratic deviations in PSE, and while the controller attempted to correct these deviations, SLEV approached its constraints.

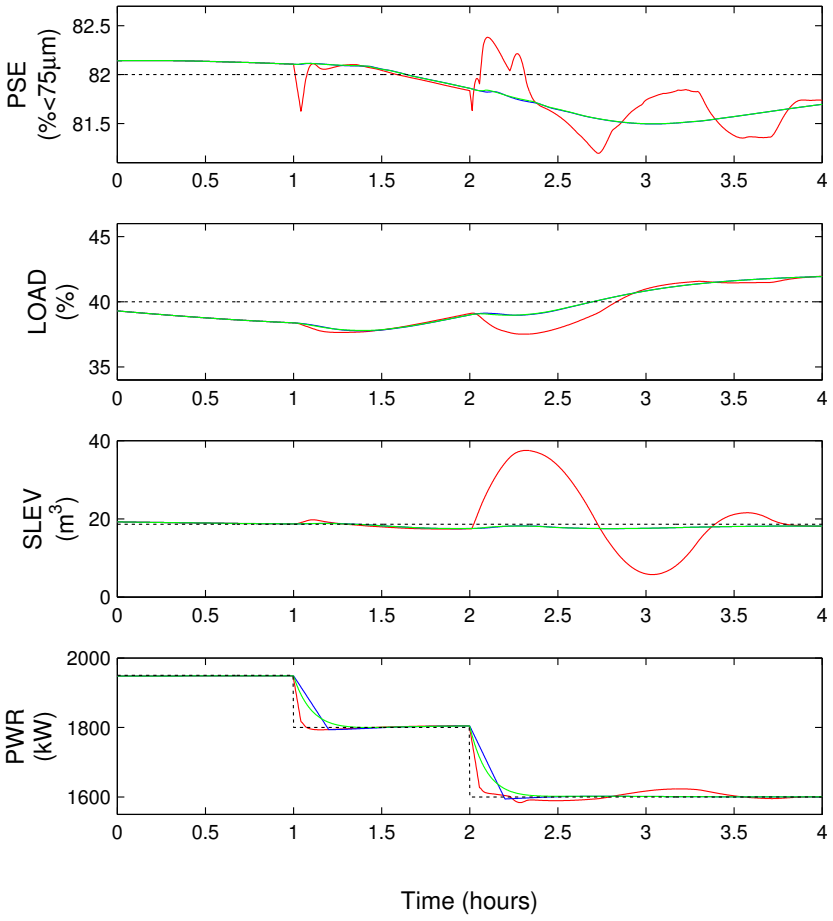

Figure 5.2: CV responses for a step change (red line), ramp change (blue line), and filtered change (green line) of the PWR set-point.

Similar responses were observed for the ramp and filtered set-point changes. Though PSE varied for these set-point changes it did so very gradually, while SLEV and LOAD varied comfortably within their respective operating ranges. Owing to the simplicity of implementing filtered as opposed to ramp set-point changes a filter was used between the supervisory and regulatory controllers.

5.3 THROUGHPUT SIMULATIONS

In order to evaluate the economic benefit of the complete load shifting controller, it was necessary to develop scenarios to compare the performance of the load shifting controller to a baseline. Two forms of simulations were performed, fixed power simulations and load

shifting simulations. For the fixed power simulations the PWR set-point was kept constant to achieve a specified throughput over the simulation horizon. For the load shifting simulations, the complete controller was used to minimize electricity costs while meeting a specified throughput target over the simulation horizon. Settings for the different simulations are given in Table 5.1.

Table 5.1: Inputs used for the load shifting controller throughput simulations.

Scenario	Throughput (t/h)	Electricity tariffs (financial year)	Mineral price (ZAR/ozt)
High throughput	94.97	2014/15	16,000
Moderate throughput	90.76	2014/15	16,000
Low throughput	88.47	2014/15	16,000

Results for the high throughput simulation are presented in Figure 5.3 and 5.4 for high and low demand periods respectively. Simulation results for the moderate throughput simulation are shown in Figure 5.5 and 5.6 for high and low demand periods respectively.

Results for the low throughput simulation are shown in Figure 5.7 and 5.8 for high and low demand periods respectively. The high demand period simulation failed as the milling circuit was moved to and maintained at an operating point where the linear plant model for the regulatory controller was no longer valid. This operating region is entered when PWR is significantly lower than the operating point around which the linear plant models were developed for long periods. In this region SLEV becomes unstable and the regulatory controller is unable to recover stability of the milling circuit.

The operating point for PWR around which the model was linearized is 1,855 kW, while during the simulation the PWR set-point was between 1,550 kW and 1,656 kW for more than 67% of the time. In order to prevent the non-linear model from moving into an operating region where the linear controller fails, the RTO constraints were modified. Lower constraints on PWR were made variable according to the electricity tariff periods. The lower PWR constraints for off-peak and standard tariff periods were both changed to 1,800 kW and for peak tariff periods the constraint was left at 1,550 kW. The simulation results are presented in Figure 5.9.

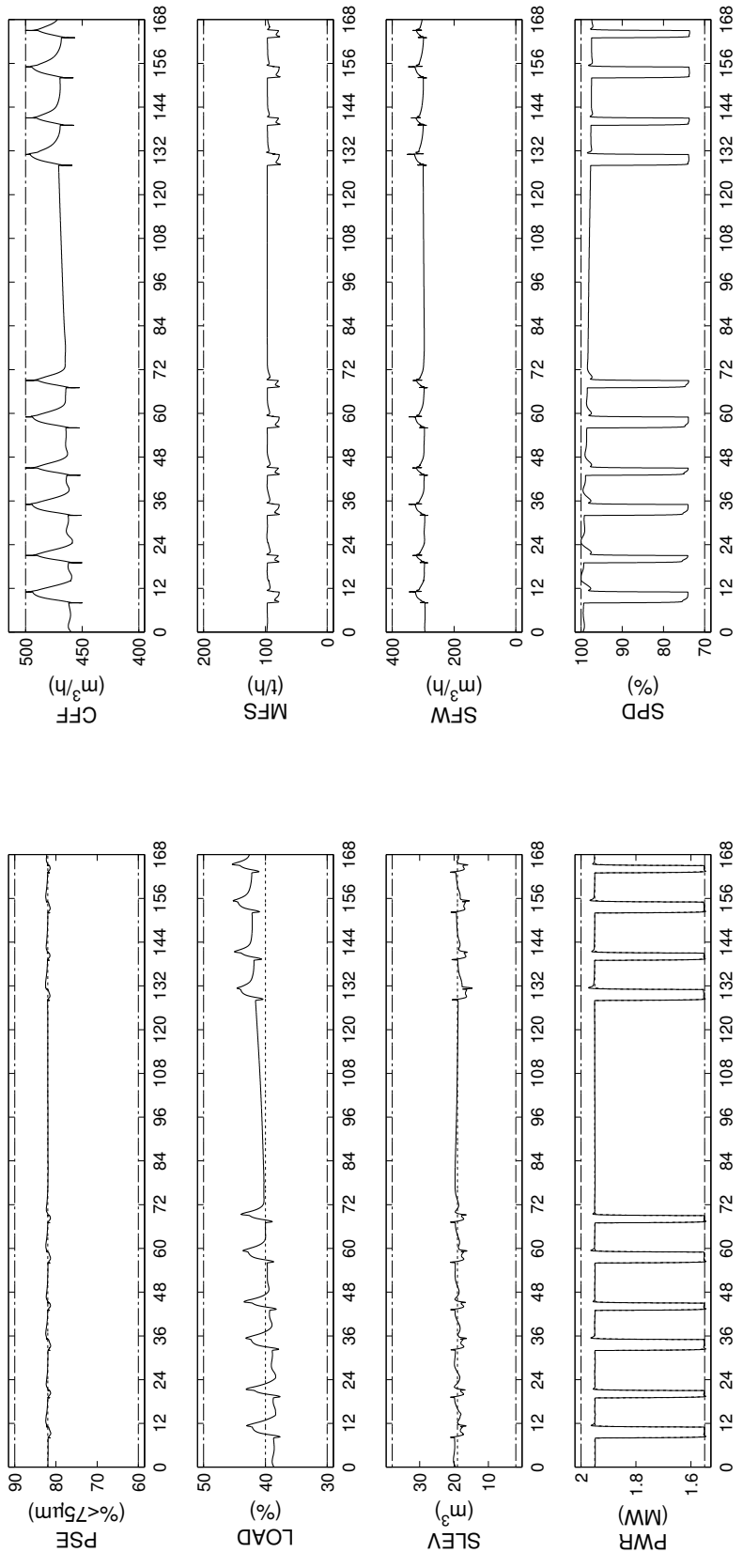

(a) CV responses for the simulation.

(b) MV responses for the simulation.

Figure 5.3: Simulation results for the high throughput scenario during the high demand tariff period. Solid lines indicate CVs and MVs, dotted lines the set-points, and dash-dotted lines the constraints.

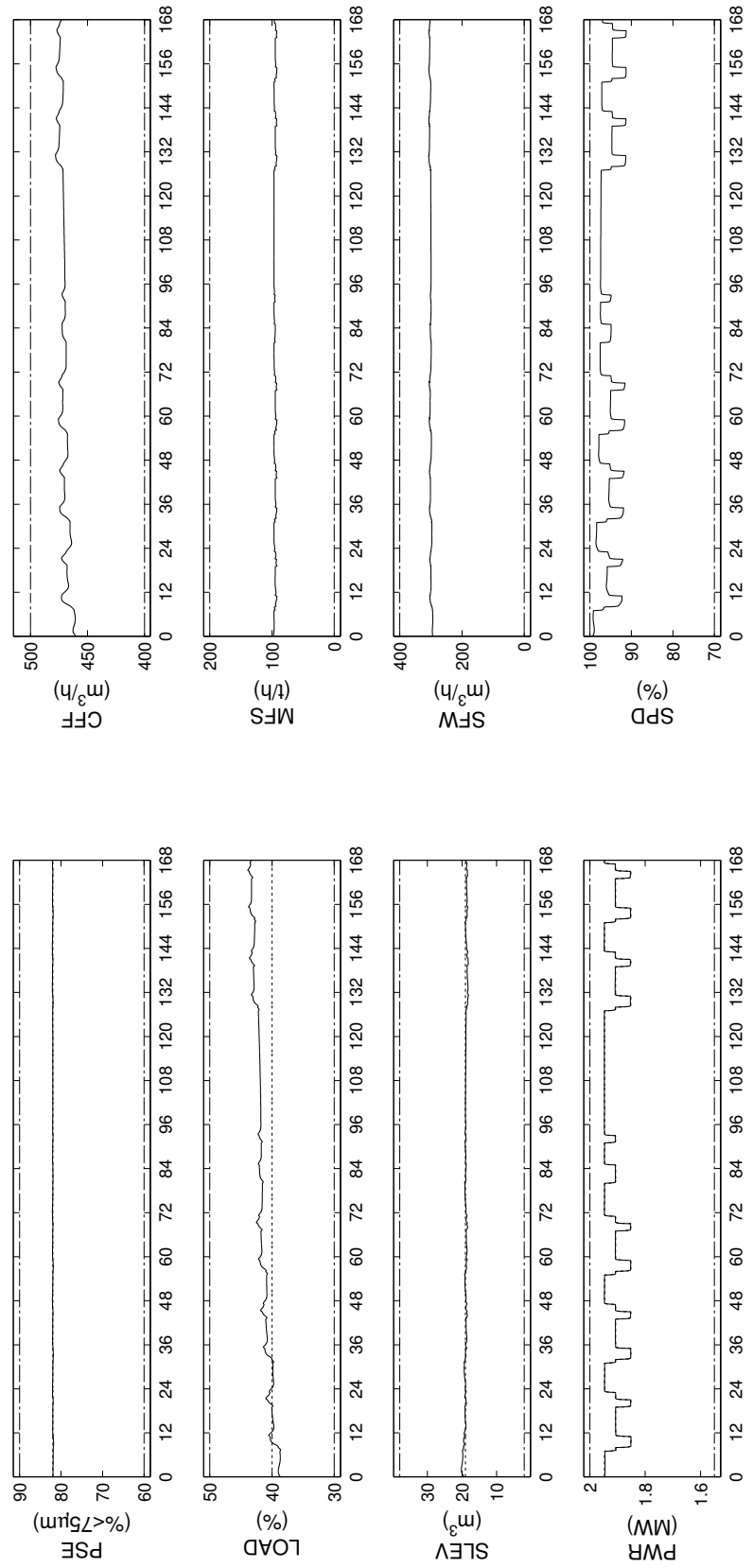

(a) CV responses for the simulation.

(b) MV responses for the simulation.

Figure 5.4: Simulation results for the high throughput scenario during the low demand tariff period. Solid lines indicate CVs and MVs, dotted lines the set-points, and dash-dotted lines the constraints.

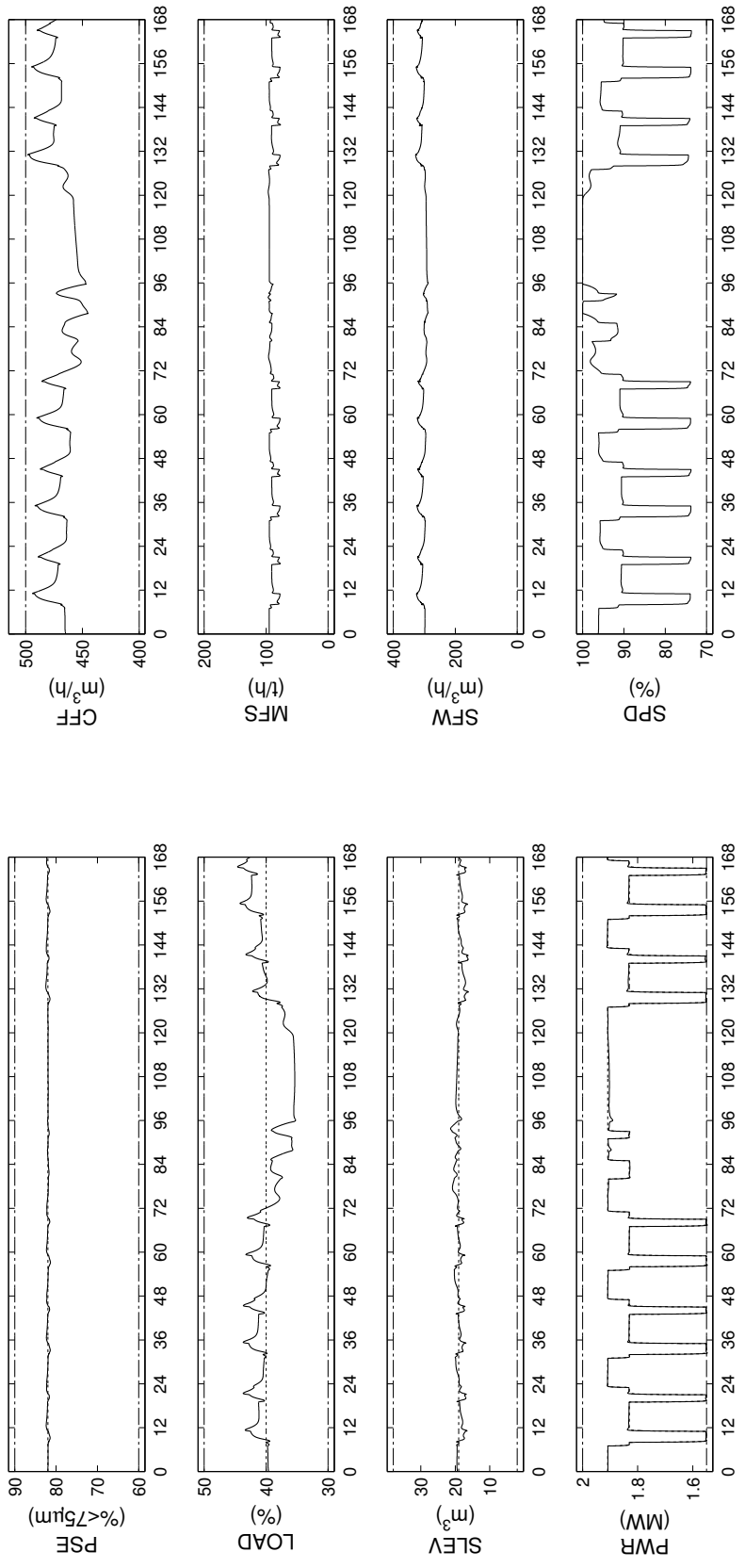

(a) CV responses for the simulation.

(b) MV responses for the simulation.

Figure 5.5: Simulation results for the moderate throughput scenario during the high demand tariff period. Solid lines indicate CVs and MVs, dotted lines the set-points, and dash-dotted lines the constraints.

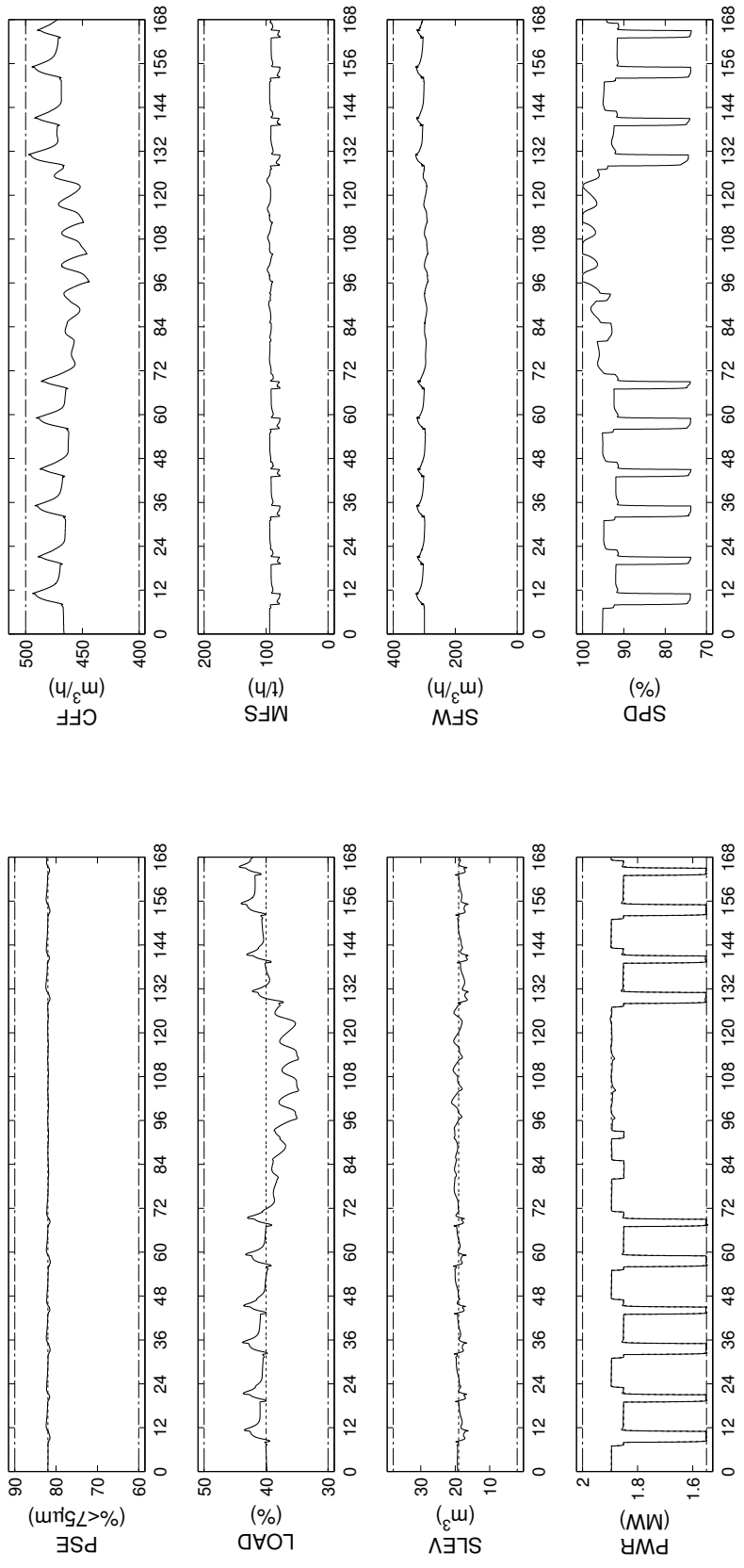

(a) CV responses for the simulation.

(b) MV responses for the simulation.

Figure 5.6: Simulation results for the moderate throughput scenario during the low demand tariff period. Solid lines indicate CVs and MVs, dotted lines the set-points, and dash-dotted lines the constraints.

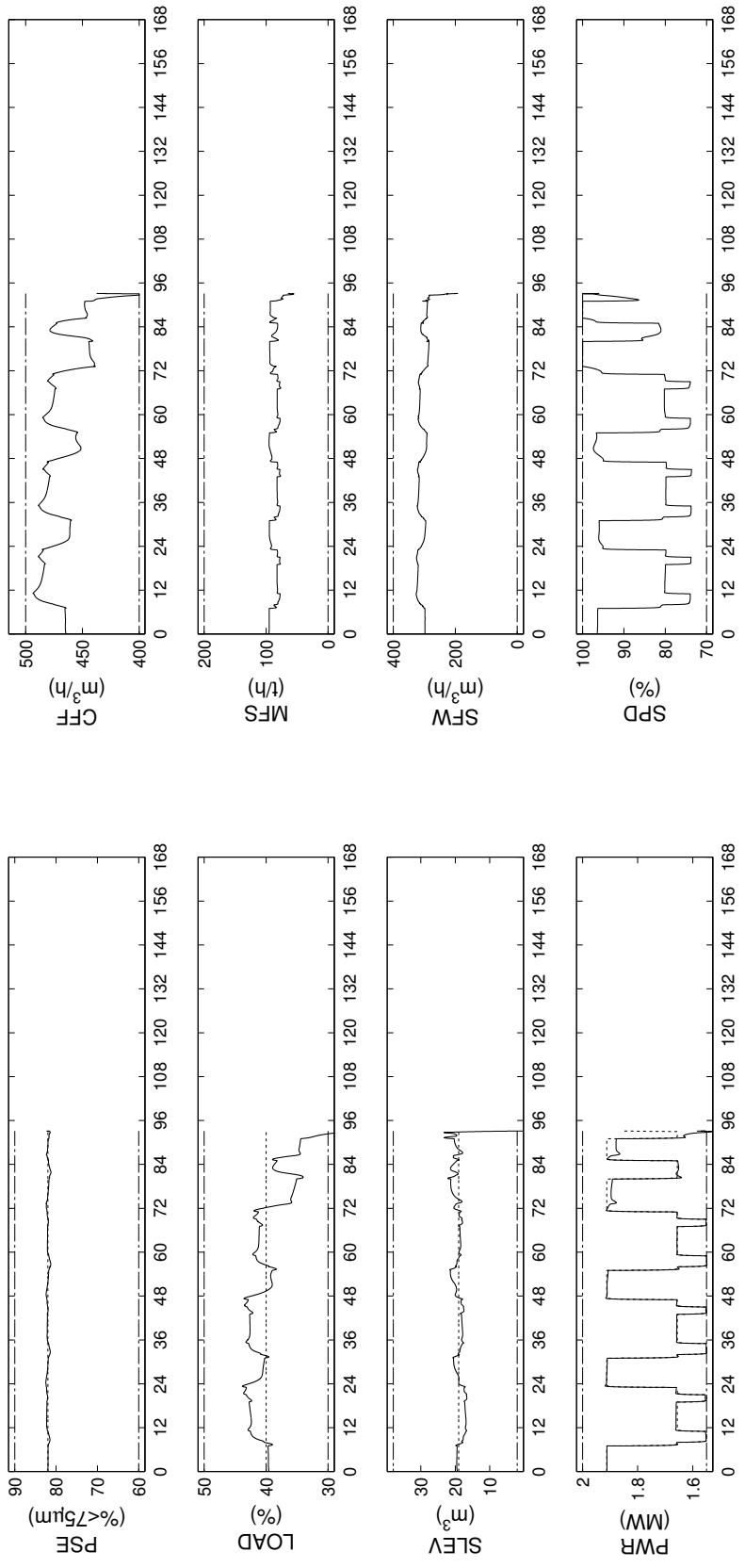

(a) CV responses for the simulation.

(b) MV responses for the simulation.

Figure 5.7: Simulation results for the low throughput scenario during the high demand tariff period. Solid lines indicate CVs and MVs, dotted lines the set-points, and dash-dotted lines the constraints.

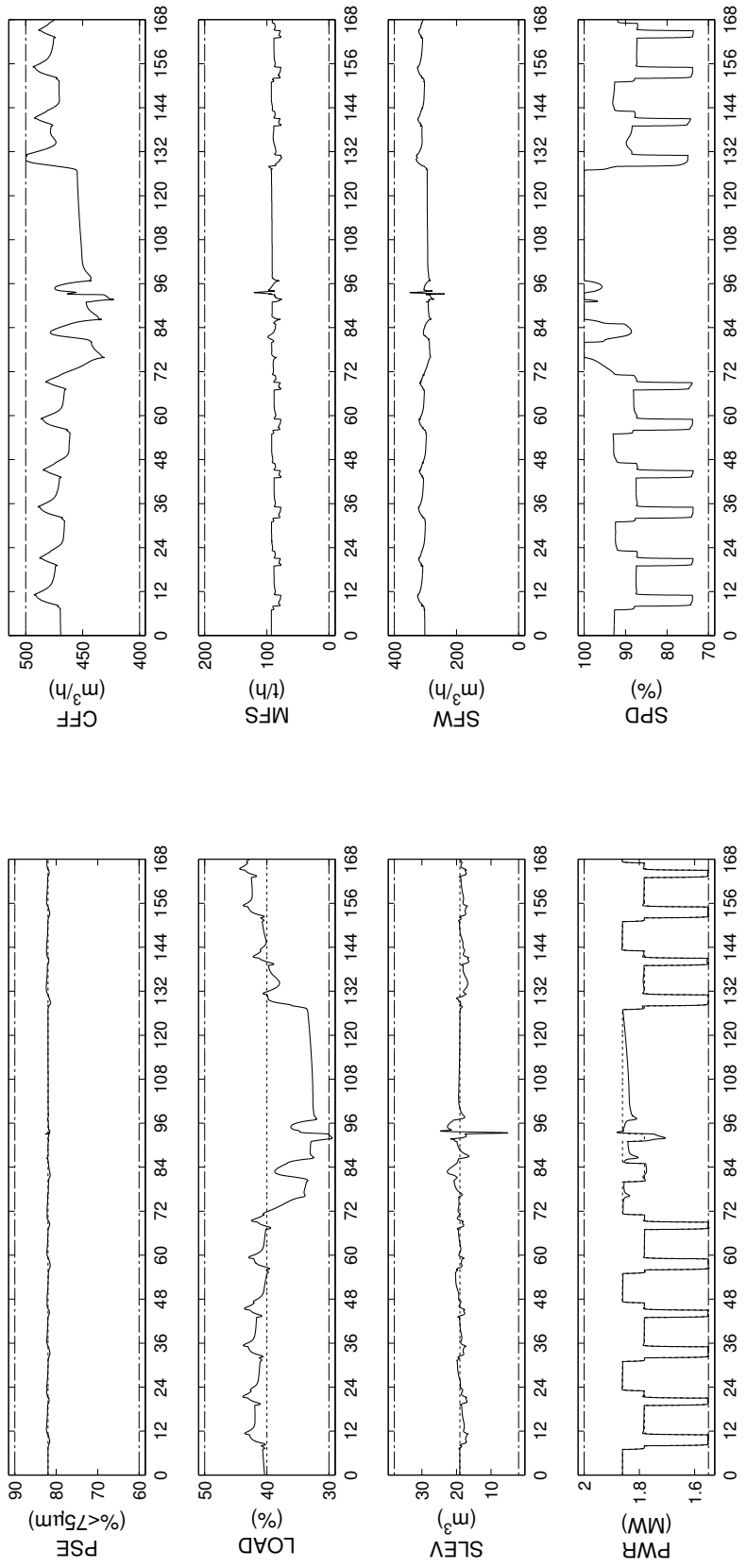

(a) CV responses for the simulation.

(b) MV responses for the simulation.

Figure 5.8: Simulation results for the low throughput scenario during the low demand tariff period. Solid lines indicate CVs and MVs, dotted lines the set-points, and dash-dotted lines the constraints.

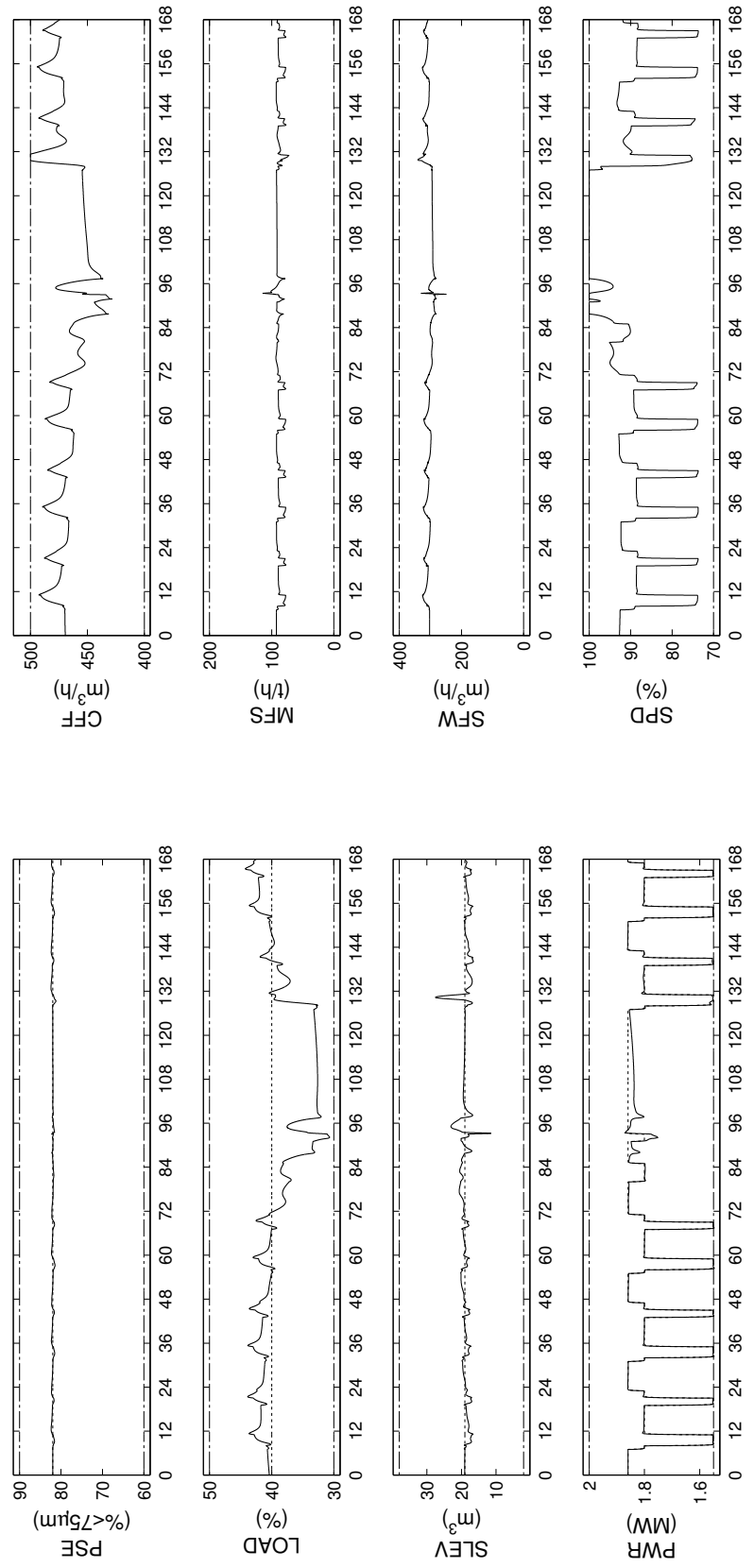

(a) CV responses for the simulation.

(b) MV responses for the simulation.

Figure 5.9: Simulation results for the low throughput scenario during the high demand tariff period using variable constraints on PWR for the RTO. Solid lines indicate CVs and MVs, dotted lines the set-points, and dash-dotted lines the constraints.

5.4 ANALYSIS OF RESULTS

Results of the simulations for the complete load shifting controller were evaluated from two points of view. First, the technical feasibility was evaluated by considering the control objectives. Second, the economic feasibility of the controller was evaluated by considering electricity cost reduction, decreased cost per unit of production, and costs attributed to to additional ore inventory storage.

5.4.1 Milling circuit stability

From the simulation results it is clear that milling circuit stability was maintained by the load shifting controller. This was, however, with exception to the low throughput, high demand period simulation. For the successful simulations the CVs and MVs remained comfortably within their constraints. In addition, CFF, MFS, and SFW maintained significant room to maneuver within their constraints if disturbances were to be introduced (see Section 3.7 for further discussion).

Through tight control of PSE, the control objective *maintain the quality of the product by decreasing product size fluctuations* was met for the high and moderate throughput simulations. The PSE mean and standard deviation for the high, moderate, and low throughput simulations are given in Table 5.2. Given the low magnitude and long time dynamic of the PSE variations, downstream processes would be minimally affected (McKee, 1991).

Table 5.2: Mean and standard deviation of PSE from simulation results.

Simulation	$\overline{\text{PSE}}$ (%)	$\sigma\overline{\text{PSE}}$ (%)
High throughput	82.009	0.101
Moderate throughput	82.008	0.208
Low throughput	82.013	0.197

The modified constraints ensure that the milling circuit operates with mill power draw at, or over, 1800 kW for approximately 67% of the time. This ensures that the milling circuit is kept within the operating region where the MPC linear model remains valid and can maintain stability. This is not necessarily an optimal solution as the region in which the RTO attempts

to minimize the objective function is limited. In order to maximize this region either gain scheduled linear MPC or non-linear MPC could be developed for the regulatory controller. Development of a different controller was not covered in this study.

5.4.2 Electricity cost reduction

Electricity costs were calculated based on the average mill power draw over every hour of the simulation billed at the applicable tariff for that hour. Total electricity cost was given by the cumulative electricity cost over the simulation horizon calculated using,

$$C_{tot} = \sum_{t=1}^{168} \left[c(t) \times \Delta T_{MPC} \sum_{i=0}^{1/\Delta T_{MPC}-1} [PWR(i + t/\Delta T_{MPC})] \right], \tag{5.3}$$

where $PWR(i + t/\Delta T_{MPC})$ is the mill power at sampling instant $i + t/\Delta T_{MPC}$, $c(t)$ is the TOU tariff applicable at time t as given in Table 4.3, and ΔT_{MPC} is the sampling interval of the MPC controller in hours.

Total electricity cost for each of the simulation scenarios is presented in Table 5.3. Load shifting the milling circuit was shown to save up to 5.8% on electricity costs when compared to running the milling circuit with a constant mill power draw.

Table 5.3: Electricity cost attributable to the milling circuit (ZAR million).

Scenario	High demand season (13 w)		Low demand season (39 w)	
	Load shifting	Baseline	Load shifting	Baseline
High throughput	0.232	0.246	0.147	0.145
Moderate throughput	0.226	0.239	0.138	0.144
Low throughput	0.223	0.234	0.134	0.138

When considering the operation of the milling circuit over a year, high and low demand season tariffs would be incurred, high demand from June to August and low demand from September to May. Combining the cost of the high demand season (approximately 13 weeks) and low demand season (approximately 39 weeks) gave an annual cost for each scenario.

Annual electricity cost for the high throughput scenario showed a 1.2% decrease from R8.85 m for the baseline to R8.75 m for load shifting. The moderate throughput scenario showed a 4.8% improvement from R8.72 m without load shifting to R8.32 m with load shifting. For the

low throughput scenario a 3.7% improvement from R8.42 m to R8.13 m with load shifting was observed.

5.4.3 Turnover

In order to compare the load shifting controller performance to a throughput constrained milling circuit the income attributed to the milling circuit was calculated by

$$I_{tot} = 168 \times HG \times P_{ADJ} \times TPT_{achieved} \times \vartheta(PSE_{achieved}), \tag{5.4}$$

where $TPT_{achieved}$ was the average throughput over the simulation horizon given by

$$TPT_{achieved} = 168/\Delta T_{MPC} \sum_{t=1}^{168/\Delta T_{MPC}} \left[TPT(t/\Delta T_{MPC})\right]. \tag{5.5}$$

$PSE_{achieved}$ was the average product particle size over the simulation horizon given by

$$PSE_{achieved} = 168/\Delta T_{MPC} \sum_{t=1}^{168/\Delta T_{MPC}} \left[PSE(t/\Delta T_{MPC})\right]. \tag{5.6}$$

HG was the head grade of the mined ore given as 3 g/t, P_{ADJ} was the adjusted price as in (4.5), and $\vartheta(PSE_{achieved})$ was the recovery based on average PSE given by (4.4). Income based on throughput and product particle size for each simulation is presented in Table 5.4.

Table 5.4: Income attributable to the milling circuit (ZAR million).

Scenario	High demand season (13 w)		Low demand season (39 w)	
	Load shifting	Baseline	Load shifting	Baseline
High throughput	12.98	13.13	13.18	13.13
Moderate throughput	12.56	12.55	12.55	12.56
Low throughput	12.28	12.23	12.23	12.23

As per the method discussed in Section 5.4.2, the total turnover for a year was calculated for the high and moderate throughput scenarios. Little difference was observed between the turnover for baseline simulations versus load shifting simulations. This was expected as the PSE mean and average throughput did not significantly differ between baseline and load shifting simulations.

Estimated turnover for the high throughput scenario was R682.95 m with load shifting and R682.94 m without. Estimated turnover for the moderate throughput scenario was R652.87 m with load shifting and R652.88 m without. Estimated throughput for the low throughput simulation was higher with load shifting (R636.61 m) than without (R635.96 m).

5.4.4 Cost improvement per unit production

Cost improvement per unit production was a direct comparison of the electricity cost of producing platinum with and without load shifting, given by

$$C_{improvement} = \frac{[C_{tot(baseline)} - C_{tot(load\,shifting)}]}{TPT_{achieved} \times HG}, \tag{5.7}$$

where $TPT_{achieved}$ was the throughput achieved, HG was the head grade (3 g/t), $C_{tot(baseline)}$ was the total electricity cost for the baseline simulation, and $C_{tot(loadshifting)}$ was the total electricity cost for the mill power load shifting simulation.

Resulting daily cost improvements over a year were R8.09 per gram, R19.22 per gram, and R20.78 per gram for the high, moderate, and low throughput scenarios respectively. This relates to R1.89 m p.a. for a milling circuit that processes on average 90 t/h. As the milling circuit operates further from maximum throughput the cost improvement increases as more load can be shifted to off-peak periods.

5.4.5 Effect on storage requirements

In order to perform load shifting on the milling circuit it is necessary to have a storage facility where excess ore can be stored during peak and standard periods where throughput is reduced. In the case where the milling circuit is a capacity constraint to the throughput, the RTO optimized the PWR set-point to the maximum in order to process the maximum throughput for that period. Storage requirements would therefore only be required during reduced throughput periods and over a week there would be no nett storage. Change in the holdup of ore within the silo can be given by

$$\frac{dX_{so}}{dt} \triangleq V_{si} - V_{so}, \tag{5.8}$$

where X_{so} [t] is the holdup of ore within the silo ($X_{so}(0) = 0$), V_{si} [t/h] is the feed-rate of ore from upstream into the silo and V_{so} [t/h] is the feed-rate of ore to the milling circuit ($V_{so} = MFS$).

The maximum additional holdup of ore within the silo would be 157.6 t for the moderate throughput scenario and 144.0 t for the high throughput scenario. The maximum holdup within the silo would be 7.24% and 6.32% of the daily average throughput for the moderate and high scenario simulations respectively.

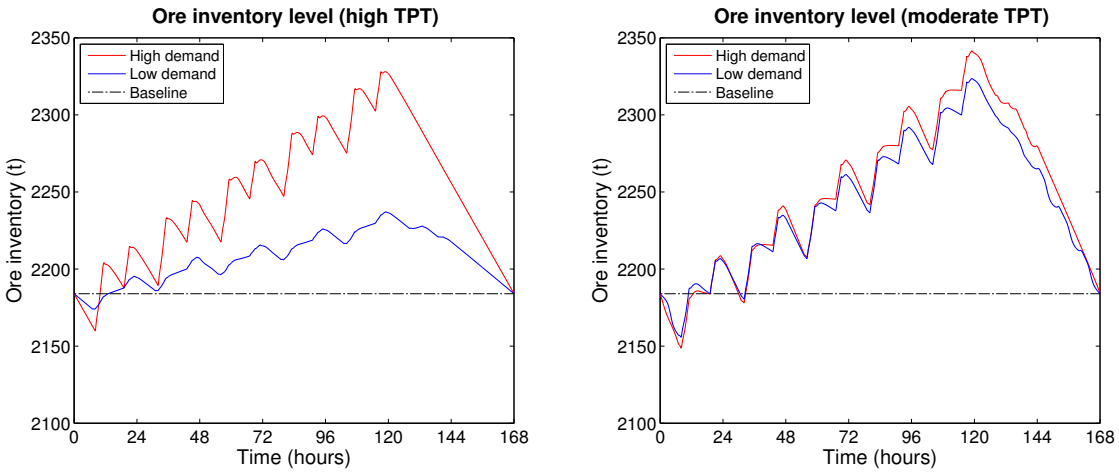

(a) High throughput scenario.

(b) Moderate throughput scenario.

Figure 5.10: The ore inventory level in tons for the high and moderate demand scenarios. The high demand periods (red line) are compared to the low demand periods (blue line).

For a safety stockpile sized to meet a week's worth of production at a throughput of 90 t/h, (Jacobs, Chase and Aquilano, 2009), the maximum additional holdup would be 1.04% and 0.95% of the week's safety stock capacity (15, 120 t) for the moderate and high throughput scenarios respectively. It is therefore not anticipated that any additional inventory costs would be incurred by implementing DSM.

5.5 CONCLUSION

Revised control objectives as discussed in Section 2.4 were met by the load shifting controller. Stability requirements *maintain milling circuit stability* and *minimize product size fluctuations* were met by the regulatory controller. The supervisory controller met the economic objectives *maintain a specified average throughput over a week* and *minimize cost attributed to electricity consumption.*

It was shown that by load shifting the milling circuit, savings of up to R20.78 per gram of

unrefined platinum could be realized. The highest savings were observed when throughput was the lowest as the maximum load could be shifted to off-peak periods. Cost savings were related to up to R1.89 m p.a. for a milling circuit that processes on average 90 t/h at a head grade of 3 g/t.

It is not anticipated that there would be any additional cost attributed to handling inventory during periods where the throughput of the milling circuit is lower. Based on the simulations, additional ore storage for 158 t would be required which is only 1.04% of the recommended inventory capacity. Additional cost required to realize the projected economic benefits would therefore be limited to the cost of implementing the advanced control system and some form of variable speed control on the mill if none exists.

The milling circuit enters an unstable operating point when the PWR is below approximately $1,800$ kW for more than 67% of the time. This is owing to the operating point around which the non-linear model was linearized. Variable constraints depending on the tariff period were implemented on the RTO to maintain stability.

The variable PWR constraints limit the feasible region of the RTO possibly reducing the economic benefit of the load shifting controller. The feasible region could be increased by implementing a regulatory controller that can guarantee stability over a wider operating region. This could be achieved by using either gain scheduled linear MPC or non-linear MPC.

CHAPTER 6

CONCLUSION

6.1 SUMMARY OF RESULTS

It was proposed that owing to developments in the South African electricity sector and platinum market, traditional control objectives for milling circuits are no longer optimal. Throughput was traditionally maximized in a trade-off between throughput and electricity consumption. Motivation for this trade-off was based on the argument that the return earned on platinum far exceeds the cost of electricity.

In order to challenge the optimality of the control objectives demand side management was implemented through load shifting. This implementation of DSM was performed using advanced process control on the non-linear Hulbert milling circuit model. A load shifting controller was developed based on a two-layer hierarchy using supervisory and regulatory controllers.

Regulatory control was implemented by using linear MPC to control the non-linear model. The objective of the regulatory controller was to maintain milling circuit stability and introduce control of mill power draw, which is traditionally not directly controlled. Mill speed was identified as the most appropriate manipulated variable to be used to achieve functional controllability.

Development of the regulatory controller required identification of a linear plant model which was achieved using SID. The identified linear model was consistent with literature based on a similar non-linear model. Simulations were used to tune the regulatory controller for receding horizon control as traditional tuning parameters were computationally infeasible. Around the

operating point of the linear plant model the controller performed well.

Supervisory control was implemented using a real-time optimizer to maximize an objective function describing milling circuit profitability based on turnover, driven by throughput, and electricity cost. The RTO was developed to achieve a given average throughput over a week-long period according to TOU tariffs. This was related to the milling circuit through a steady-state plant model.

Implementation of DSM on a milling circuit shows that it is viable to reduce operating costs associated with electricity consumption and increase profitability on a milling circuit. This was shown to be possible while maintaining milling circuit stability for average weekly throughput as low as 90 t/h. As throughput was decreased below 90 t/h the milling circuit was required to operate outside the region for which the linear MPC models were developed which resulted in instability.

In order to prevent the load shifting controller from entering the unstable operating region the supervisory controller was modified by adding variable constraints on PWR. A lower constraint of $1,800$ kW during off-peak and standard tariff periods was introduced for PWR while during peak periods the lower constraint remained $1,550$ kW. This ensured that the milling circuit remained stable with the linear regulatory controller. In order to increase the operating region of the controller it is proposed that either gain scheduled linear MPC or non-linear MPC be investigated.

Sensitivities to optimization of the milling circuit were identified to be mineral price, electricity tariffs, and average throughput requirements. Mineral price sensitivities indicated that the optimization of the PWR set-points is proportional to the relationship between mineral price and electricity tariffs. This is consistent with traditional control objectives where throughput was maximized owing to high returns compared to historically low electricity tariffs.

Electricity tariff sensitivities were interesting as optimization of the PWR set-points was not affected by the absolute electricity tariff but rather the relationship between tariffs during off-peak, standard, and peak periods. This was consistent with expectations as turnover of the milling circuit significantly exceeds the operating costs associated with electricity. Cost savings using load shifting are achieved through the exploitation of the TOU tariff structure

given specific milling circuit throughput requirements.

It is shown that the load shifting controller responded to changes in weekly average throughput by varying the PWR set-point. The controller was most effective in the operating range between 90% and 100% of maximum throughput. When the milling circuit was throughput constrained the load shifting controller maximized the PWR set-point which effectively disables load shifting. This is consistent with traditional operation of milling circuits. As throughput requirements were reduced, a wider range of PWR set-points were implemented resulting in operating cost savings.

Operating cost savings associated with electricity consumption were realized when implementing the load shifting controller on the non-linear Hubert milling circuit model. Based on comparisons between baseline and load shifting controller simulations it was estimated that cost savings of between R16.51 and R20.78 per gram of unrefined platinum could be made. This was equivalent to an annual cost saving of up to R1.89 m for a milling circuit that processes an average of 90 t/h of 3 g/t head grade ROM ore.

6.2 CONCLUDING REMARKS

DSM implemented through process control to load shift a milling circuit according to TOU tariffs is a viable solution to address rising operating costs through electricity tariff increases. Load shifting was implemented using a linear MPC controller and a non-linear RTO at the recovery and supervisory control layers respectively. Load shifting does not reduce operating costs for a throughput constrained milling circuit.

Implementation of a load shifting controller requires a milling circuit that has a some form of mill speed control capability. In an industry-wide survey addressing milling circuit control 90% of the respondents indicated that electric motors are used as the actuator for mill speed (Wei and Craig, 2009a).

It is necessary to have capacity for ore inventory storage in order to load shift the milling circuit. It is expected, however, that such a storage facility would be available for any given milling circuit. Based on the assumption that a storage facility would exist, no additional inventory storage costs would be anticipated to implement load shifting. Additional storage

capacity required to meet load shifting requirements is negligible compared to standard design capacities.

6.3 SUGGESTIONS FOR FURTHER WORK

In order to improve the operating range of the load shifting controller, gain scheduled linear MPC and non-linear MPC should be investigated to replace the regulatory controller. It is also possible that further improvement of the regulatory controller could be achieved by increasing the prediction horizon using a multi-rate controller (Halldorsson et al., 2005). Exploration of Jacobian linearization should be investigated to potentially improve linear MPC. This can be expanded using closed-loop steady-state gain models for the supervisory controller.

Expansion of the supervisory controller to evaluate other costs associated with load shifting the milling circuit should be investigated. Additional costs that should be investigated and added to the RTO model include

- steel ball consumption,
- mill liner wear, and
- water consumption.

Validation of the complete load shifting controller should be performed based on incorporation of the peripheral tools developed for milling circuit control. These tools include state and parameter estimation which could improve performance of the regulatory controller (Olivier and Craig, 2013).

REFERENCES

Amestica, R., Gonzalez, G. D., Menacho, J. and Barria, J. (1996). A mechanistic state equation model for semiautogenous mills, *International Journal of Mineral Processing* **44-45**(SPEC. ISS.): 349–360.

Apelt, T. A., Asprey, S. P. and Thornhill, N. F. (2002). Inferential measurement of sag mill parameters ii: State estimation, *Minerals Engineering* **15**(12): 1043–1053.

Atkins, A. R. and Hinde, A. L. (1975). Measurement and control of particle size in a milling circuit, *ISA Transactions* **14**(4): 318–323.

Atkins, A. R., Hinde, A. L., Lloyd, P. J. D. and Mackay, J. G. (1974). Control of milling circuits, *Journal of the South African Institute of Mining and Metallurgy* **74**(11): 388–395.

Badenhorst, W., Zhang, J. and Xia, X. (2011). Optimal hoist scheduling of a deep level mine twin rock winder system for demand side management, *Electric Power Systems Research* **81**(5): 1088–1095.

Bauer, M. and Craig, I. K. (2008). Economic assessment of advanced process control – A survey and framework, *Journal of Process Control* **18**(1): 2–18.

Bemporad, A., Morari, M. and Ricker, N. L. (2004). Model predictive control toolbox, *The Matlab user's guide* .

Borell, M., Bäckström, P.-O. and Söderberg, L. (1996). Supervisory control of autogenous grinding circuits, *International Journal of Mineral Processing* **44-45**: 337–348.

Camacho, E. F. and Bordons, C. (2004). *Model predictive control*, Vol. 2, Springer London.

Chen, X. S., Li, Q. and Fei, S. M. (2008a). Constrained model predictive control in ball mill grinding process, *Powder Technology* **186**(1): 31–39.

Chen, X. S., Li, Q. and Fei, S. M. (2008b). Supervisory expert control for ball mill grinding circuits, *Expert Systems with Applications* **34**(3): 1877–1885.

Chen, X. S., Zhai, J. Y., Li, S. H. and Li, Q. (2007). Application of model predictive control in ball mill grinding circuit, *Minerals Engineering* **20**(11): 1099–1108.

Coetzee, L. C. (2009). *Robust nonlinear model predictive control of a closed run-of-mine ore milling circuit*, PhD thesis, University of Pretoria.

Coetzee, L. C., Craig, I. K. and Kerrigan, E. C. (2010). Robust nonlinear model predictive control of a run-of-mine ore milling circuit, *IEEE Transactions on Control Systems Technology* **18**(1): 222–229.

Craig, I. K. (2012). Grinding mill modeling and control: Past, present and future, *Chinese Control Conference, CCC* pp. 16–21.

Craig, I. K., Hulbert, D. G., Metzner, G. and Moult, S. P. (1992). Optimized multivariable control of an industrial run-of-mine milling circuit., *Journal of the South African Institute of Mining and Metallurgy* **92**: 169–176.

Craig, I. K. and Koch, I. (2003). Experimental design for the economic performance evaluation of industrial controllers, *Control Engineering Practice* **11**(1): 57–66.

Craig, I. K. and MacLeod, I. M. (1995). Specification framework for robust control of a run-of-mine ore milling circuit, *Control Engineering Practice* **3**(5): 621–630.

Craig, I. K. and MacLeod, I. M. (1996). Robust controller design and implementation for a run-of-mine ore milling circuit, *Control Engineering Practice* **4**(1): 1–12.

Cramer, L. A. (2008). What is your pgm concentrate worth?, *3rd International Platinum Conference 'Platinum in Transformation', SAIMM* pp. 387–394.

Cutler, C. and Perry, R. (1983). Real time optimization with multivariable control is required to maximize profits, *Computers and Chemical Engineering* **7**(5): 663–667.

Daniel, M. J. (2011). Comminution efficiency attracts attention, *AusIMM Bulletin* **5**: 20–24.

Desbiens, A., Núñez, E., Del Villar, R., Hodouin, D. and Poulin, E. (2008). Using process control to increase the energy efficiency of mineral and metal processing plants, *International Journal of Power and Energy Systems* **28**(2): 146–151.

Duarte, M., Sepúlveda, F., Castillo, A., Contreras, A., Lazcano, V., Giménez, P. and Castelli, L. (1999). A comparative experimental study of five multivariable control strategies applied to a grinding plant, *Powder Technology* **104**(1): 1–28.

Engell, S. (2007). Feedback control for optimal process operation, *Journal of Process Control* **17**(3): 203–219.

Eskom (2007). Annual report 2007, Web site: http://financialresults.co.za/2007/eskomar2007_launch/ [Last accessed: 14 Sep 2014].

Eskom (2011). Tariffs and charges booklet 2011/2012, Web site: http://www.eskom.co.za/CustomerCare/TariffsAndCharges/Documents/Tariff_brochure_20112.pdf [Last accessed: 14 Sep 2014].

Eskom (2012). Integrated report 2012, Web site: http://www.financialresults.co.za/2012/eskom_ar2012/ [Last accessed: 14 Sep 2014].

Eskom (2014a). Integrated report 2014, Web site: http://integratedreport.eskom.co.za/ [Last accessed: 14 Sep 2014].

Eskom (2014b). Tariffs and charges booklet 2014/2015, Web site: http://www.eskom.co.za/CustomerCare/TariffsAndCharges/Documents/TariffBrochureV9.pdf [Last accessed: 14 Sep 2014].

Galán, O., Barton, G. W. and Romagnoli, J. A. (2002). Robust control of a SAG mill, *Powder Technology* **124**(3): 264–271.

Gellings, C. W. (1985). Concept of demand-side management for electric utilities, *Proceedings of the IEEE* **73**(10): 1468–1470.

Gellings, C. W. and Limaye, D. R. (1984). Demand-side management: Market planning for

electrical utilities, *Energy Technology XI: Proceedings of the Eleventh Energy Technology Conference* pp. 126–136.

Halldorsson, U., Fikar, M. and Unbehauen, H. (2005). Nonlinear predictive control with multirate optimisation step lengths, *IEE Proceedings: Control Theory and Applications* **152**(3): 273–284.

Herbst, J. A., Pate, W. T. and Oblad, A. E. (1992). Model-based control of mineral processing operations, *Powder Technology* **69**(1): 21–32.

Hodouin, D. (2011). Methods for automatic control, observation, and optimization in mineral processing plants, *Journal of Process Control* **21**(2): 211–225.

Hulbert, D. G., Craig, I. K., Coetzee, M. L. and Tudor, D. (1990). Multivariable control of a run-of-mine milling circuit, *Journal of the South African Institute of Mining and Metallurgy* **90**(7): 173–181.

Hulbert, D. G., Koudstaal, J., Braae, M. and Gossman, G. I. (1981). Multivariable control of an industrial grinding circuit, *IFAC Automation in Mining, Mineral, and Metal Processing* **3**: 311–315.

Hulbert, D. G. and Woodburn, E. T. (1983). Multivariable control of a wet-grinding circuit, *AIChE Journal* **29**(2): 186–191.

Jacobs, F. R., Chase, R. B. and Aquilano, N. J. (2009). *Operations & Supply Management*, 12th edn, McGraw-Hill, NY.

Jansen, W. (2012). Quarterly commodity insights bulletin Q2-2012 – platinum, Web site: http://www.kpmg.com/ZA/en/IssuesAndInsights/ArticlesPublications/Quarterly-Commodity-Insights/Documents/Platinum%20Q2%202012.pdf [Last accessed: 14 Sep 2014].

Le Roux, J. D. and Craig, I. K. (2013). Reducing the number of size classes in a cumulative rates model used for process control of a grinding mill circuit, *Powder Technology* **246**: 169–181.

Le Roux, J. D., Craig, I. K., Hulbert, D. G. and Hinde, A. L. (2013). Analysis and validation of a run-of-mine ore grinding mill circuit model for process control, *Minerals Engineering* **43-44**: 121–134.

Lestage, R., Pomerleau, A. and Hodouin, D. (2002). Constrained real-time optimization of a grinding circuit using steady-state linear programming supervisory control, *Powder Technology* **124**(3): 254–263.

Ljung, L. (1988). System identification toolbox, *The Matlab userŠs guide* .

Ljung, L. (1999). *System Identification – Theory for the User*, 2nd edn, Prentice Hall, Upper Saddle River, NJ.

Lynch, A. J. and Dredge, K. H. (1969). Automatic control system for mineral grinding circuits, *Institution of Engineers of Australia, Electrical Engineering Transactions* **EE5**(1): 101–108.

Mayne, D. Q., Rawlings, J. B., Rao, C. V. and Scokaert, P. O. M. (2000). Constrained model predictive control: Stability and optimality, *Automatica* **36**(6): 789 – 814.

McKee, D. J. (1991). Automatic flotation control - a review of 20 years of effort, *Minerals Engineering* **4**(7-11): 653 – 666.

Middelberg, A., Zhang, J. and Xia, X. (2009). An optimal control model for load shifting - with application in the energy management of a colliery, *Applied Energy* **86**(7-8): 1266–1273.

Morrell, S. (2004). A new autogenous and semi-autogenous mill model for scale-up, design and optimisation, *Minerals Engineering* **17**(3): 437–445.

Morrison, R. D. and Richardson, J. M. (2002). *Mineral Processing Plant Design, Practice, and Control*, SME, chapter JKSimMet: A Simulator for analysis, optimisation and design of comminution circuits, pp. 442–460.

Muller, B. and De Vaal, P. L. (2000). Development of a model predictive controller for a milling circuit, *Journal of the South African Institute of Mining and Metallurgy*

100(7): 449–453.

Nageswararao, K., Wiseman, D. M. and Napier-Munn, T. J. (2004). Two empirical hydrocyclone models revisited, *Minerals Engineering* **17**(5): 671–687.

Naidoo, M. A., Olivier, L. E. and Craig, I. K. (2013). Combined neural network and particle filter state estimation with application to a run-of-mine ore mill, *IFAC Proceedings Volumes (IFAC-PapersOnline)* **10**(PART 1): 397–402.

Najim, K., Hodouin, D. and Desbiens, A. (1995). Adaptive control: State of the art and an application to a grinding process, *Powder Technology* **82**(1): 59–68.

Napier-Munn, T. J. and Wills, B. A. (2006). *Wills' Mineral Processing Technology, Seventh Edition: An Introduction to the Practical Aspects of Ore Treatment and Mineral Recovery.*, Butterworth-Heinemann, Linacre House, Jordan Hill, Oxford, UK.

NERSA (2013). Reason for decision: Revenue application – multi year price determination 2013/14 to 2017/18 (MYPD3)., *Technical report*, National Energy Regulator of South Africa.

Niemi, A. J., Tian, L. and Ylinen, R. (1997). Model predictive control for grinding systems, *Control Engineering Practice* **5**(2): 271–278.

Olivier, L. E. and Craig, I. K. (2013). Model-plant mismatch detection and model update for a run-of-mine ore milling circuit under model predictive control, *Journal of Process Control* **23**(2): 100–107.

Olivier, L. E., Craig, I. K. and Chen, Y. Q. (2012). Fractional order and BICO disturbance observers for a run-of-mine ore milling circuit, *Journal of Process Control* **22**(1): 3–10.

Olivier, L. E., Huang, B. and Craig, I. K. (2012). Dual particle filters for state and parameter estimation with application to a run-of-mine ore mill, *Journal of Process Control* **22**(4): 710–717.

Palensky, P. and Dietrich, D. (2011). Demand side management: demand response, intelligent energy systems, and smart loads, *IEEE Transactions on Industrial Informatics*

7(3): 381–388.

Pauw, O. G., King, R. P., Garner, K. C. and Van Aswegen, P. C. (1985). The control of pebble mills at Buffelsfontein gold mine by use of a multivariable peak-seeking controller, *Journal of the South African Institute of Mining and Metallurgy* **85**(3): 89–96.

Powell, M. S., Morrell, S. and Latchireddi, S. (2001). Developments in the understanding of South African style SAG mills, *Minerals Engineering* **14**(10): 1143–1153.

Powell, M. S., van der Westhuizen, A. P. and Mainza, A. N. (2009). Applying grindcurves to mill operation and optimisation, *Minerals Engineering* **22**(7-8): 625–632.

Radhakrishnan, V. R. (1999). Model based supervisory control of a ball mill grinding circuit, *Journal of Process Control* **9**(3): 195–211.

Rajamani, R. K. and Herbst, J. A. (1991a). Optimal control of a ball mill grinding circuit-I. Grinding circuit modeling and dynamic simulation, *Chemical Engineering Science* **46**(3): 861–870.

Rajamani, R. K. and Herbst, J. A. (1991b). Optimal control of a ball mill grinding circuit-II. Feedback and optimal control, *Chemical Engineering Science* **46**(3): 871–879.

Ramasamy, M., Narayanan, S. S. and Rao, C. D. P. (2005). Control of ball mill grinding circuit using model predictive control scheme, *Journal of Process Control* **15**(3): 273–283.

Seborg, D. E., Edgar, T. F. and Mellichamp, D. A. (2004). *Process Dynamics and Control*, 2nd edn, Wiley, NJ.

Shi, F. N. and Napier-Munn, T. J. (2002). Effects of slurry rheology on industrial grinding performance, *International Journal of Mineral Processing* **65**(3-4): 125–140.

Skogestad, S. and Postlethwaite, I. (2006). *Multivariable Feedback Control – Analysis and Design*, 2nd edn, Wiley, Chichester.

Steyn, C. W., Brooks, K. S., de Villiers, P. G. R., Muller, D. and Humphries, G. (2010). A holistic approach to control and optimization of an industrial run-of-mine ball milling circuit, *IFAC Automation in Mining, Mineral, and Metal Processing* **13**: 137–141.

Tang, Y., Zheng, G. and Zhang, S. (2014). Optimal control approaches of pumping stations to achieve energy efficiency and load shifting, *International Journal of Electrical Power and Energy Systems* **55**: 572–580.

Valenzuela, J., Bourassa, M., Najim, K. and Del Villar, R. (1994). Dynamic matrix control of an autogenous grinding circuit, *Minerals Engineering* **7**(1): 105–114.

van Staden, A. J., Zhang, J. and Xia, X. (2011). A model predictive control strategy for load shifting in a water pumping scheme with maximum demand charges, *Applied Energy* **88**(12): 4785–4794.

Wei, D. (2010). *Development of performance functions for economic performance assessment of process control systems*, PhD thesis, University of Pretoria.

Wei, D. and Craig, I. K. (2009a). Economic performance assessment of two ROM ore milling circuit controllers, *Minerals Engineering* **22**(9-10): 826–839.

Wei, D. and Craig, I. K. (2009b). Grinding mill circuits – A survey of control and economic concerns, *International Journal of Mineral Processing* **90**(1-4): 56–66.

Yang, J., Li, S. H., Chen, X. S. and Li, Q. (2010). Disturbance rejection of ball mill grinding circuits using DOB and MPC, *Powder Technology* **198**(2): 219–228.

Zhang, S. and Xia, X. (2010). Optimal control of operation efficiency of belt conveyor systems, *Applied Energy* **87**(6): 1929–1937.